MULTIPHASE IMMISCIBLE FLOW THROUGH POROUS MEDIA

by

Jopan Sheng

Dissertation submitted to the Faculty of the

Virginia Polytechnic Institute and State University

in partial fulfillment of the requirements for the degree of

Doctor of Philosophy

in

Civil Engineering

APPROVED:

T. Kuppusamy

T. L. Brandon

D. Frederick

J. H. Hunter

R. D. Krebs

July, 1986

Blacksburg, Virginia

MULTIPHASE IMMISCIBLE FLOW THROUGH POROUS MEDIA

by

Jopan Sheng

T. Kuppusamy

Civil Engineering

(ABSTRACT)

A finite element model is developed for multiphase flow through soil involving three immiscible fluids: namely air, water, and an organic fluid. A variational method is employed for the finite element formulation corresponding to the coupled differential equations governing the flow of the three fluid phase porous medium system with constant air phase pressure. Constitutive relationships for fluid conductivities and saturations as functions of fluid pressures which may be calibrated from two-phase laboratory measurements, are employed in the finite element program. The solution procedure uses iteration by a modified Picard method to handle the nonlinear properties and the backward method for a stable time integration. Laboratory experiments involving soil columns initially saturated with water and displaced by p-cymene (benzene-derivative hydrocarbon) under constant pressure were simulated by the finite element model to validate the numerical model and formulation for constitutive properties. Transient water outflow predicted using independently measured capillary head-saturation data agreed well with observed outflow data. Two-dimensional simulations are presented for eleven hypothetical field cases involving introduction of an organic fluid near the soil surface due to leakage from an underground storage tank. The subsequent transport of the organic fluid in the variably saturated vadose and ground water zones is analysed.

Acknowledgements

The author would like to express special thanks to Dr. T. Kuppusamy for his guidance and encouragement. The author also directs a special appreciation to Dr. J. H. Hunter for his great efforts in correcting the writing of this thesis. The sound advice of Dr. T. L. Brandon, Dr. D. Frederick, and Dr. R. D. Krebs are appreciated by the author.

The author would like to express his thanks to Dr. J. C. Parker and Dr. R. J. Lenhard, who supervised and conducted the experimental study for this research at the Department of Agronomy.

The author is grateful to his wife for her encouragement, patience, and love.

This study was supported by the U. S. Environmental Protection Agency through the R. S. Kerr Environmental Research Laboratory under assistance agreement CR-812073-02.

Table of Contents

List of Illustrations

List of Tables

CHAPTER 1

Introduction

Rapid increases in industrial and agricultural productivity, have resulted in ground water resources becoming increasingly important during the last decade. Consequently, the potential danger of ground water contamination is proportionally greater.

Ground water contamination may be due to several causes such as an industrial accident, careless treatment of hazardous waste material, poor maintenance of underground liquid containers, and inadequate design of ground water pumping and recharging systems among other things. The physical phenomena involved in these contamination causes can be classified into two categories. One is miscible contamination in which the hazardous material dissolves into the water phase. The propagation of the contaminant involves convection and diffusion. The other one is immiscible contamination in which the contaminant flows simultaneously with the water phase as an independent fluid phase. The latter is commonly called immiscible flow. This three-phase immiscible flow usually consists of an air phase, a water phase, and another immiscible fluid phase. The interfacial tension between the different

fluid phases result in a fluid-fluid interface within a porous material. The term porous material refers mainly to soils in this study.

The objective of this study is to develop a numerical model to analyse three-phase immiscible flow behavior in porous media. It is important and of great interest to understand how immiscible fluid flows underground along with water. For example, in the case of a leaking underground oil tank, an accurate prediction of the propagation of the oil phase in the soil provides necessary information for a remedy.

A thorough study of the literature related to the subject of immiscible flow behavior is presented in Chapter 2. It includes general descriptions of immiscible flow phenomena, the major factors controlling flow behavior, the empirical research based on laboratory work, the mathematical derivation of the flow equations, and the numerical analyses for this specific topic.

Chapter 3 introduces the whole system of three-phase immiscible flow. The system includes the porous medium, the air phase, the oil phase, and the water phase. The assumptions made for the porous medium and the fluids are presented and discussed. The three-phase flow equations are then derived based on these assumptions.

An empirical study of immiscible flow behavior is outlined in Chapter 4. The procedures for the laboratory tests and for estimation of the model parameters are described in that chapter.

Chapter 5 gives a numerical analysis using the finite element method. The formulation is based on the variational method and uses iteration techniques for nonlinearity and a time integration scheme.

In Chapter 6 a complete validation is made for the finite element model by comparing the model prediction with laboratory test data. The tests used for comparison are one-dimensional static tests and a transient test. A problem of seepage through an earth dam is analysed using the numerical model and this result is compared with a well known graphic solution.

Some applications of the developed numerical model are presented in Chapter 7. A hypothetical underground leaking oil tank is analysed under different water table levels, different boundary conditions, and different soil properties. A cutoff wall is constructed near the leaking oil tank and the effect of this cutoff wall on the spreading of the oil plume is analysed.

Conclusions that can be derived from this study along with some recommendations for further research are presented in Chapter 8.

CHAPTER 2

Multiphase Immiscible Flow

The study of immiscible flow behavior for hydrocarbon and water in oil reservoirs has attracted researchers in petroleum engineering for more than twenty years. In the 1970's, groundwater contamination from leaking underground storage tanks received increased attention from researchers in environmental science and soil physics. In recent years, geotechnical engineers have become involved in cleaning up contaminated sites. Hence, the civil engineering attention also is directed towards understanding the mechanics of immiscible flow of fluids through soils.

Research related to immiscible flow falls into two major categories. One of these is the analytical study of flow behavior supported by experimental results, and the other is numerical simulation. The analytical studies laid the foundation for the basic governing equations developed from the laws of physics, and experimental studies permitted valuation of various material parameters necessary for use of the basic equations. Numerical simulation yielded valuable models for solutions of practical problems.

Saturated Flow

The systematic study of the fundamentals of flow through porous media started early in the 1850's. H. Darcy and J. Dupuit were pioneers in the studying of groundwater flow. One of the most important contributions to the study of the groundwater flow is the well-known Darcy's law proposed in 1856.

Many researchers used different models to derive Darcy's law analytically. The capillary tube model (Scheidegger 1960) started from the Hagen-Poisseuille's law governing steady flow through a single straight circular tube and extended to the case of nonuniform capillary tubes with tortuosity considered. The fissure model (Irmay 1955, Snow 1965, Parsons 1966) started with the average velocity solved from the Navier-Stoke's equation for the specific condition of a single fissure of constant width bounded by two parallel impervious planes. The hydraulic radius model (Blake 1922, Carman 1937, Wyllie and Spangler 1952, Carman 1956) applies the Hagen-Poisseuille's law using an *equivalent hydraulic radius* and a *porosity factor*. The flow resistance model (Iberall 1950, Rumer and Drinker 1966) considers the drag force as the fluid flows past particles of porous media. The statistical model (Scheidegger 1954) considers a *disordered* porous medium which is highly simplified in most of theoretical or mathematical analyses. Ferrandon (Bear 1972) uses fundamental aspects of anisotropic permeability in a porous medium for the development of his model, and most soils are anisotropic with respect to permeability (Casagrande 1940).

Intrinsic Permeability

From the analytic derivations of Darcy's law mentioned above, Nutting (1930) obtained an expression for the hydraulic conductivity K. He showed that $K = \frac{k\gamma}{\eta}$ where k is the *intrinsic permeability* of the porous medium, γ is the unit weight of the fluid, and η is the dynamic viscosity of the fluid. Thus the intrinsic permeability depends upon the porous medium only.

Some of the formulas derived in the literature relating the intrinsic permeability to the various properties of the porous material are purely empirical (see Bear 1972 for Krumbein and Monk 1943), some are semi-empirical (Fair and Hatch 1933), and some are purely theoretical (Bear 1972). The semi-empirical functions are most commonly used for practical purposes. The purely empirical formulas are less accurate in general even though they are simple to use. The purely theoretical formulas require too many parameters which are some times difficult to estimate. The semi-empirical formulas are derived using a theoretical basis with some empirical coefficients left to be determined experimentally. The laboratory or field tests required to provide the necessary information in determining these coefficients are relatively simple and practical.

Validity of Darcy's Law

Since Darcy's law is an experimental conclusion, its validity is a proper topic for researchers. Many investigators (e.g., Rose 1945) found that Darcy's law no longer holds as the specific discharge increases beyond certain limits. The dimensionless Reynold number R_e is used as a criterion to indicate the flow pattern, laminar or turbulent. For flow through porous media R_e is defined as $R_e = q\frac{d}{\nu}$ where q is the discharge, d some length dimension of the porous medium, and ν the kinematic viscosity of the fluid. Different suggestions have been made for selecting d. Collins (1961) used $d = (k/\varphi)^{1/2}$ where k is intrinsic permeability and φ is porosity. Ward (1964) chose $k^{1/2}$ for d.

It is generally accepted that at low Reynolds numbers, flow in a porous material is laminar, viscous forces are predominant, and Darcy's law is valid. As the Reynold number increases inertial forces govern the flow and experimental results deviate from Darcy's law. This is the upper limit for the application of Darcy's law.

Many investigators (von Engelhardt and Tunn 1955, Low 1961, Swartzendruber 1962, Kutilek 1969, Bolt and Groenevelt 1969) noticed that if the hydraulic gradient of a fluid in a porous material is lower than a critical value there exists very little flow and Darcy's law be-

comes invalid. The flow under this condition is called non-Darcian laminar flow. This leads to the lower limit for the application of Darcy's law. For practical purposes, Bear (1972) suggests that Darcy's law is valid as long as the maximum value of R_e , based on average grain diameter, does not exceed some value between 1 and 10.

Unsaturated Flow

In the analysis of groundwater flow , the capillary zone above the phreatic surface was neglected until the 1960's (Wesseling 1961, Remson and Randolph 1962, Swartzendruber 1969, Philip 1970). Before 1950, problems involving the flow of two fluids, a gas and oil, through porous media were analysed for the most part by petroleum engineers (Muskat 1937, Buckley and Leverett 1942). Two major topics, capillary pressure and relative permeability, have been studied since then to aid in the understanding of the mechanics of unsaturated flow.

Capillary Pressure

In an unsaturated soil capillarity is the evidence of surface tension in the fluid, which is generally water. Capillarity enables a dry soil to draw water through continuous pores to elevations above the phreatic line, or enables an initially saturated soil to keep the water at a certain elevation above the phreatic line in a draining process (Lambe and Whitman 1969). Not all the pores below these elevations are filled by water. This induces variations in both the degree of saturation and the hydraulic conductivity with respect to the elevation of points within the capillary zone.

In a circular capillary tube the height of rise $h_c = \frac{2T_s}{R\gamma}\cos\alpha$ where the T_s is the liquid surface tension, γ the unit weight of liquid, α the contact angle between the liquid and the tube, and R the tube radius. This capillary rise h_c is called the capillary head. In soils the pore size varies depending on the shape, size, and packing condition of the soil particles. These vari-

ables make the analytic approach in determining the capillary head extremely difficult. On the other hand, direct measurement of the capillary head by installing a standpipe is fairly simple. Table 1 gives some test data obtained by Lane and Washburn (1946) and Silin-Bekchurin (1958) in the soil column test for the height of capillary rise.

An increase or decrease of the air pressure at the top of the soil sample column produces different values of the capillary rise h_c and the corresponding water saturation S. Collins (1961) derived an equation to calculate the degree of saturation by considering the case of vertical circular rods with radius R in a cubic packing mode as a porous medium. Smith (1933) analysed the case of uniform size spheres as a three-dimensional porous material.

It is of great interest to measure the relationship between capillary head and degree of saturation for porous media. The laboratory methods can be classified into two groups. The displacement methods are based on hydrostatic equilibrium at successive states, e.g., the desaturation method (Welge and Bruce 1947), the mercury injection method (Purcell 1949), and the centrifuge method. Amyx et al. (1960) compared results from various methods. The dynamic method (Brown 1951) used a horizontal soil sample and controlled the capillary pressure at both ends of the soil sample. This ensured uniform capillary pressure throughout the soil sample. Many investigators (Millington and Quirk 1961, Brooks and Corey 1964, van Genuchten 1980, and Diment 1983) developed empirical equations to fit the *soil-water retention curve*, and these equations are called the *capillary function* for generality.

It was found that the soil-water retention curve is not unique. In other words, at a given capillary head h_c the corresponding water saturation S depends on the wetting or drying history experienced by the soil column sample. This is called *hysteretic* behavior which has gained the attention of some investigators (Muskat 1937, Bear 1972).

Relative Permeability

In the unsaturated flow problem, only part of the pore space in the neighborhood of a point in a porous material is occupied by water. Hence the unsaturated permeability of the

Table 1. Values of capillary rise.

Soil type	Height of capillary rise (cm)
Silin-Bekchurin (1958) :	
Coarse sand	2-5
Sand	12-35
Fine sand	35-70
Silt	70-150
Clay	200-400 and greater
Lane and Washburn (1946) :	
Coarse gravel	5.4
Sandy gravel	28.4
Fine gravel	19.5
Silty gravel	106.
Coarse sand	82.
Medium sand	239.6
Fine sand	165.5
Silt	359.2

porous material will be less than the saturated permeability. Experimental evidence (e.g., Botset 1940) supports this idea which can be stated as *the relative permeability depends on the water saturation* where the relative permeability is defined as the ratio between the unsaturated and the saturated permeabilities.

As mentioned in the previous section, there exists a relationship between the capillary head and the water saturation provided the wetting or drying history of the porous material is known. Thus the relative permeability can be expressed in terms of the capillary head, or the water saturation, or both (e.g., Mualem 1976).

A detailed review on the relative permeability is given in the next section where the multiphase immiscible flow problem is reviewed.

Immiscible Flow

The simultaneous flow of two or more fluids results in the immiscible flow problem. In oil reservoir engineering, the flowing phases consists of gas, oil, and water. The unsaturated flow mentioned in the previous section can be viewed as a simple case of the immiscible flow problem where water and air are the two immiscible fluids.

Most of the concepts and terminology introduced for unsaturated flow are applicable to immiscible flow (Dullien 1979).

Wettability

Since there can be more than one flowing liquid in an immiscible flow problem, an assumption is commonly made in most studies relating to wettability. It is assumed here that there can be no direct contact between fluid A and fluid C if fluid B exists and the wettability of fluid B is in between those of fluids A and C. The term wettability is related to the interfacial tension of the fluids involved. Bikerman (1958), Scheidegger (1960), and Adamson (1967)

made an extensive study on this subject. Pirson (1958) adopted the concept of wettability to distinguish three types of fluid saturation between the limits 0 % and 100 % . These are the equilibrium saturation, the funicular saturation, and the insular saturation. A clear explanation on these saturation terms is given by Scheidegger (1960) and Bear (1972).

Capillary Pressure

Based on the concept of wettability, there can be no interface between more than two fluids. This makes the capillary pressure measurement for a multiphase immiscible flow the same as for an unsaturated flow. All the information required to determine the capillary function for a multiphase immiscible flow problem can be obtained from the results generated by sufficient two-phase flow studies (Stone 1970, Parker et al. 1985).

Relative Permeability

One way to determine the relative permeability is by direct measurement from laboratory experiments. In the steady flow test, two liquids are introduced simultaneously at the inflow end through separate tubing systems while keeping the ratio of the quantities of the two fluids constant. When a steady flow is reached (total inflow equals total outflow) the pressures at both ends are recorded for each fluid. The rate of flow q and saturation S are determined for each fluid. The relative permeabilities are calculated by using the equation $q_{w,o} = (k_{w,o}/\eta_{w,o})\Delta P_{w,o}/L$. The test is repeated under different injecting ratio until a complete relative permeability curve is established. Brownscombe et al. (1950) and Rose (1951) presented a general review of this type of test.

Figure 1 gives typical relative permeability curves for a porous medium saturated by oil and water. The rapid decline of the relative permeability of the water phase indicates that the oil phase (nonwetting phase) occupies the larger pores first as the water saturation decreases.

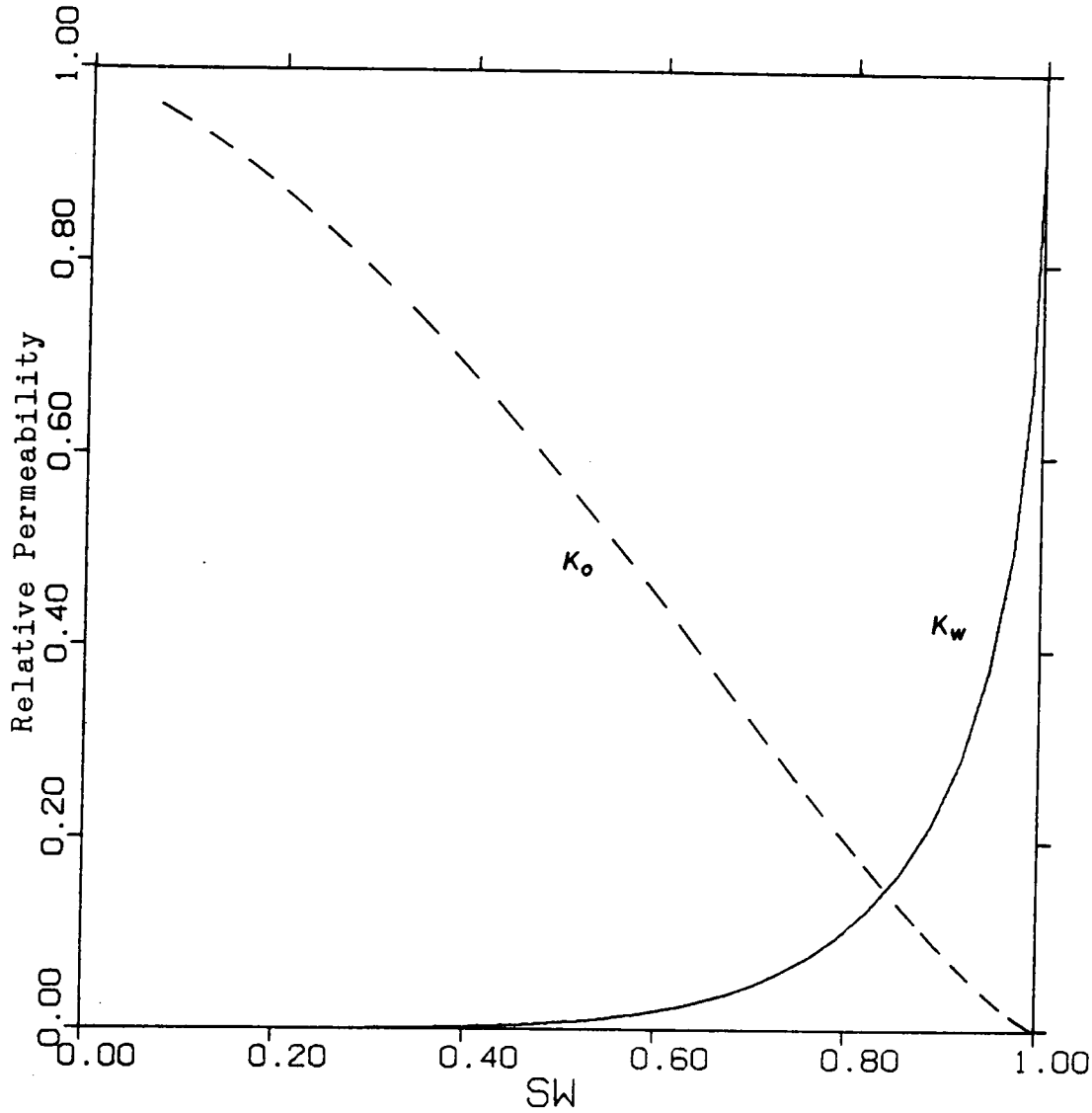

Figure 1. Relative permeabilities in an oil-water system.

Researchers found that the sum $k_{rw} + k_{ro}$ is generally less than unity even though the pores are fully saturated by oil and water. On the other hand, Russell and Charles (1959) found that a thin layer of water on the solid surfaces may reduce the resistance to the flow of oil. This makes the relative permeability of the oil phase greater than unity. All these observations contradict the assumption that relative permeability is dependent on the properties of the porous medium alone. The effect of pressure gradient on relative permeability was studied by Muskat (1937) and he concluded that the effect is negligible.

As mentioned in the previous section, Mualem (1976) proposed a semi-empirical model to predict the relative permeability. The analytic part of the model is similar to Burdine's equation which was derived (Burdine 1953) based on the hydraulic radius theory and the observation that the nonwetting phase tends to occupy the larger part of the pore first. Brooks and Corey (1964) described the hydraulic radius theory in detail. The empirical part of Mualem's model was done by examining 45 soil samples and suggested a value of 0.5 for the power of the effective saturation term. This model requires an accurate capillary function which must be determined experimentally. Scheidegger (1960) reviewed several models of capillary function (e.g., Rose and Bruce 1949, Fatt and Dykstru 1951, and Rapoport and Leas 1951). Corey et al. (1956) worked on the three-phase relative permeability with $CaCl_2$ brine as the wetting phase. Brooks and Corey (1964) suggested the equation $S_e = (P_b/P_c)^{\lambda}$ where S_e is the effective degree of saturation, P_b the minimum value of P_c on the drying curve, and λ a pore size distribution index. Van Genuchten (1980) proposed a capillary function (see Eq. 4.4) with two parameters α and n to be determined from the laboratory experiments. He substituted this capillary function into two models (Burdine 1953 and Mualem 1976) for the relative permeabilities. Diment and Watson (1983) used a simple polynomial $K = K_s(\theta/\theta_s)^T$ for relative permeability and a hyperbolic tangent capillary function $\theta = (\theta_s - \theta_r)$ $\tanh[R(h + S)] + \theta_s - F$ where K_s is intrinsic permeability, T the degree of the polynomial, θ_s the saturated moisture content, θ_r the residual moisture content, R and S the model parameters, and $F = (\theta_s - \theta_r) \tanh(RS)$. Since the polynomial expression for relative permeability has no clear theoretical basis, its validity still needs more studies.

Solution Methods for Flow Through Porous Media

The governing differential equations for an immiscible flow problem can be set up by using the mass conservation principle. The constitutive laws are to be experimentally determined. The unknowns to be solved for are total head, saturation, and flow rate for each fluid phase considered in a flow problem. The independent variables are spatial coordinates and time.

There are basically three types of solutions available. The first type is the analytical solution which expresses the dependent variables (solutions) in terms of the independent variables explicitly. The second type is the model or the analog solution. It reproduces as many the aspects of a physical problem as possible by constructing an analog model using materials which may or may not be the same as the materials of the physical problem. The third type is the numerical solution which gives solutions at each discrete point in space and time within the domain of the physical problem. Information on the material properties and the boundary and initial conditions of a physical problem are necessary for any type of solution method.

Analytical Solution

Due to the complexity of immiscible flow behavior very few problems can be solved analytically. For an analytical solution, either the problem is idealized and over-simplified, or the analytical solution obtained is expressed in the form of an infinite series or a complex integral. An over-simplified problem has less value for practical purpose. An analytical solution involving any form of infinite series or a complex integral may still need a digital computer for calculating an precise answer.

Bear (1972) gives an extensive review of the methods that may be used for an analytical solution of boundary and initial value problems of flow through porous media. Collins (1961)

gave an analytical solution of the linear displacement problem in which gravity and capillary effects were not considered. Eckberg and Sunada (1984) analytically evaluated a three-phase distribution under static equilibrium condition caused by a petroleum spill in an unconfined aquifer.

Model and Analog Solutions

A model is usually constructed of the same or similar materials as is the physical problem to be modelled. The main difference between a model and a physical problem is the scale which should satisfy geometric similarity, kinematic similarity, and dynamic similarity in general (Bear 1972). A sand box model is frequently used in petroleum reservoir engineering (e.g., Muskat 1937 and van Meurs 1957).

An analog system is made of completely different materials from the physical problem. However, there is a one-to-one correspondence between each dependent variable in the analog and the physical systems, and the independent variables are related to each other in the same manner in the two systems. The common mathematical equations developed to describe flow through porous media are similar to those in heat flow, electricity, and other branches of physics (Scheidegger 1957). This provides an opportunity for adapting a well developed testing technique from other field to analyse the flow problem.

One important advantage of the model and analog approach is that the solution is continuous in the time domain as it is in the analytical solution. In the numerical simulation, which is reviewed in the next section, the time domain is discrete, and this leads to a certain degree of inaccuracy.

Numerical Solution

Due to the nonlinear characteristics of the governing differential equations used in simulating a flow behavior, it is extremely difficult to obtain an analytical solution. The model or

analog solution requires much effort in building a physical model. Furthermore, the model is usually used only for a very specific problem. On the other hand, a numerical method is fairly flexible in handling different problems. In the last decade, the advances in high technology not only provide a higher speed for calculation but also offer better quality output devices so that the interpretation of the calculated results is easier and clearer than ever. All of these indicate that numerical analyses are approaching a brilliant and challenging era.

There are basically two methods of solving differential equations numerically, the finite difference method (Shaw 1953, Smith 1965, and Peaceman 1977) and the finite element method (Bathe 1976, Zienkiewicz 1977, and Reddy 1984).

Finite Difference Method

Generally speaking, the finite difference method is quite straightforward mathematically. The spatial derivative terms of the dependent variable are approximated by the *finite differences* of the variables and the distances between adjacent discrete grid points. For time dependent problem, similar finite difference approximation is made for the time derivative terms. The solution proceeds for each discrete time step Δt. The differential equation turns out to be a series of algebraic equations involving all the dependent variables. After substituting the given boundary conditions, the algebraic equations are solved one by one or simultaneously depending on how the approximation is made for the derivative terms.

It is obvious that a finer grid (a shorter distances between adjacent points) leads to a better approximation for the spatial derivative terms and thus a better solution. However, finer grid means more algebraic equations to be solved for a given domain. Furthermore, if the explicit scheme is used in a time dependent problem, it is known (Richtmeyer 1957) that the discrete length ΔL and the time step Δt are constrained to the condition $\Delta t/(\Delta L)^2 \leq 1/2$ so that a stable solution is guaranteed. The implicit scheme avoids this constraint but the algebraic equations have to be solved simultaneously.

The finite difference method has been widely used in solving the flow problems. Douglas et al. (1959), Quon et al. (1966), and Carter (1967) discussed the multiphase flow problem in

reservoir engineering. Watson (1967) dealt with the unsaturated flow problem. Peery and Herron (1969) made a three-phase reservoir simulation. Huppler (1970) investigated the effects of common core heterogeneities on waterflood relative permeabilities. Freeze (1971a) studied three-dimensional transient unsaturated flow in a groundwater basin. Settari and Aziz (1972) used an irregular grid in oil reservoir simulation. Narasimhan and Witherspoon (1976) used the integrated finite difference method to solve a groundwater flow problem. Narasimhan (1982) analysed the fluid flow in fractured porous media. Casulli and Greenspan (1982) simulated miscible and immiscible flow in porous media. Faust (1984) modelled the transport of immiscible flow within and below the unsaturated zone. Abriola and Pinder (1985a,b) studied multiphase contamination in porous media.

Finite Element Method

Instead of approximating the differential equation directly as does the finite difference method, the finite element method constructs a functional associated with the governing differential equation. By the variational method or the residual method, a series of algebraic equations for each finite element is developed. Lumping together the element level algebraic equations and applying the given boundary conditions result in the global algebraic equations from which the dependent variables are solved simultaneously. A number of books on this subject are available (Zienkiewicz 1977, Hinton and Owen 1979, Bathe 1982, Brebbia 1982, Segerlind 1984, Logan 1986, Grandin, 1986).

The soils involved in the flow problem are usually nonhomogeneous and the geometric domain may be irregular. The finite element method has a greater flexibility and capability in handling complex geometric conditions. than does the finite difference method. Thus more and more researchers have applied the finite element method to flow problem since the 1970's.

Use of the finite element method for flow problems is exemplified in many publications. Shamir (1967) analysed steady flow in nonhomogeneous anisotropic aquifer. Javandel and Witherspoon (1968) studied transient flow through porous media. Zienkiewicz et al. (1977)

coupled the boundary solution procedures with the finite element method. This coupled procedure reduced the the number of unknowns to approximately the unknowns involved along the boundaries, and handled the infinite boundaries reasonably well. Bettess (1977) introduced shape functions which are applicable to a flow problem having a domain extended to infinity. Belytschko et al. (1983) proposed a special time integration procedure which allowed different time steps and integrators within different parts of a domain. Van Genuchten (1982) compared the finite element methods for one-dimensional unsaturated flow with mass transport problems. Neuman et al. (1982) studied the groundwater flow and land subsidence due to pumpage in multiaquifer systems. Van Genuchten (1983) used an Hermitian finite element formulation to solve the two-dimensional unsaturated flow equation. Huyakorn et al. (1984) used an influence coefficient technique to avoid costly numerical integration. Lewis et al. (1984) analysed a plan pattern of two-dimensional multiphase flow. Osborne and Sykes (1986) simulated the migration of an immiscible organic solvent in groundwater from a chemical waste disposal site in the upper state of New York.

CHAPTER 3

Theory of Multiphase Immiscible Flow in Porous Media

This chapter introduces the physics of multiphase immiscible flow followed by a complete derivation of the governing equations.

Physical Phenomena

The industrial waste spill, the underground gas tank leaking, initiate the study of multiphase flow in soils. Some of these hazardous fluids are practically immiscible with groundwater and present certain behaviors as they seep through soils. The observed physical phenomena give the key to analyse these immiscible flow behaviors in porous media.

Porous Media

There are many examples of porous materials in engineering practice. Soil, limestone, sandstone, or even concrete may be treated as a porous material with a certain value of hydraulic conductivity. A common characteristic of these porous media is that they are permeable to a variety of fluids. If a medium is permeable to a fluid then the fluid must be able to penetrate the porous material no matter how much resistance the material offers. This implies that only pores *interconnected* all the way through a porous medium contribute to the flow behavior; one of the basic requirements for flow to occur is a channel through which flow can occur. For example, a sample of vesicular igneous rock such as pumice can have a large percentage of its volume occupied by non-solid material but since these gas bubbles are closed it follows that the permeability of the pumice can be zero.

Those pores affecting flow can be characterized by a ratio called *effective porosity*. Effective porosity is defined as V_v/V_{bulk} where V_v is the volume of those *interconnected* pores and V_{bulk} is the total volume of the porous material. The term *porosity* used here is the effective porosity unless otherwise noted. The porosity φ of a porous material (the symbol n, used in geotechnical engineering, is identical to φ) is assumed to remain constant throughout the analysis. More specifically, the porous skeleton is assumed to behave as a rigid material. This implies that V_{bulk} and V_v of a porous material remains unchanged during flow. This is a sound assumption insofar as the flow of water through most soils and rocks. If the compressibility of the soil skeleton is taken into account then it leads to the Biot's consolidation theory (1941). However, in this study only flow through porous media is analysed.

Flow in Porous Media

Flow in porous media can be described in many ways. The characteristics of the medium can affect the flow. The characteristics of the fluid or fluids flowing can affect the flow, and

jointly the medium and the fluid can have mutually interactive characteristics. Flow can occur with only one fluid or with more than one fluid flowing.

Fluid-Media Factors

Capillary pressure : Capillary phenomenon in a porous medium involves a solid phase (the porous skeleton) and at least two fluid phases. One of these two fluid phases can be said to *wet* the solid more preferentially than the other. The contact angle between the two fluids determines which one of them is the wetting phase.

In an air-water-solid system, for example, if the contact angle γ is less than 90° as shown in Figure 2 then the water phase is the wetting phase. In this example, the air and water phases are separated by a thin layer called the *interface*. The pressure difference between these two phases is defined as the *capillary pressure*, p_c. The capillary pressure is the pressure in the nonwetting phase minus the pressure in the wetting phase, or $p_c = p_a - p_w$.

Capillary pressure is a fundamental factor in the study of multiphase flow through porous media. From Figure 2, one may expect that the air phase will penetrate further into the capillary space as the air pressure increases. This will result in an increase in capillary pressure. This points to a relationship between capillary pressure and degree of saturation. This relationship will be discussed later.

Degree of Saturation : The degree of saturation S is defined as V_{fluid}/V_v where V_{fluid} is the volume of fluid in the pores. In soil physics another term used to describe the degree of saturation is called the *volumetric moisture content* θ, and θ is defined as V_{fluid}/V_{bulk}. It is clear that $\theta = \varphi S$. The value of S ranges from 0 for complete dry to 1 for full saturation.

Capillary Head vs. Fluid Saturation

As mentioned above, a close relationship between capillary head and degree of saturation is expected. Figure 3 shows a typical wetting and draining curves commonly observed for an air-water-solid system. Hysteretic behavior is exhibited between the wetting and drying

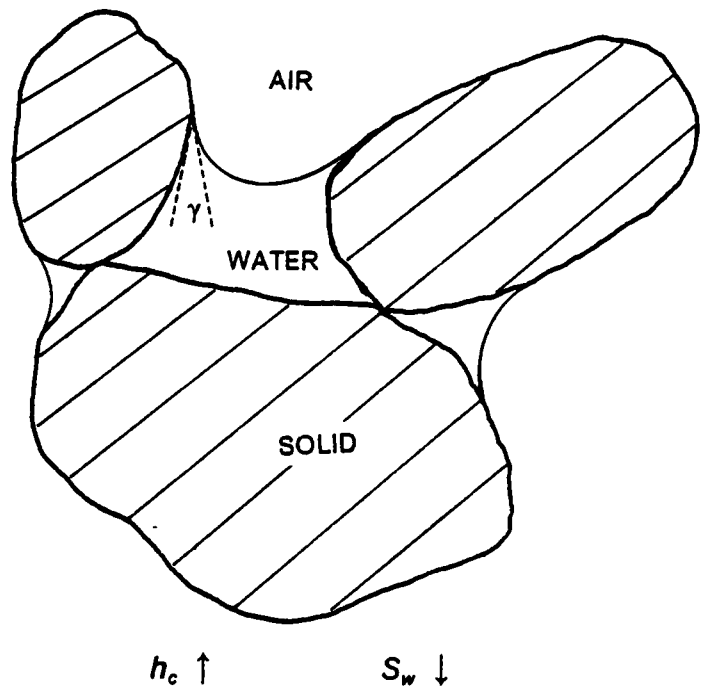

Figure 2. Contact angle for an air-water-solid system.

cycles. This figure also points out some important aspects of flow behavior for the system. The capillary head h_c is a decreasing function of the wetting phase saturation S_w. There is a deflection point on each of the two curves. A certain degree of saturation for the wetting phase is retained, and this appears to be independent of further increases of the capillary head h_c. This specific value of saturation is defined as the *residual saturation* S_{rw} for the wetting phase of the system. A mathematical function can be developed which will adequately model the h_c-S relationship.

Fluid Conductivity

In soil physics *permeability* k is used to describe the ability of a porous medium to be permeated by a fluid. Permeability to a soil physicist is a physical property of the porous medium which is independent of both fluid properties and flow mechanisms. In ground water hydrology and soil mechanics, *hydraulic conductivity* K is commonly used rather than permeability as defined above. For a particular fluid, K becomes K_{fluid} and hydraulic conductivity can be generalized to *fluid conductivity*. Fluid conductivity is defined as $K_{fluid} = k\,\rho_{fluid}\,g/\eta_{fluid}$ where ρ_{fluid} is the fluid density, η_{fluid} the fluid viscosity, and g the acceleration due to gravity. Geotechnical engineers use K but they commonly call it permeability and use as its symbol k. Thus, two conflicting definitions of permeability exist. In multiphase flow problems fluids other than water are flowing thus the use of K_{fluid} is appropriate. To avoid confusion of terms this will be referred to as fluid conductivity K although it is very nearly the same quantity geotechnical engineers call permeability.

Similar to fluid saturation S, fluid conductivity K is a decreasing function of the capillary head h_c. The function curve is quite similar to that in Figure 3. In fact, there is a close relationship among capillary head h_c, fluid saturation S, and fluid conductivity K. The $h_c - S - K$ relationship plays a key role in multiphase flow behavior.

Multiphase Immiscible Flow

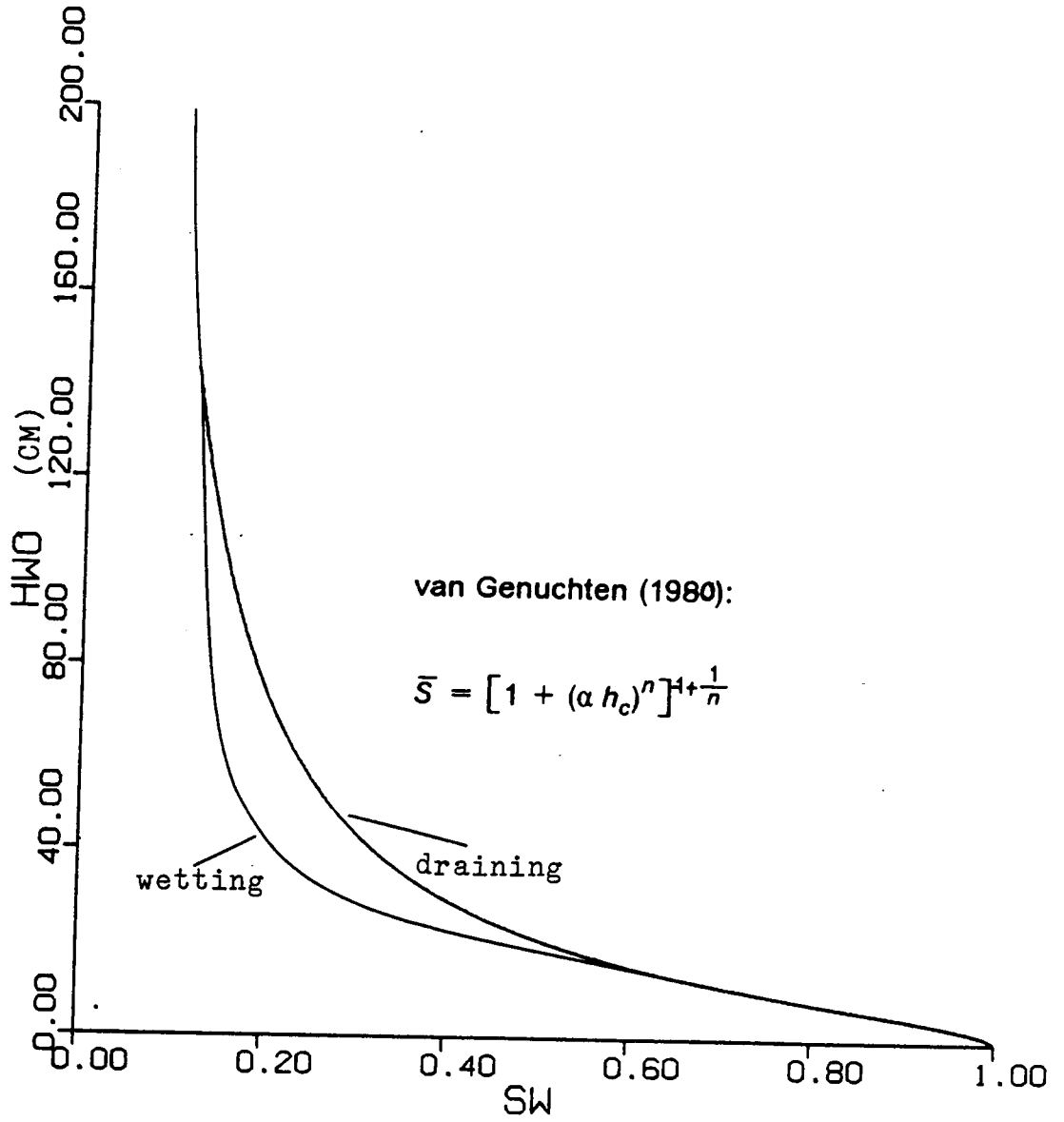

Figure 3. Capillary head vs. degree of saturation.

Multiphase immiscible flow involves two or more fluid phases flowing simultaneously through porous media. They are separated from one another by interfaces. No interphase transfer is considered in this study.

Unsaturated flow through soils is a simple example of multiphase flow. A most common case of unsaturated flow which routinely happens is the infiltration of rain fall through unsaturated soils. The infiltration process really involves two phases of fluids in which the wetting phase is water and the nonwetting phase is air. During the process of infiltration, the water phase displaces the air phase. Another example of unsaturated flow is the seepage through an earth dam due to first filling of the reservoir (Freeze 1971b). The capillary zone above the phreatic surface is important because of the seepage in this zone and the initial moisture content variations.

The fluid conductivity of gases in soils is generally very much greater than that of most liquids in soils. This will permit some simplification of the mathematical model for multiphase systems if one of the fluids is a gas. In this study the gas is always ordinary air which is a mixture of gases. The simplification can be achieved by neglecting the head lost within the gaseous phase. Specifically, this implied assumption can be stated as *the pressure in the air is assumed to remain constant and equal to atmospheric pressure throughout the soil domain under consideration.* This assumption may not hold in all cases. An example in which this assumption is not valid is the case in which air is introduced under high pressure for the purpose of forcing some liquid such as oil from a soil.

Channel flow concept originated from direct visual observation of two-phase flow (Craig 1971) is applied in this study. The concept states that *each fluid phase flows through its own network of interconnected channels.* Any increase in the saturation of one fluid phase corresponds to an increase in the number of channels carrying that fluid. At the same time, there is a corresponding decrease in the number of channels occupied by the other fluid phase. At all times the sum of the degrees of saturation for all the fluids equals unity, i.e., $\sum_{i=1}^{n} S_i = 1$, where n is the total number of fluid phases and S_i is the degree of saturation of each fluid phase i, including air phase as one of the fluid.

The wettability of each fluid phase strongly affect the multiphase flow behavior. Wetting fluids tend to occupy the smaller pores while nonwetting fluids fill the larger pores. In a multiphase system wettability is relative. For example, in an air-oil-water multiphase system, water is the wetting phase while oil is a nonwetting phase with respect to water and is a wetting phase with respect to air.

Figure 4 shows a wedge-shaped pore containing these three phases. Water occupies the smallest portion of the pore, the tip of the wedge, for it is the wetting phase. The oil lies in between the water and the air for it is a wetting phase with respect to air but nonwetting with respect to water. In this study it is assumed that so long as the oil phase exists, there can be no direct contact between the air and water phases. This assumption leads to the conclusion that the total degree of saturation S_t is a function of the capillary head h_{ao} alone. The head h_{ao} is the capillary head between the air and oil phases. The saturation of the water phase S_w is a function of the capillary head h_{ow} between the oil and water phases. Since $S_t = S_o + S_w$, the saturation of the oil phase S_o is affected by both capillary heads h_{ao} and h_{ow}.

Capillary head affects not only the degree of saturation but also the fluid conductivity. Fluid conductivity and degree of saturation are not independent, and thus the effects of capillary head on both of these factors are similar. Usually fluid conductivity K is presented as a function of the degree of saturation. For water $K_w = f_1(S_w)$ and for oil $K_o = f_2(S_w, S_o)$. Figure 5 shows the typical variations of K_o and K_w as functions of S_w in an oil-water system in which $S_o = 1 - S_w$.

Governing Equations of Immiscible Flow

Both one- and two-dimensional multiphase immiscible flow equations are derived in this section. Since air pressure is assumed to be atmospheric throughout the whole flow domain,

THREE-PHASE IMMISCIBLE FLOW

AIR-WATER-HYDROCARBON SYSTEM

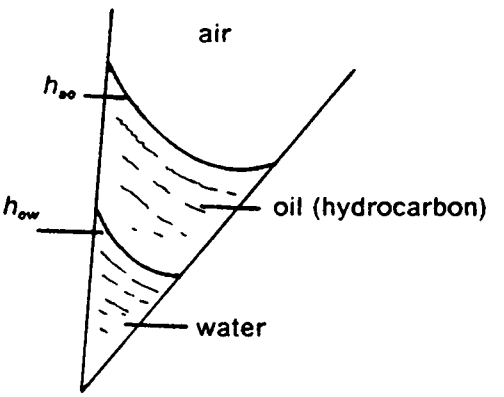

No direct contact between water and air if oil exists.

Figure 4. Wetting and nonwetting phases in an air-oil-water system.

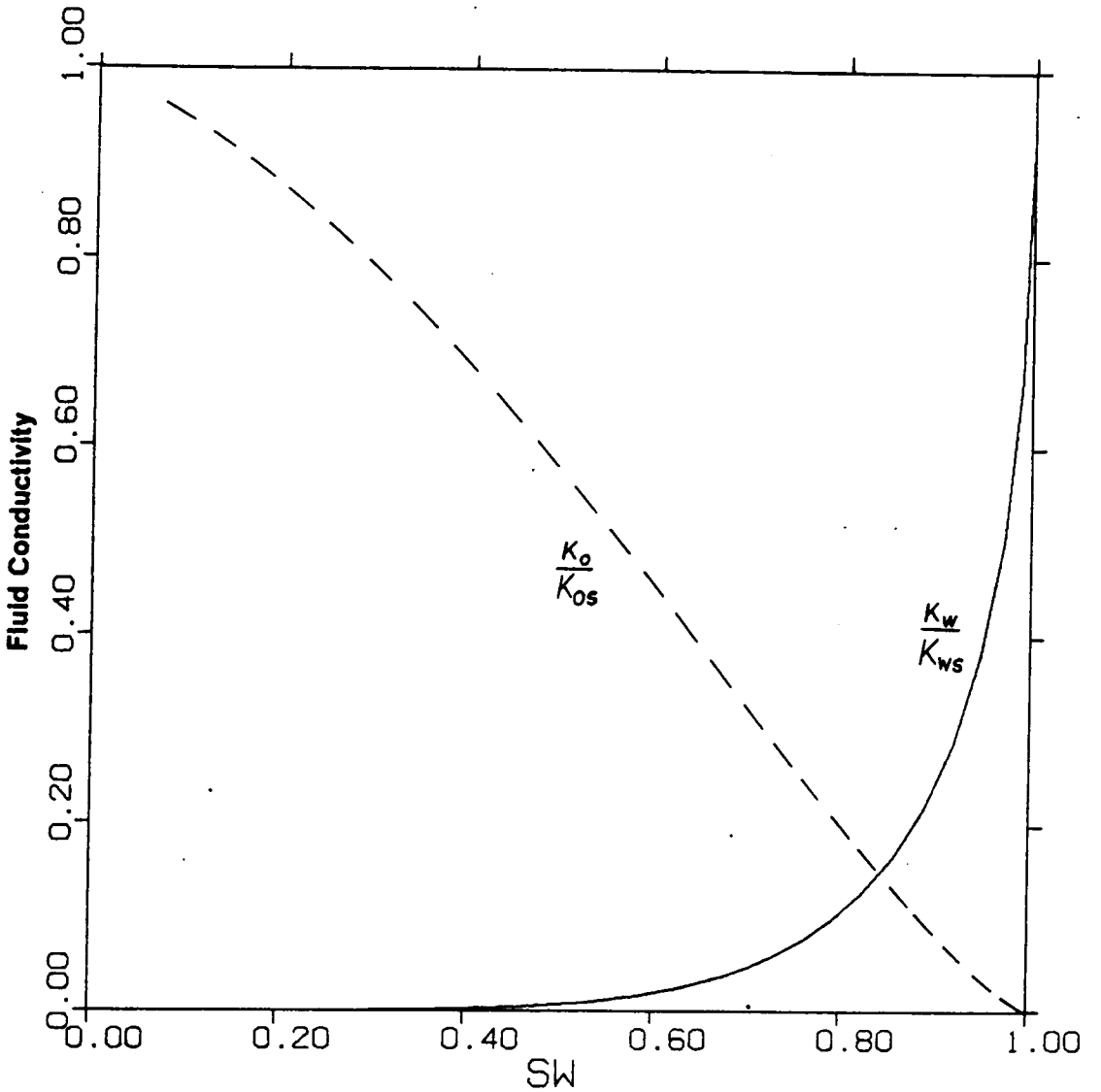

Figure 5. Variations of fluid conductivities in an oil-water system.

only those equations governing the flows of the liquid phases are derived. These liquid phases are considered as incompressible fluids.

Equation of Continuity

The equation of continuity is the mathematical expression of the principle of conservation of mass. Since the porous skeleton is assumed to be rigid and the liquid phases are considered as incompressible, the continuity equation of each liquid phase is expressed in terms of volumetric flux rather than mass flux. As commonly expressed in literature of fluid mechanics (e.g., Li and Lam 1972), the net volumetric outflow of liquid phase i from a specific domain dV during time dt is $\nabla \cdot \bar{q}_i dt dV$. The corresponding decrease in the degree of saturation of the same liquid phase is $-(\partial\theta_i/\partial t)dtdV$.

Equating the net outflow to the decrease of moisture saturation leads to the equation of continuity for the liquid phase i flowing in rigid porous media:

$$\nabla \cdot \bar{q}_i = -\frac{\partial \theta_i}{\partial t} = -\varphi \frac{\partial S_i}{\partial t} \qquad [3.1]$$

where $\bar{q}_i$ is the volumetric flux vector of liquid phase i with dimension L^3/L^2T.

Eq. 3.1 can be written in explicit form for both the one- and two-dimensional cases. For the one-dimensional case

$$\frac{\partial q_{zi}}{\partial z} = -\frac{\partial \theta_i}{\partial t} = -\varphi \frac{\partial S_i}{\partial t} \qquad [3.2]$$

and for the two-dimensional case

$$\frac{\partial q_{xi}}{\partial x} + \frac{\partial q_{yi}}{\partial y} = -\frac{\partial \theta_i}{\partial t} = -\varphi \frac{\partial S_i}{\partial t} \qquad [3.3]$$

Darcy's Law

Darcy's law plays the most important role in flow through porous media and is commonly expressed in differential form for multiphase flow as

$$\bar{q}_l = - \tilde{K}_l \nabla H_l \qquad [3.4]$$

where $\bar{q}_l$ is the volumetric flux vector, $\tilde{K}_l$ the fluid conductivity tensor, and H_l the total head, of liquid phase i. The subscript i stands for liquid phase i, not a tensor notation.

Eq. 3.4 holds as long as the fluid conductivity $\tilde{K}_l$ is independent of the total head gradient ∇H_l at a given moisture saturation. Experimental evidence indicates that this is the case for laminar flow through porous media (e.g., Calhoun 1951).

The one-dimensional form for Eq. 3.4 is

$$q_{zl} = - K_{zl} \frac{\partial H_l}{\partial z} \qquad [3.5]$$

and the two-dimensional form is

$$\begin{aligned} q_{xl} &= - (K_{xx} \frac{\partial H}{\partial x})_l + (K_{xy} \frac{\partial H}{\partial x})_l \\ q_{yl} &= - (K_{yx} \frac{\partial H}{\partial y})_l + (K_{yy} \frac{\partial H}{\partial y})_l \end{aligned} \qquad [3.6]$$

If the principal direction of tensor $\tilde{K}_l$ is chosen as the spatial directions x and y, Eq. 3.6 reduces to

$$\begin{aligned} q_{xl} &= - (K_x \frac{\partial H}{\partial x})_l \\ q_{yl} &= - (K_y \frac{\partial H}{\partial y})_l \end{aligned} \qquad [3.7]$$

Multiphase Flow Equations

The multiphase flow equation for liquid phase *i* is obtained by substituting Eq. 3.4 into Eq. 3.1 and this yields

$$\nabla \cdot (\tilde{K}_i \nabla H_i) = \frac{\partial \theta_i}{\partial t} \qquad [3.8]$$

The one-dimensional form of Eq. 3.8 becomes

$$\frac{\partial}{\partial z}(K_z \frac{\partial H}{\partial z})_i = \frac{\partial \theta_i}{\partial t} \qquad [3.9]$$

and the corresponding two-dimensional form is

$$\frac{\partial}{\partial x}(K_x \frac{\partial H}{\partial x})_i + \frac{\partial}{\partial y}(K_y \frac{\partial H}{\partial y})_i = \frac{\partial \theta_i}{\partial t} \qquad [3.10]$$

with spatial directions *x* and *y* coincident with the principal directions of the fluid conductivity tensor $\tilde{K}_i$.

In Eq. 3.8, the total head H_i and the moisture content θ_i of liquid phase *i* are the unknowns to be solved. It is convenient mathematically to express θ_i in terms of H_i for solving the flow equation.

In the following paragraphs, subscripts *i-1*, *i*, and *i+1* stand for the orders of wettability of liquid phases *i-1*, *i*, and *i+1*. Phase *i+1* has the highest wettability.

Based on the concept introduced in Figure 4, θ_i is a function of the capillary heads of phases *i-1*, *i*, and *i+1*. Again, there is no direct contact between phases *i-1* and *i+1* as long as phase *i* exists.

In immiscible flow problems *head* is more useful then *pressure* since pressure is only one component of head. Then the total, pressure, elevation, and capillary heads of each liquid phase are converted to the head of phase *n* which has the highest wettability in the multiphase

flow system. Total head H, pressure head h and capillary head h_c along with proper subscripts are

$$\begin{aligned} H_i &= h_i + z\,\rho_i/\rho_n \\ h_i &= P_i/\rho_n g \\ h_c &= h_{i-1,\,i} = h_{i-1} - h_i \end{aligned} \qquad [3.11]$$

where P_i is the pressure and ρ_i is the density, of phase i. The density of phase n is ρ_n and the acceleration of gravity is g.

Using Eq. 3.11, the right hand side of Eq. 3.8 is rewritten as

$$\frac{\partial \theta_i}{\partial t} = \frac{\partial \theta_i}{\partial h_{i-1}}\frac{\partial h_{i-1}}{\partial t} + \frac{\partial \theta_i}{\partial h_i}\frac{\partial h_i}{\partial t} + \frac{\partial \theta_i}{\partial h_{i+1}}\frac{\partial h_{i+1}}{\partial t} \qquad [3.12]$$

For z, ρ_i, and ρ_n constant in Eq. 3.11,

$$\frac{\partial H_i}{\partial t} = \frac{\partial h_i}{\partial t} \qquad [3.13]$$

Eq. 3.12 can be rewritten in terms of total heads as

$$\begin{aligned} \frac{\partial \theta_i}{\partial t} &= \frac{\partial \theta_i}{\partial h_{i-1}}\frac{\partial H_{i-1}}{\partial t} + \frac{\partial \theta_i}{\partial h_i}\frac{\partial H_i}{\partial t} + \frac{\partial \theta_i}{\partial h_{i+1}}\frac{\partial H_{i+1}}{\partial t} \\ &= C_{i,i-1}\frac{\partial H_{i-1}}{\partial t} + C_{i,i}\frac{\partial H_i}{\partial t} + C_{i,i+1}\frac{\partial H_{i+1}}{\partial t} \end{aligned} \qquad [3.14]$$

where C is called the *moisture capacity* which is the slope of the $\theta - h$ curve as those in Figure 3. A detailed description and derivation for C is given in Chapter 4 where the empirical functions of $h_c - \theta - K$ are constructed.

A final form for the flow equation is obtained by substituting $\partial\theta_i/\partial t$ as defined in Eq. 3.14 back into Eq. 3.8

$$\nabla \cdot (\tilde{K}_i \nabla H_i) = C_{i,i-1}\frac{\partial H_{i-1}}{\partial t} + C_{i,i}\frac{\partial H_i}{\partial t} + C_{i,i+1}\frac{\partial H_{i+1}}{\partial t} \qquad [3.15]$$

In practice, a typical multiphase flow problem involving air, water, and one organic immiscible liquid phase is quite common. To simplify the mathematical expressions, the air-oil-water system is used as a general example throughout the rest of this study.

Flow equations for the water and oil phases are

$$\nabla \cdot (\tilde{K}_w \nabla H_w) = \frac{\partial \theta_w}{\partial h_o}\frac{\partial H_o}{\partial t} + \frac{\partial \theta_w}{\partial h_w}\frac{\partial H_w}{\partial t} = C_{wo}\frac{\partial H_o}{\partial t} + C_{ww}\frac{\partial H_w}{\partial t}$$
$$\nabla \cdot (\tilde{K}_o \nabla H_o) = \frac{\partial \theta_o}{\partial h_o}\frac{\partial H_o}{\partial t} + \frac{\partial \theta_o}{\partial h_w}\frac{\partial H_w}{\partial t} = C_{oo}\frac{\partial H_o}{\partial t} + C_{ow}\frac{\partial H_w}{\partial t} \qquad [3.16]$$

while the air phase is assumed to be at atmospheric pressure and is not in the computation.

From the definition of the moisture capacity, C_{wo}, C_{ww}, and C_{ow} can be related to each other. As mentioned before, θ_w is a function of the capillary head h_{ow} only and thus $\theta_w(h_{ow})$ or $\theta_w(h_o - h_w)$. Therefore

$$\frac{\partial \theta_w}{\partial h_o} = -\frac{\partial \theta_w}{\partial h_w}$$

or

$$C_{wo} = -C_{ww} \qquad [3.17]$$

where h_o and h_w are independent to each other. Furthermore, based on the assumption that there is no direct contact between the air and water phases when the oil phase exists, it is clear that the total moisture content θ_t is a function of h_o only or $\partial\theta_t/\partial h_w = 0$ where $\theta_t = \theta_o + \theta_w$. Thus

$$\frac{\partial \theta_o}{\partial h_w} = \frac{\partial(\theta_t - \theta_w)}{\partial h_w} = \frac{\partial \theta_t}{\partial h_w} - \frac{\partial \theta_w}{\partial h_w} = 0 - \frac{\partial \theta_w}{\partial h_w}$$

or

$$C_{ow} = -C_{ww} \qquad [3.18]$$

Eqs. 3.17 and 3.18 reduce the moisture capacities from four to two and this simplifies the coefficient calculations in solving Eq. 3.16. Nevertheless, $\tilde{K}_w$, $\tilde{K}_o$, C_{ww}, C_{wo}, C_{ow}, and C_{oo} are functions of H_w and H_o. Thus Eq. 3.16 becomes nonlinear and coupled since both H_w and H_o appear in the derivative of time terms.

Finally, in one-dimensional form Eq. 3.16 becomes

$$\begin{aligned} \frac{\partial}{\partial z}(K_w\frac{\partial H_w}{\partial z}) &= C_{wo}\frac{\partial H_o}{\partial t} + C_{ww}\frac{\partial H_w}{\partial t} \\ \frac{\partial}{\partial z}(K_o\frac{\partial H_o}{\partial z}) &= C_{oo}\frac{\partial H_o}{\partial t} + C_{ow}\frac{\partial H_w}{\partial t} \end{aligned} \qquad [3.19]$$

and in two-dimensional form it becomes

$$\begin{aligned} \frac{\partial}{\partial x}(K_{xw}\frac{\partial H_w}{\partial x}) + \frac{\partial}{\partial y}(K_{yw}\frac{\partial H_w}{\partial y}) &= C_{wo}\frac{\partial H_o}{\partial t} + C_{ww}\frac{\partial H_w}{\partial t} \\ \frac{\partial}{\partial x}(K_{xo}\frac{\partial H_o}{\partial x}) + \frac{\partial}{\partial y}(K_{yo}\frac{\partial H_o}{\partial y}) &= C_{oo}\frac{\partial H_o}{\partial t} + C_{ow}\frac{\partial H_w}{\partial t} \end{aligned} \qquad [3.20]$$

Again, spatial directions x and y are in the principal directions of the fluid conductivity $\tilde{K}_w$ (and $\tilde{K}_o$).

Summary

The governing differential equations for an air-oil-water system are derived here. The porous media are assumed as rigid materials and the fluids are taken as incompressible. The air phase is assumed to be at constant atmospheric pressure throughout the porous domain, and it is not coupled with other fluids in the flow equations. The relationship among capillary head, degree of saturation, and fluid conductivity are briefly described. The equations of continuity and Darcy's law are combined to obtain the flow equation for each immiscible liquid phase. The flow equations are nonlinear and coupled.

CHAPTER 4

Laboratory Modelling of Immiscible Flow in Porous Media

Laboratory tests serve as the basis for developing an adequate flow model and estimating the model parameters. Static and transient tests are described, and empirical relationships among capillary head, degree of saturation, and fluid conductivity are developed from these test results. All the laboratory tests presented in this chapter were performed by R. J. Lenhard in the Soil Laboratory of the Agronomy Department at VPI&SU.

Fundamental Material Properties

The fundamental material properties involved in a multiphase immiscible flow problem are the porosity φ of the porous medium, the density ρ, and the saturated fluid conductivity K_s of each liquid phase. The soil used in this study is a laboratory processed sandy soil. The grain size distribution of the soil is given in Figure 6. The liquids used are water, benzene, and p-cymene. These materials were chosen for the experimental portion of this study since

they were readily available in the laboratory and their properties are well established. Thus they provide reliable parameters for use in the finite element programs developed as a part of this investigation. The basic properties of the soil and liquids used in the laboratory are listed in Table 2. The properties of the soil were determined in accordance with standard procedures which are widely used. One source of the standardized procedure is Lambe (1951). The pertinent properties of the liquids come from a chemistry handbook (Dean 1979).

Static Test

The static test provides important information for developing the capillary pressure function. Data obtained from static tests are the capillary pressure head and the degree of saturation of the wetting phase under the static condition. The term *head* refers to the head of water.

Figure 7 gives a sketch of the equipment setup for the static tests. Typical static test results for a three-phase flow system is shown on Figure 8. There are three sets of data in the figure and each corresponds to a pair of fluids. Each set of data is fitted by a *S* shape solid curve using van Genuchten's capillary function.

Testing Procedure

Three types of flow system were conducted, namely the air-water system, the air-oil system, and the oil-water system.

Air-Water System

A soil sample with known weight w_s and porosity φ is initially saturated with water. The soil sample and the sample container is then weighed as the total weight w_t. The air is then introduced from the top of the sample under a constant head h_1 while the water phase is

Table 2. Fundamental material properties.

Material	Porosity φ	Density ρ g/cm ^{3}
Soil	0.42	
Water		1.00
Benzene		0.88
P-cymene		0.86

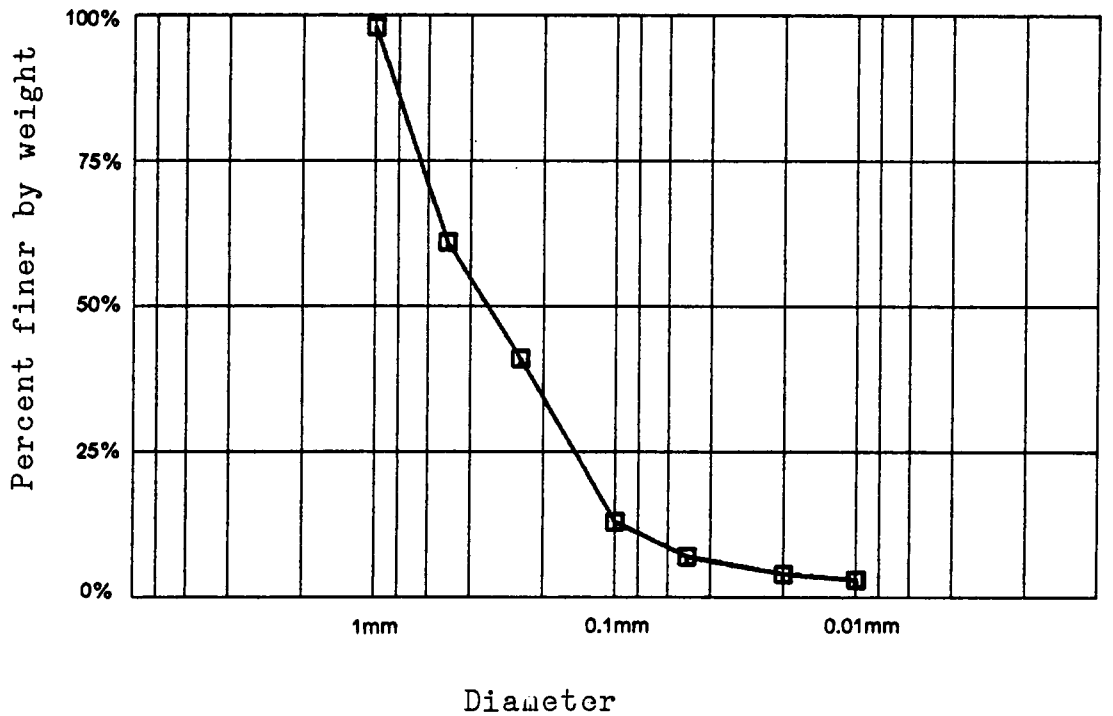

Figure 6. Grain size distribution of soil used.

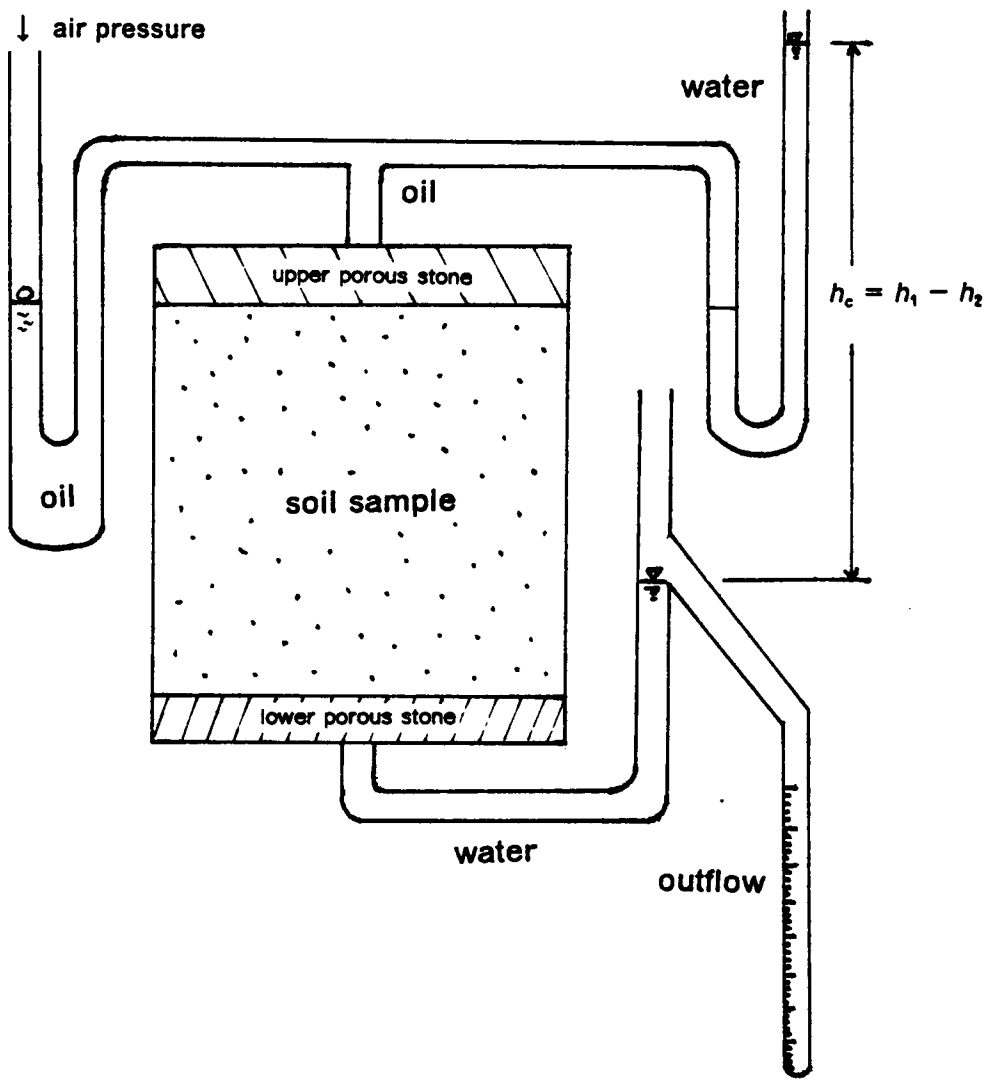

Figure 7. Equipment setup for static tests.

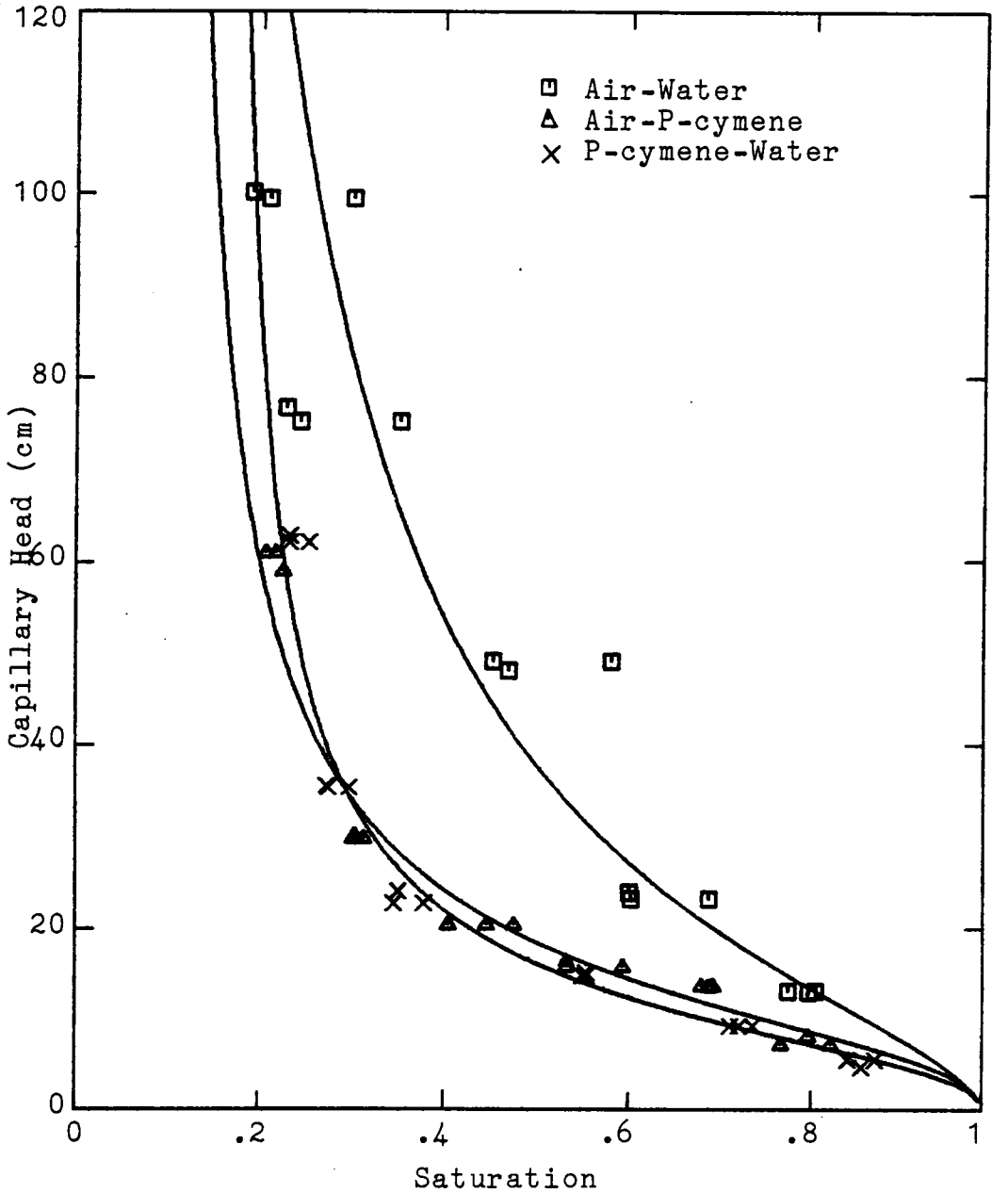

Figure 8. Typical static test results from three two-phase flow systems.

subjected to a constant head h_2 at the bottom of the sample such that the air begins to displace the water. The outflow of water is measured when the static condition is reached. It takes about 24 hours to reach static equilibrium depending on the heads applied. The soil sample is weighed again with the container. The degree of saturation of water can be calculated as

$$S_w = \frac{(w_t - w_c - w_s)}{\gamma_w V_{bulk} \varphi}$$

where w_c is the weight of the soil container and γ_w the unit weight of water. The difference in the externally applied heads $h_1 - h_2$ is taken as the capillary head h_c for the soil sample since it is small with a height of only 5.15 cm. The sample is treated as a single point in space even though it is of finite size. This combination of S and h_c provides one data point for Figure 8. The head of the air phase is then increased by one step (5 cm) and this gives another data point when a new static equilibrium condition is reached.

Air-Oil System

The fluid p-cymene is used as the wetting phase in the air-oil system test. The soil sample is initially saturated with p-cymene and pressurized air is introduced to displace the p-cymene. The testing procedure is exactly the same as in the air-water system.

Oil-Water System

In the oil-water system test, the soil sample is saturated with water as it is in the test for the air-water system. The oil (p-cymene) is then introduced from the top of the soil sample under a constant head h_1. The rest of the test is similar to the test for the air-water system. Both the inflow of the oil phase and the outflow of the water phase are measured for comparison. They should be very close to each other if the test is properly conducted. The degree of saturation of the water phase at equilibrium is calculated based upon the measured outflow, i.e., $S_{static} = (\varphi V_{bulk} - V_{outflow})/\varphi V_{bulk}$.

Effective Saturation

In Figure 8, a residual saturation S_r is observed even at very high capillary head h_c. In order to fit an empirical curve for these data, it is desirable to normalize the degree of saturation S such that it varies from 0 to 1. A term called the *effective saturation* $\bar{S}$ is defined as $(S - S_r)/(1 - S_r)$. Thus $\bar{S} = 0$ when $S = S_r$ and $\bar{S} = 1$ when $S = 1$.

By definition, the effective saturations of two-phase flow systems are

$$\bar{S}_w^{aw} = \frac{S_w - S_{rw}^{aw}}{1 - S_{rw}^{aw}}$$

$$\bar{S}_w^{ow} = \frac{S_w - S_{rw}^{ow}}{1 - S_{rw}^{ow}} \qquad [4.1]$$

$$\bar{S}_o^{ao} = \frac{S_o - S_{ro}^{ao}}{1 - S_{ro}^{ao}}$$

where each superscript stands for a flow system, e.g., *aw* means the air-water system.

In modelling the air-oil-water system, the same normalizing procedures are followed as is demonstrated in Eq. 4.1. This results in

$$\bar{S}_w = \frac{S_w - S_{rw}}{1 - S_{rw} - S_{ro}}$$

$$\bar{S}_o = \frac{S_o - S_{ro}}{1 - S_{rw} - S_{ro}} \qquad [4.2]$$

$$\bar{S}_t = \frac{S_w + S_o - S_{rw} - S_{ro}}{1 - S_{rw} - S_{ro}}$$

where superscript *aow* is omitted for simplicity. In Eq. 4.2, $S_{rw} = S_{rw}^{aw}$ if $S_o = 0$ and $S_{rw} = S_{rw}^{ow}$ when $S_o > 0$. The latter is again based on the *no direct contact* assumption. For S_{ro}, instead of fixing $S_{ro} = S_{ro}^{ao} - S_{rw}^{ow}$, it is assumed to vary linearly with S_o so that

$$S_{ro} = \frac{S_o(S_{ro}^{ao} - S_{rw}^{ow})}{1 - S_{rw}^{ow}} \qquad [4.3]$$

Based on this assumption, S_{ro} is zero when oil is first flowing into an air-water system and then it increases linearly with the oil inflow until it reaches the value $S_{ro}^{ao} - S_{rw}^{ow}$. However, for the condition of oil draining from an air-oil-water system, S_{ro} does not decrease with the decrease in S_o when $S_o > S_{ro}^{ao} - S_{rw}^{ow}$. It stays at $S_{ro}^{ao} - S_{rw}^{ow}$ until $S_o = S_{ro}^{ao} - S_{rw}^{ow}$. When S_o drops further, it is assumed that $S_{ro} = S_o$.

Capillary Head vs. Effective Saturation

By using the definition of effective saturation, the three curves of Figure 8 are replotted in Figure 9. Each curve in this figure can be modelled by an empirical mathematical function proposed by van Genuchten (1980) as

$$\bar{S} = \left[1 + (\alpha h_c)^n\right]^{-1+\frac{1}{n}} \qquad [4.4]$$

in which α and n are two parameters which are to be determined. Eq. 4.4 is basically an empirical expression for the curves in Figure 9 with two parameters α and n. Qualitatively, α and n are inversely related to the air-entry tension and the width of the pore size distribution function for a porous medium. For a given porous medium, the values of parameter n are found fairly close to each other in different two-phase flow systems. For example in Figure 9 the values of n are 1.745 for air-water, 2.339 for air-oil, and 2.335 for oil-water system. On the other hand, the values of parameter α are substantially different from each other in different fluid systems. For example in Figure 9 the values of α are 0.058 cm^{-1} for air-water, 0.088 for air-oil, and 0.109 for oil-water system. This implies that n is practically fluid-independent and α is dependent on both porous medium and fluid. It is desirable, if possible, to have parameters related either to the porous media or to the fluids only. A scaling factor β is introduced for this purpose (Parker et al. 1986) and Eq. 4.4 is modified as

$$\bar{S} = \left[1 + (\beta\alpha h_c)^n\right]^{-1+\frac{1}{n}} \qquad [4.5]$$

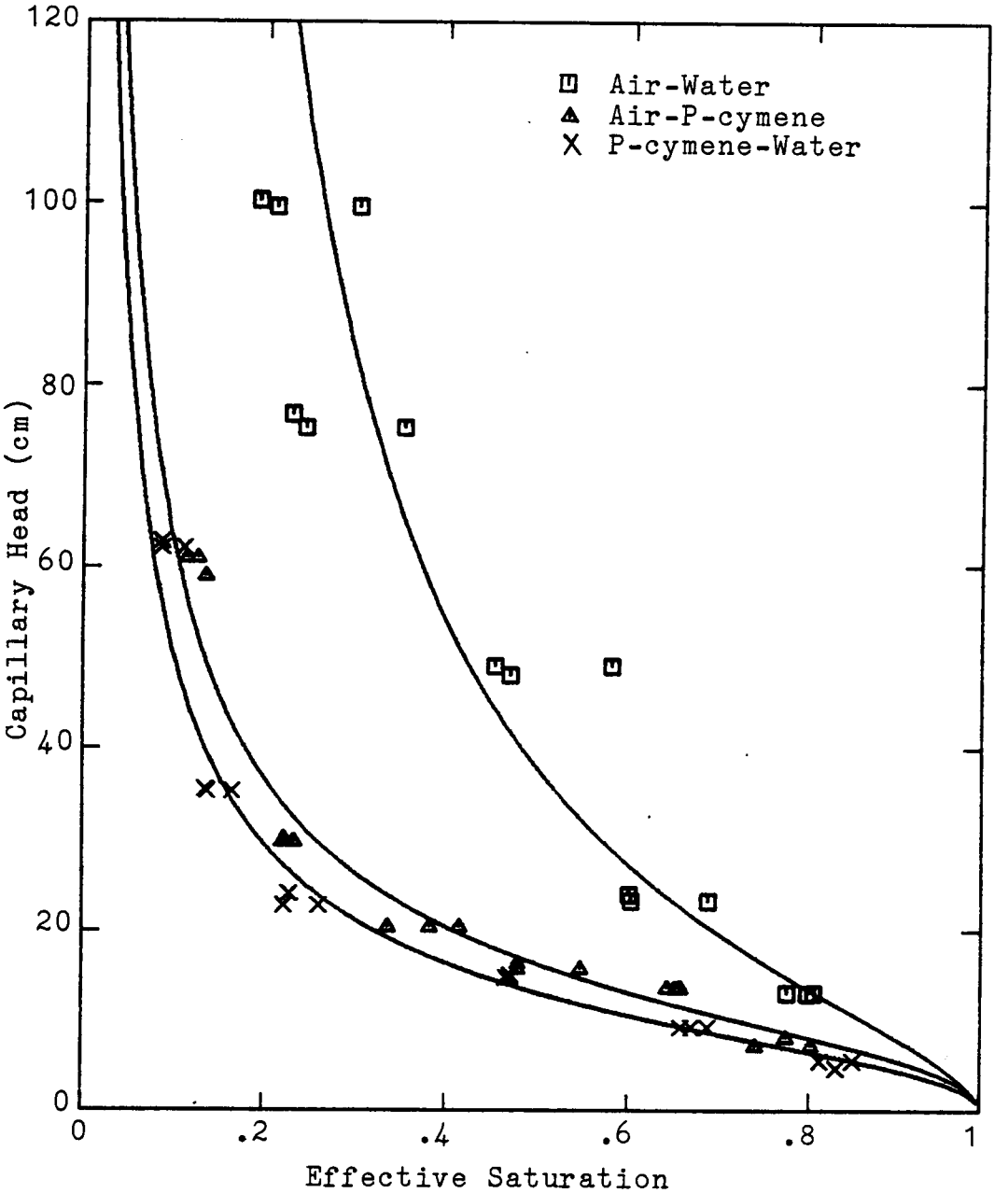

Figure 9. Capillary head vs. effective saturation.

where α and n are material parameters and β is fluid parameter. Using the Eq. 4.5 and choosing appropriate values of β, the three curves in Figure 9 can be transformed into one single curve. For this purpose, the air-water system is chosen as a reference and β_w^{aw} is set to 1. The other two curves representing the air-oil and the oil-water systems are scaled with scaling factors $\beta_o^{ao} = 1.52$ and $\beta_w^{ow} = 1.88$ and the resulting curves are shown in Figure 10. In this figure, curves for the air-oil and oil-water systems are very close to each other because these two systems have very close values of n (2.335 and 2.339). However, they are deviating from the curve for the air-water system. This is mainly due to the value of parameter n (1.744) of the system. This figure implies that parameter n is not absolutely fluid-independent. Taking all the data and using nonlinear least-squares fitting procedure a new set of parameters, α ($0.054 cm^{-1}$), n (2.03) , β_{ao} (1.72), and β_{ow} (2.14), are obtained. Figure 11 shows the final single fitting curve.

A complete expression of Eq. 4.5 can be stated. For an air-water system ($\beta_o^{aw} = 1$)

$$\bar{S}_t = \bar{S}_w = \left[1 + (\alpha h_{aw})^n\right]^{-1+\frac{1}{n}} \qquad [4.6]$$

For an air-oil system

$$\bar{S}_t = \bar{S}_o = \left[1 + (\beta_o^{ao}\alpha h_{ao})^n\right]^{-1+\frac{1}{n}} \qquad [4.7]$$

and for an air-oil-water system

$$\begin{aligned} \bar{S}_w &= \left[1 + (\beta_w^{ow}\alpha h_{ow})^n\right]^{-1+\frac{1}{n}} \\ \bar{S}_t &= \left[1 + (\beta_o^{ao}\alpha h_{ao})^n\right]^{-1+\frac{1}{n}} \\ \bar{S}_o &= \bar{S}_t - \bar{S}_w \end{aligned} \qquad [4.8]$$

Eqs. 4.6, 4.7, and 4.8 describe the relationship between capillary heads and effective saturations for any combination in an air-oil-water system.

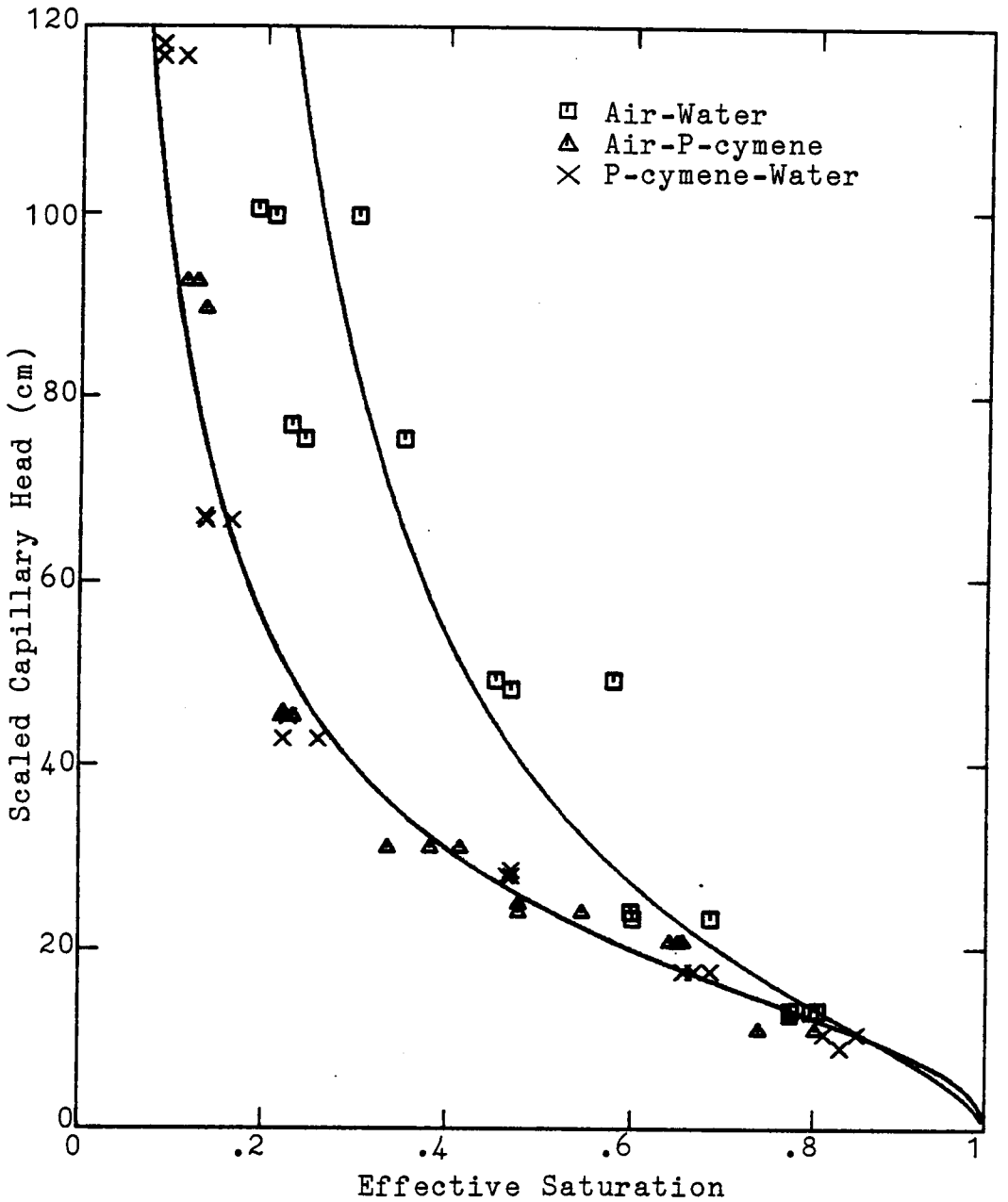

Figure 10. Scaled capillary head vs. effective saturation.

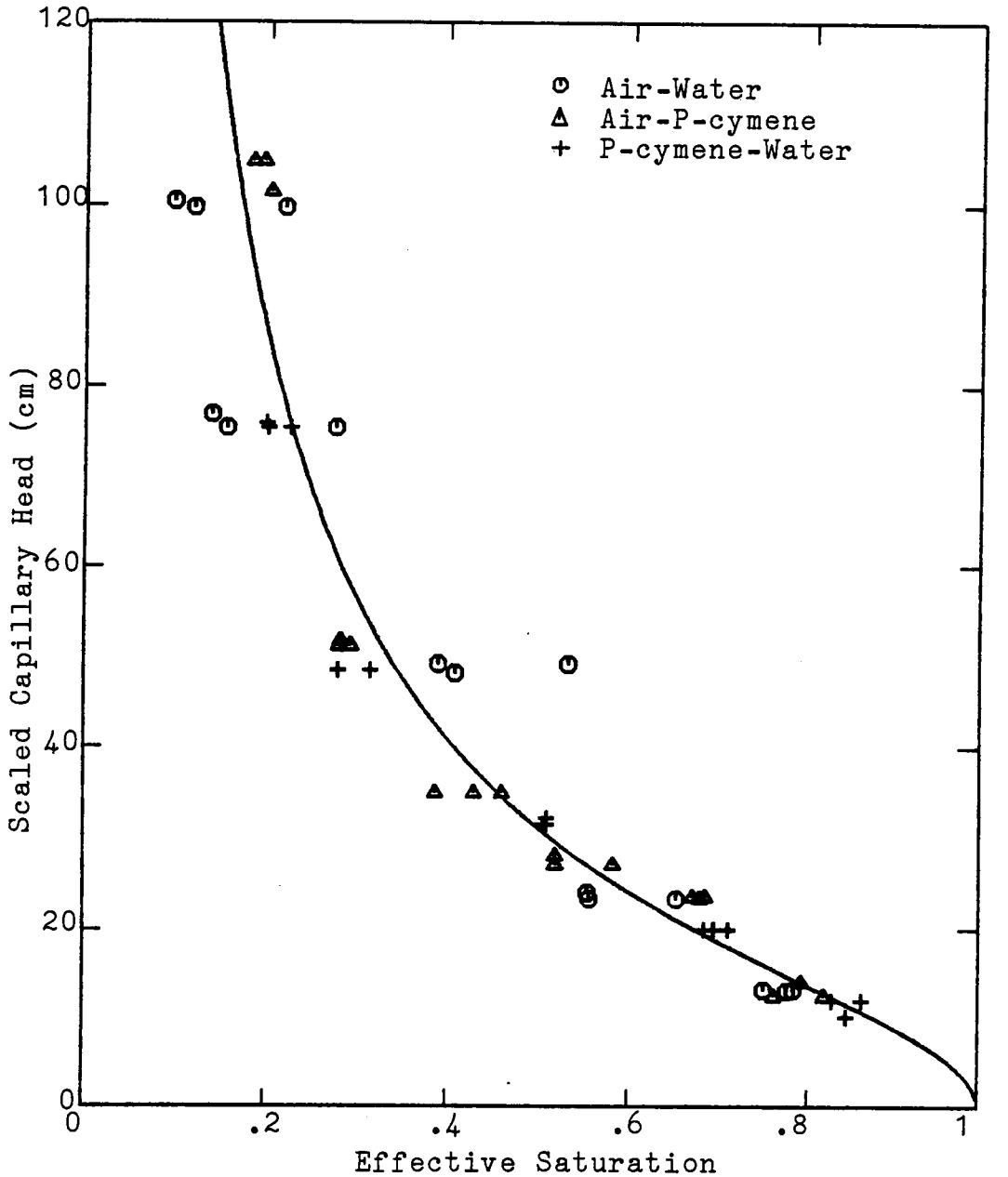

Figure 11. Final single curve for scaled capillary head and effective saturation.

Unsaturated Fluid Conductivity

By considering the pore size distribution function $f(r)$, the channel flow concept, and the tortuosity of the flow path, Mualem (1976) proposed a function to predict the unsaturated fluid conductivity as

$$K = K_s \bar{S}^n \left[\frac{\int_{R_{min}}^{R_{max}} r f(r)\, dr}{\int_{R_{min}}^{R_{max}} r f(r)\, dr} \right]^2$$

where R (or r) is the pore radius, n may be positive or negative, and $f(r)dr = d\theta$. Applying the capillary law $r \propto 1/h_c$, the final form for the fluid conductivity K is

$$K = K_s \bar{S}^{0.5} \left[\frac{\int_o^{\bar{S}} 1/h_c(\xi)\, d\xi}{\int_o^1 1/h_c(\xi)\, d\xi} \right]^2 \qquad [4.9]$$

where K_s is the saturated fluid conductivity and ξ is a dummy variable for $\bar{S}$. The power 0.5 in the term $S^{0.5}$ in the above equation was determined by examining the test data from 45 soils (Mualem 1976). Thus, this is a semi-empirical model for predicting the unsaturated fluid conductivity. Figure 12 shows the unsaturated fluid conductivity K vs. the capillary head h_c in an air-water system.

In an air-oil-water system, the water phase conductivity is

$$K_w = K_{sw} \bar{S}_w^{0.5} \left[\frac{\int_o^{\bar{S}_w} 1/h_{ow}\, d\xi_w}{\int_o^1 1/h_{ow}\, d\xi_w} \right]^2 \qquad [4.10]$$

and the oil phase conductivity

$$K_o = K_{so} \bar{S}_o^{0.5} \left[\frac{\int_{\bar{S}_w}^{\bar{S}_t} 1/h_{ao}\, d\xi_t}{\int_o^1 1/h_{ao}\, d\xi_t} \right]^2 \qquad [4.11]$$

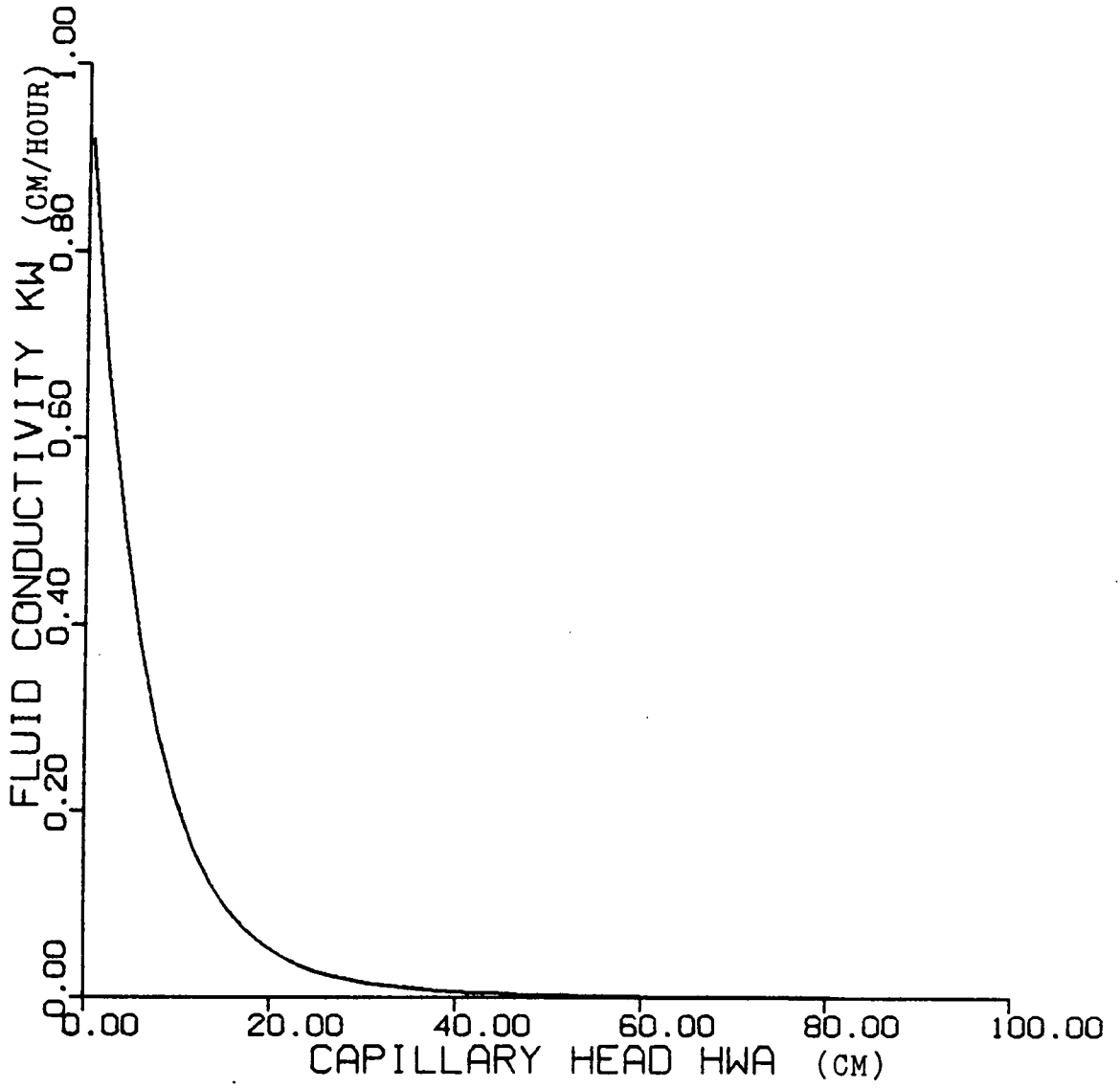

Figure 12. Unsaturated fluid conductivity vs. capillary head in an air-water system.

where ξ_w and ξ_t are the dummy variables for $\bar{S}_w$ and $\bar{S}_t$ respectively.

Since Eq. 4.9 is developed for a single liquid phase flow system, any application of this equation for a multiphase flow system must be justified. Based on the *no direct contact* assumption, Eq. 4.10 holds for an air-oil-water system. For an air-water system h_{ow} becomes h_{aw}. Eq. 4.11, however, extends the same assumption one step further and still needs more research work for justification.

From Eq. 4.8, $\bar{S}$'s can be expressed in terms of h's. Substituting $\bar{S}$'s for h's in Eqs. 4.10 and 4.11 and carrying out the integrations, the unsaturated fluid conductivities can be expressed in terms of effective saturations as

$$\begin{aligned} K_w &= K_{sw}\bar{S}_w^{0.5}\left[1-(1-\bar{S}_w^{1/m})^m\right]^2 \\ K_o &= K_{so}\bar{S}_o^{0.5}\left[(1-\bar{S}_w^{1/m})^m-(1-\bar{S}_t^{1/m})^m\right]^2 \end{aligned} \qquad [4.12]$$

where $m = 1 - 1/n$. Figure 13 shows K_w vs. $\bar{S}_w$ and Figure 14 shows K_o vs. $\bar{S}_o$ in an air-oil-water system.

Moisture Capacity

Moisture capacity is defined in Eq. 3.14 in Chapter 3. It is the derivative of the volumetric fluid content with respect to fluid pressure head. This can be found easily once the relationship between the capillary head and the effective saturation is known. For an air-oil-water system, moisture capacities are

$$C_{ww} = \frac{\partial\theta_w}{\partial h_w} = \varphi\frac{\partial S_w}{h_w} = \varphi(1 - S_{rw} - S_{ro})\frac{\partial\bar{S}_w}{\partial h_w}$$

and using Eq. 4.8,

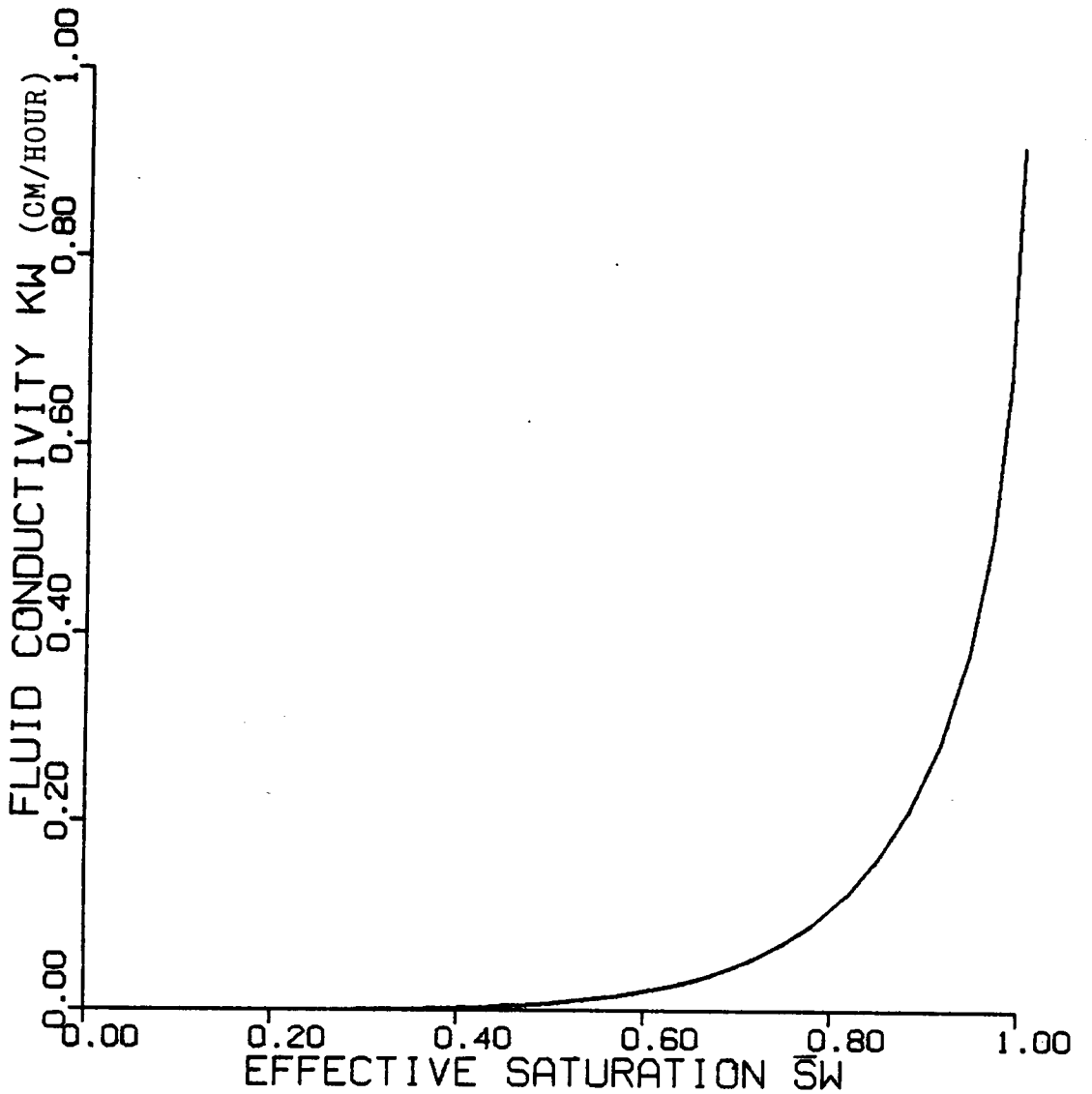

Figure 13. Fluid conductivity vs. effective saturation of water phase in an air-oil-water system.

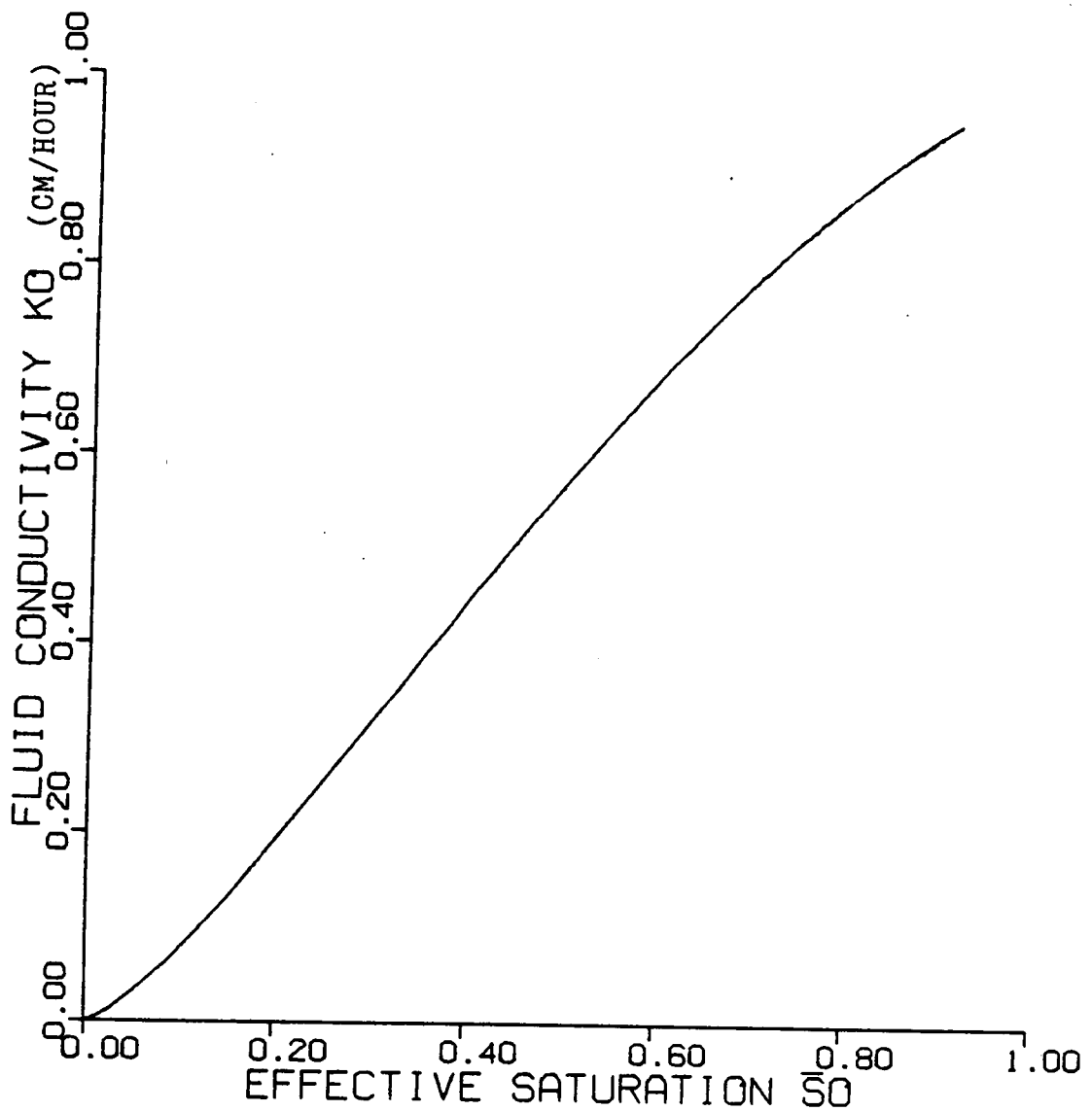

Figure 14. Fluid conductivity vs. effective saturation of oil phase in an air-oil-water system.

$$C_{ww} = \varphi(1 - S_{rw} - S_{ro})\beta_w^{ow}\alpha(n-1)\bar{S}_w^{1/m}(1 - \bar{S}_w^{1/m})^m$$

$$C_{oo} = \frac{\partial\theta_o}{\partial h_o} = \frac{\partial\theta_t}{\partial h_o} - \frac{\partial\theta_w}{\partial h_o} = \varphi\frac{\partial S_t}{\partial h_o} - C_{wo} \qquad [4.13]$$

$$= \varphi(1 - S_{rw} - S_{ro})\beta_o^{ao}\alpha(n-1)\bar{S}_t^{1/m}(1 - \bar{S}_t^{1/m})^m + C_{ww}$$

while $C_{wo} = C_{ow} = C_{oo} = 0$ if $S_o \leq S_{ro}$. Figure 15 shows the variation of C_{ww} with respect to $\bar{S}_w$.

For an air-water system, Eq. 4.13 reduces to

$$C_{ww} = \varphi(1 - S_{rw})\alpha(n-1)\bar{S}_w^{1/m}(1 - \bar{S}_w^{1/m})^m$$
$$C_{wo} = C_{ow} = C_{oo} = 0 \qquad [4.14]$$

Eq. 4.13 holds for an air-oil system with $C_{wo} = C_{ow} = -C_{ww} = 0$.

Model Parameters

Parameters α and n were introduced in Eq. 4.4. Their effects on the capillary head function are given in Figures 16 and 17. The scaling factor β was then employed in Eqs. 4.7 and 4.8. These parameters describe the relationship between capillary head and fluid saturation in a multiphase flow problem. As explained before, parameters α and n characterize the porous media while β takes care of the types of fluids. The available information on these three parameters is limited and some typical values for them are listed in Table 3.

Transient Test

The static test provides information for estimating the mathematical parameters under equilibrium conditions. Usually flow in soils is quite slow and equilibrium conditions should closely approximate the true state in the soil. However, this should be verified by transient

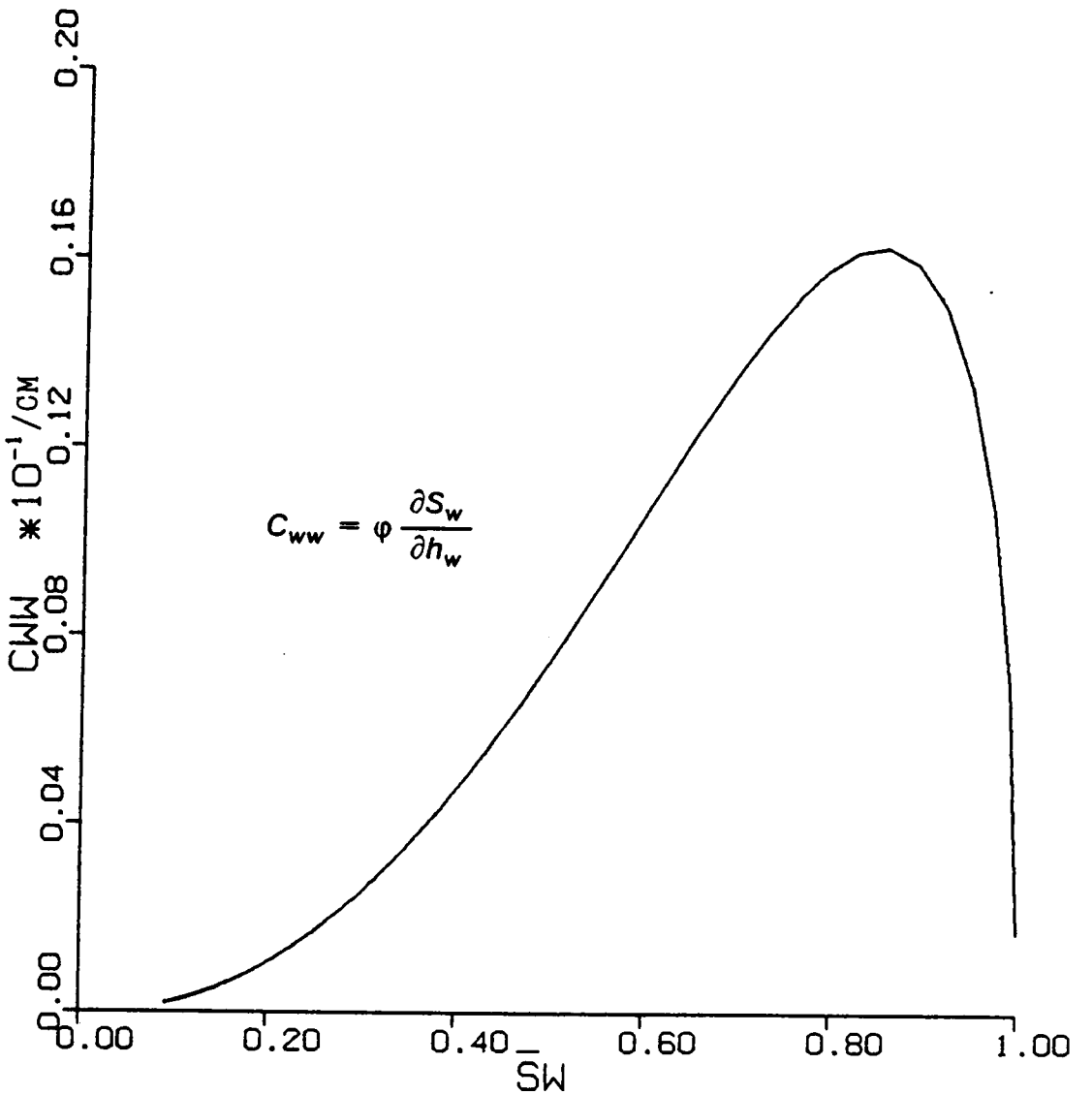

Figure 15. Moisture capacity C_{ww} vs. effective saturation $\bar{S}_w$.

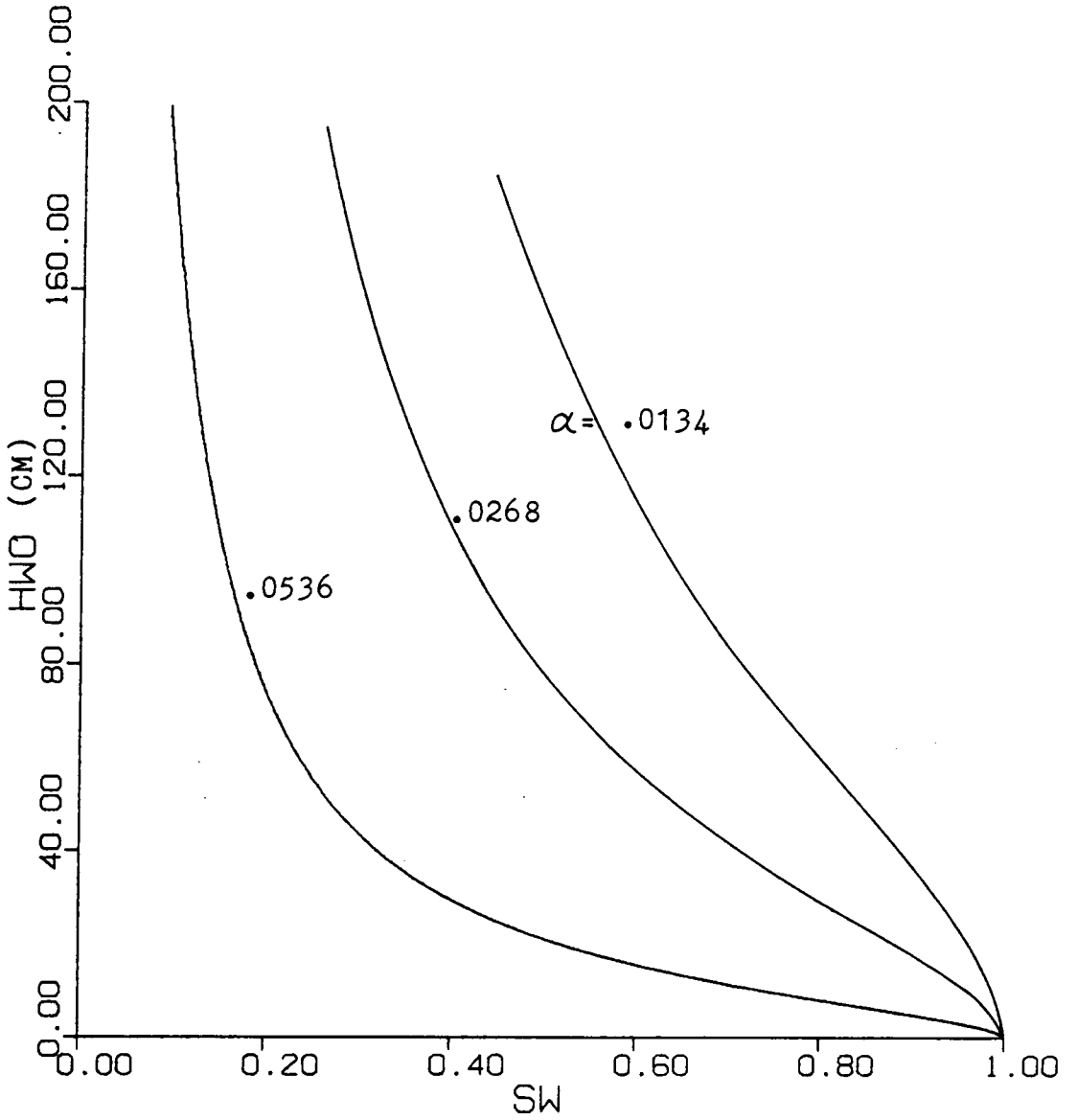

Figure 16. Effect of parameter α on the capillary head function.

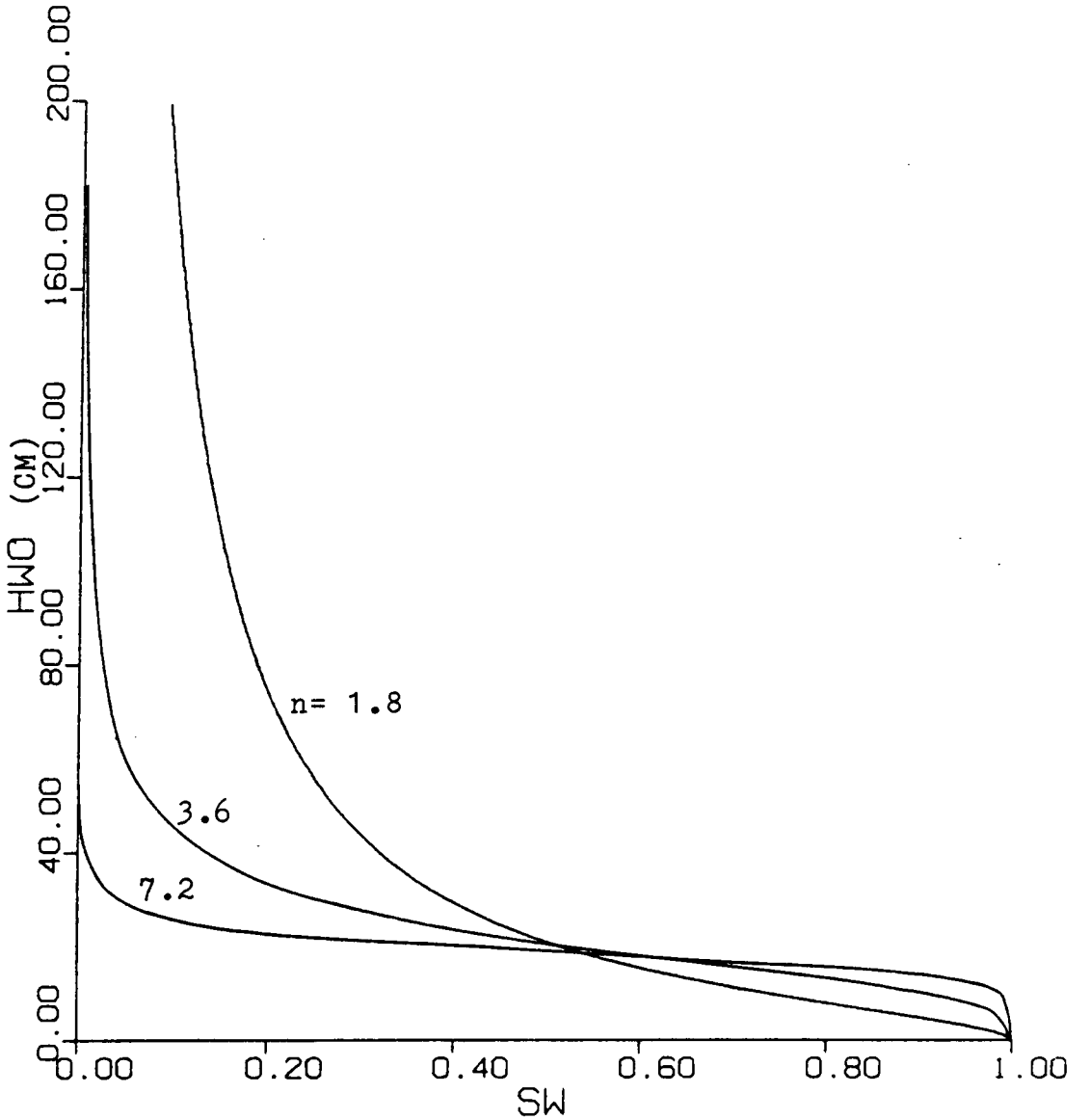

Figure 17. Effect of parameter n on the capillary head function.

Table 3. Model parameters

Soil and water	$\alpha\ (m^{-1})$	n	S_{wr}	K_{ws} (m/day)
Parker et al. (1985) :				
Sandy loam	1.53	1.265	0.208	0.06
Silt loam	3.46	1.289	0.265	1.296
Sandy clay loam	0.82	1.275	0.276	0.095
Clay	0.07	1.419	0.185	0.00019
van Genuchten (1980) :				
Hygiene sandstone	0.79	10.4	0.612	1.08
Touchet silt loam G.E.3	0.5	7.09	0.405	3.03
Silt loam G.E.3	0.423	2.06	0.331	0.05
Beit Netofa clay	0.152	1.17	0.0	0.00082

Soil and Oil	β_{ao}	β_{ow}
Lenhard and Parker (1986) : (from interfacial tension measurements)		
p-cymene -sand	1.938	2.098
benzene -sand	1.898	2.073
o-xylene -sand	2.170	2.325

flow tests. If the model, using equilibrium parameters, predicts transient behavior as verified by transient flow tests, then the equilibrium parameters are adequate.

Transient tests were conducted to verify parameter evaluation. The equipment setup for a transient test is exactly the same as that for a static test. The sample preparation and initial conditions for a transient test are also the same as in a static test. However, rather than recording only the static condition as in a static test, the outflow of the replaced wetting phase fluid in a transient test is recorded for various time intervals. Figure 18 shows a typical transient test result.

Summary

The relationship between capillary head and fluid saturation is obtained by using the laboratory static test data. An empirical function as given by van Genuchten (1980) is fitted to the laboratory data and this results in the evaluation of the model parameters α, n, and β as given in Table 3. The unsaturated fluid conductivities of the three-phase system are predicted by using a semi-empirical expression proposed by Mualem (1976). The moisture capacities are derived from the capillary head function.

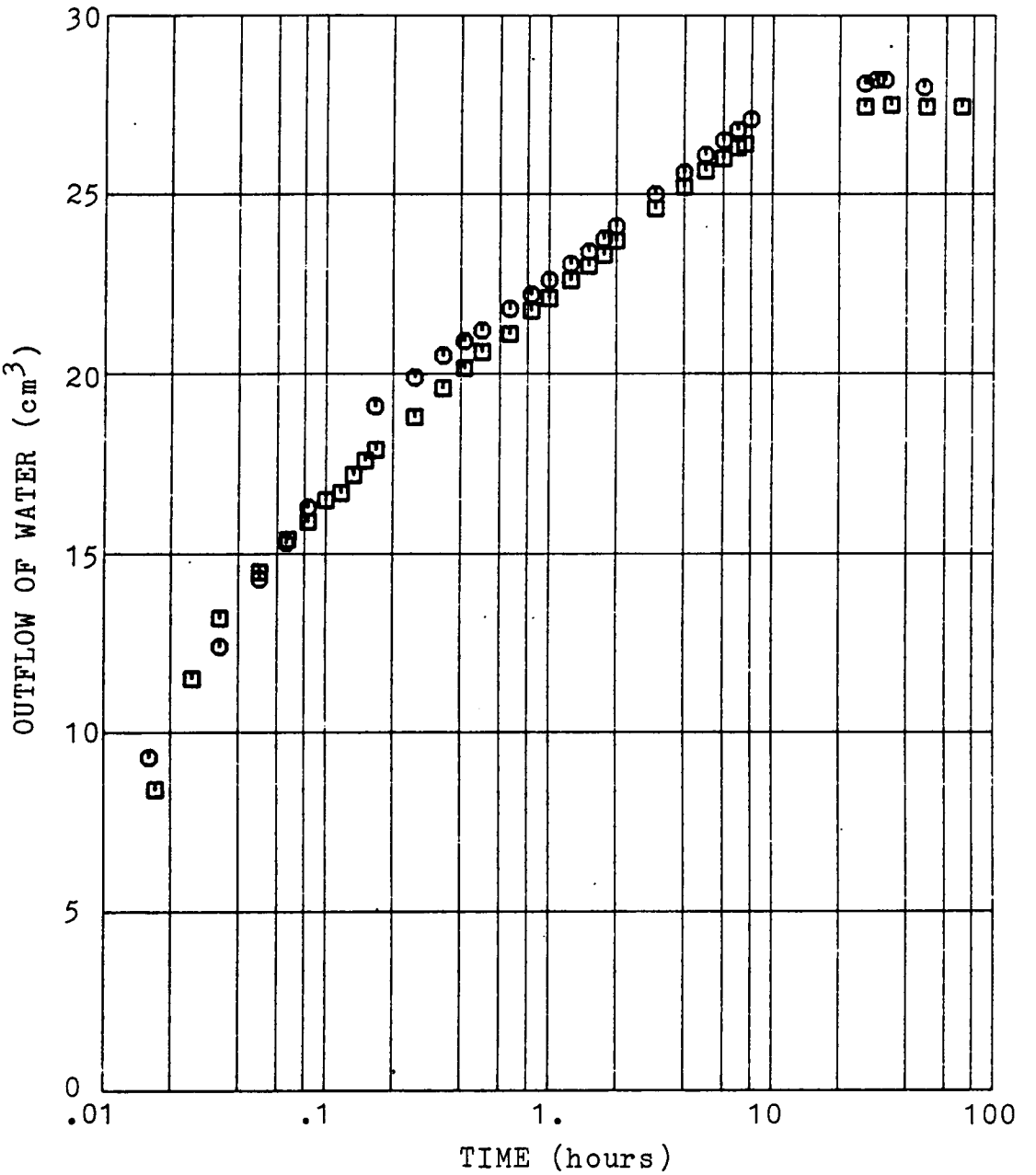

Figure 18. Transient test results on an oil-water system.

CHAPTER 5

Finite Element Formulation on Multiphase Immiscible Flow in Porous Media

The governing equations of multiphase immiscible flow in porous media are derived in Chapter 3. Since the equations are nonlinear, numerical analysis becomes the only practical way to solve them. The finite element method is one of the most common numerical methods used to solve this type of problem. These problems involve an arbitrary domain with heterogeneous and nonlinear materials. All these complexities can be elegantly handled by finite element method (Zienkiewicz 1977).

Variational Approach

Variational principle is considered to be the most important concept in analyzing a continuum problem and is widely used in finite element formulation. The first step in the

variational approach is to construct the functional. Through the variation operation on the functional, the corresponding Euler's equation precisely reproduces the governing differential equation of the problem. Thus the functional is an alternative way of describing the problem.

One-dimensional Formulation

The functionals corresponding to Eq. 3.19 in Chapter 3 are

$$\Pi_w = \int_z \frac{1}{2} K_{zw} \left(\frac{\partial H_w}{\partial z}\right)^2 dz + \int_z \left(C_{wo} H_w \frac{\partial H_o}{\partial t} + C_{ww} H_w \frac{\partial H_w}{\partial t}\right) dz - H_w \bar{q}_w \Big|_{boundary}$$
$$\Pi_o = \int_z \frac{1}{2} K_{zo} \left(\frac{\partial H_o}{\partial z}\right)^2 dz + \int_z \left(C_{oo} H_o \frac{\partial H_o}{\partial t} + C_{ow} H_o \frac{\partial H_w}{\partial t}\right) dz - H_o \bar{q}_o \Big|_{boundary} \qquad [5.1]$$

where $\bar{q}_w$ and $\bar{q}_o$ are the flux of the water and oil phases at the boundary.

By equating the variations of Π_w and Π_o to zero,

$$\delta\Pi_w = \int_z \delta H_w \left[\frac{\partial}{\partial z}\left(K_{zw} \frac{\partial H_w}{\partial z}\right) - C_{wo} \frac{\partial H_o}{\partial t} - C_{ww} \frac{\partial H_w}{\partial t}\right] dz + \delta H_w \left(K_{zw} \frac{\partial H_w}{\partial z} - \bar{q}_w\right) = 0$$
$$\delta\Pi_o = \int_z \delta H_o \left[\frac{\partial}{\partial z}\left(K_{zo} \frac{\partial H_o}{\partial z}\right) - C_{oo} \frac{\partial H_o}{\partial t} - C_{ow} \frac{\partial H_w}{\partial t}\right] dz + \delta H_o \left(K_{zo} \frac{\partial H_o}{\partial z} - \bar{q}_o\right) = 0 \qquad [5.2]$$

the Euler's equations, the terms within the brackets [ ], are found to be identical to Eq. 3.19.

The second step is to choose an approximation function for finite element analysis. A two-noded line element is used in the one-dimensional formulation. For this element,

$$H = N_i H_i = [N] \{H_n\}^T = [N_1 \;\; N_2]\{H_1 \;\; H_2\}^T$$
$$\frac{\partial H}{\partial z} = [B] \{H_n\}^T \qquad [5.3]$$

where N_i is the linear shape function, H_i the nodal variable, and $[B] = \partial[N]/\partial z$.

Substitute Eq. 5.3 into Eq. 5.1 and take the variation to obtain the equations in general matrix form as

$$[K]\{H_n\} + [K_{tw}]\{\dot{H}_n\}_w + [K_{to}]\{\dot{H}_n\}_o = \{Q\} \qquad [5.4]$$

where the dot means time derivative.

For the water phase, the terms in Eq. 5.4 are

$$\{H_n\}^T = \{H_{w1} \;\; H_{w2}\}$$
$$\{Q\}^T = \{\bar{q}_{w1} \;\; \bar{q}_{w2}\}$$
$$\{\dot{H}_n\}_w^T = \{\dot{H}_{w1} \;\; \dot{H}_{w2}\}$$
$$\{\dot{H}_n\}_o^T = \{\dot{H}_{o1} \;\; \dot{H}_{o2}\}$$

and

$$[K] = [K]_w = \int K_{zw}[B]^T[B]dz$$
$$[K_{tw}] = [K_{tw}]_w = \int C_{ww}[N]^T[N]dz \qquad [5.5]$$
$$[K_{to}] = [K_{to}]_w = \int C_{wo}[N]^T[N]dz$$

For the oil phase, the terms in Eq. 5.4 are

$$\{H_n\}^T = \{H_{o1} \;\; H_{o2}\}$$
$$\{Q\}^T = \{\bar{q}_{o1} \;\; \bar{q}_{o2}\}$$

and

$$[K] = [K]_o = \int K_{zo}[B]^T[B]dz$$
$$[K_{tw}] = [K_{tw}]_o = \int C_{ow}[N]^T[N]dz \qquad [5.6]$$
$$[K_{to}] = [K_{to}]_o = \int C_{oo}[N]^T[N]dz$$

The water phase and the oil phase can be coupled as

$$[K]\{H_n\} + [K_t]\{\dot{H}_n\} = \{Q\} \qquad [5.7]$$

where

$$\{H_n\}^T = \{H_{w1} \;\; H_{w2} \;\; H_{o1} \;\; H_{o2}\}$$
$$\{\dot{H}_n\}^T = \{\dot{H}_{w1} \;\; \dot{H}_{w2} \;\; \dot{H}_{o1} \;\; \dot{H}_{o2}\}$$
$$\{Q\}^T = \{\bar{q}_{w1} \;\; \bar{q}_{w2} \;\; \bar{q}_{o1} \;\; \bar{q}_{o2}\}$$

and

$$[K] = \begin{bmatrix} [K]_w & [0] \\ [0] & [K]_o \end{bmatrix} \qquad [K_t] = \begin{bmatrix} [K_{tw}]_w & [K_{to}]_w \\ [K_{tw}]_o & [K_{to}]_o \end{bmatrix}$$

Eq. 5.7 describes a two-degree-of-freedom continuum problem with two variables, H_w and H_o, at each node. The integrations in Eqs. 5.5 and 5.6 can be carried out directly without difficulty. The explicit form of these matrices are given in Appendix A.

Two-dimensional Formulation

The two-dimensional formulation follows a similar procedure as in the one-dimensional case. The functionals of Eq. 3.20 are

$$\Pi_w = \frac{1}{2}\int_x\int_y\left[K_{xw}\left(\frac{\partial H_w}{\partial x}\right)^2 + K_{yw}\left(\frac{\partial H_w}{\partial y}\right)^2\right]dxdy + \int_x\int_y\left(C_{wo}H_w\frac{\partial H_o}{\partial t} + C_{ww}H_w\frac{\partial H_w}{\partial t}\right)dxdy - \int_l H_w\bar{q}_w dl \qquad [5.8]$$

and

$$\Pi_o = \frac{1}{2}\int_x\int_y\left[K_{xo}\left(\frac{\partial H_o}{\partial x}\right)^2 + K_{yo}\left(\frac{\partial H_o}{\partial y}\right)^2\right]dxdy + \int_x\int_y\left(C_{oo}H_o\frac{\partial H_o}{\partial t} + C_{ow}H_o\frac{\partial H_w}{\partial t}\right)dxdy - \int_l H_o\bar{q}_o dl \qquad [5.8]$$

where the natural boundary conditions on the line l are

$$\bar{q}_w = K_{xw}\frac{\partial H_w}{\partial x}n_x + K_{yw}\frac{\partial H_w}{\partial y}n_y$$

$$\bar{q}_o = K_{xo}\frac{\partial H_o}{\partial x}n_x + K_{yo}\frac{\partial H_o}{\partial y}n_y$$

For the line l, n_x and n_y are directional cosines with $dx = n_y ds$ and $dy = n_x ds$.

A four-noded quadrilateral element and a bilinear shape function (see Appendix A) are used in this study. The variable H within a quadrilateral element is approximated as

$$H = N_i H_i = [N]\{H_n\}^T = [N_1 \;\; N_2 \;\; N_3 \;\; N_4]\{H_1 \;\; H_2 \;\; H_3 \;\; H_4\}^T \qquad [5.9]$$

where N_i is the bilinear shape function and H_i the nodal value.

Eq. 5.4 holds for the two-dimensional case. For the water phase, the terms in Eq. 5.4 are

$$\{H_n\}^T = \{H_{w1} \;\; H_{w2} \;\; H_{w3} \;\; H_{w4}\}$$

$$\{Q\}^T = \{\bar{q}_{w1} \;\; \bar{q}_{w2} \;\; \bar{q}_{w3} \;\; \bar{q}_{w4}\}$$

$$\{\dot{H}_n\}_w^T = \{\dot{H}_{w1} \;\; \dot{H}_{w2} \;\; \dot{H}_{w3} \;\; \dot{H}_{w4}\}$$

$$\{\dot{H}_n\}_o^T = \{\dot{H}_{o1} \;\; \dot{H}_{o2} \;\; \dot{H}_{o3} \;\; \dot{H}_{o4}\}$$

and

$$[K] = [K]_w = \int_x\int_y [B]^T \begin{bmatrix} K_{xw} & 0 \\ 0 & K_{yw} \end{bmatrix} [B]dxdy$$

$$[K_{tw}] = [K_{tw}]_w = \int_x\int_y C_{ww}[N]^T[N]dxdy \qquad [5.10]$$

$$[K_{to}] = [K_{to}]_w = \int_x\int_y C_{wo}[N]^T[N]dxdy$$

where $[B] = [\partial N_i/\partial x \;\; \partial N_i/\partial y]^T$ (see Appendix A).

For the oil phase, the terms in Eq. 5.4 are

$$\{H_n\}^T = \{H_{o1} \;\; H_{o2} \;\; H_{o3} \;\; H_{o4}\}$$

$$\{Q\}^T = \{\bar{q}_{o1} \;\; \bar{q}_{o2} \;\; \bar{q}_{o3} \;\; \bar{q}_{o4}\}$$

and

$$[K] = [K]_o = \int_x \int_y [B]^T \begin{bmatrix} K_{xo} & 0 \\ 0 & K_{yo} \end{bmatrix} [B] dxdy$$

$$[K_{tw}] = [K_{tw}]_o = \int_x \int_y C_{ow} [N]^T [N] dxdy \qquad [5.11]$$

$$[K_{to}] = [K_{to}]_o = \int_x \int_y C_{oo} [N]^T [N] dxdy$$

Eq. 5.7 holds for the two-dimensional case with the terms

$$\{H_n\}^T = \{H_{w1} \; H_{w2} \; H_{w3} \; H_{w4} \; H_{o1} \; H_{o2} \; H_{o3} \; H_{o4}\}$$

$$\{\dot{H}_n\}^T = \{\dot{H}_{w1} \; \dot{H}_{w2} \; \dot{H}_{w3} \; \dot{H}_{w4} \; \dot{H}_{o1} \; \dot{H}_{o2} \; \dot{H}_{o3} \; \dot{H}_{o4}\}$$

$$\{Q\}^T = \{\bar{q}_{w1} \; \bar{q}_{w2} \; \bar{q}_{w3} \; \bar{q}_{w4} \; \bar{q}_{o1} \; \bar{q}_{o2} \; \bar{q}_{o3} \; \bar{q}_{o4}\}$$

Eqs. 5.10 and 5.11 are carried out using the four-point Gaussian integration technique which is widely used in numerical analysis. The matrix form for $[K]$ and $[K_t]$ remain the same as in the one-dimensional case except that the orders of these matrices change from 4 in the one-dimensional case to 8 in the two-dimensional case.

Time Integration

The time derivative terms in a transient problem are analyzed by the finite difference method. The θ method is the most common technique used for this purpose. At time t, Eq. 5.7 is written as

$$[K_t]_t \{\dot{H}_n\}_t + [K]_t \{H_n\}_t = \{Q\}_t \qquad [5.12]$$

and at time $t + \Delta t$

$$[K_t]_{t+\Delta t} \{\dot{H}_n\}_{t+\Delta t} + [K]_{t+\Delta t} \{H_n\}_{t+\Delta t} = \{Q\}_{t+\Delta t} \qquad [5.13]$$

From Eq. 5.12, $\{\dot{H}_n\}_t$ is derived as

$$[K_t]_t \{\dot{H}_n\}_t = \{Q\}_t - [K]_t \{H_n\}_t$$

$$\{\dot{H}_n\}_t = [K_t]_t^{-1}[\{Q\}_t - [K]_t \{H_n\}_t]$$

The θ method states that

$$\{H_n\}_{t+\Delta t} = \{H_n\}_t + \theta\,\Delta t\{\dot{H}_n\}_{t+\Delta t} + (1-\theta)\Delta t\{\dot{H}_n\}_t \qquad [5.14]$$

where $0 \le \theta \le 1$ and $\{\dot{H}_n\}_{t+\Delta t}$ can then be written as

$$\{\dot{H}_n\}_{t+\Delta t} = \frac{\{H_n\}_{t+\Delta t} - \{H_n\}_t - (1-\theta)\Delta t\{\dot{H}_n\}_t}{\theta\ \Delta t} \qquad [5.15]$$

Substitute Eq. 5.15 into Eq. 5.13 and multiply both sides by θ

$$\left(\frac{[K_t]_{t+\Delta t}}{\Delta t} + \theta[K]_{t+\Delta t}\right)\{H_n\}_{t+\Delta t} = \frac{[K_t]_{t+\Delta t}}{\Delta t}\{H_n\}_t + [K_t]_{t+\Delta t}(1-\theta)\{\dot{H}_n\}_t + \theta\{Q\}_{t+\Delta t}$$

Substitute $\{\dot{H}_n\}_t$ into the above equation and rearrange terms

$$\left(\frac{[K_t]_{t+\Delta t}}{\Delta t} + \theta[K]_{t+\Delta t}\right)\{H_n\}_{t+\Delta t}$$

$$= \left(\frac{[K_t]_{t+\Delta t}}{\Delta t} - (1-\theta)[K_t]_{t+\Delta t}[K_t]_t^{-1}[K]_t\right)\{H_n\}_t + (1-\theta)[K_t]_{t+\Delta t}[K_t]_t^{-1}\{Q\}_t + \theta\{Q\}_{t+\Delta t} \qquad [5.16]$$

Eq. 5.16 is the most general expression for of the θ method on Eq. 5.7. If $[K_t]_t = [K_t]_{t+\Delta t}$, i.e., $[K_t]_{t+\Delta t}[K_t]_t^{-1} = 1$, Eq. 5.16 is simplified to

$$\left(\frac{[K_t]_{t+\Delta t}}{\Delta t} + \theta[K]_{t+\Delta t}\right)\{H_n\}_{t+\Delta t}$$

$$= \left(\frac{[K_t]_{t+\Delta t}}{\Delta t} - (1-\theta)[K]_t\right)\{H_n\}_t + (1-\theta)\{Q\}_t + \theta\{Q\}_{t+\Delta t} \qquad [5.17]$$

If $\{Q\}_t = \{Q\}_{t+\Delta t}$, Eq. 5.17 is further simplified as

$$\left(\frac{[K_t]_{t+\Delta t}}{\Delta t} + \theta[K]_{t+\Delta t}\right)\{H_n\}_{t+\Delta t} = \left(\frac{[K_t]_{t+\Delta t}}{\Delta t} - (1-\theta)[K]_t\right)\{H_n\}_t + \{Q\}_t \qquad [5.18]$$

In a transient flow problem, $[K_t]_t \neq [K_t]_{t+\Delta t}$ and $\{Q\}_t$ is not necessarily equal to $\{Q\}_{t+\Delta t}$. While θ may have any value between and including 0 and 1, taking $\theta = 1$ simplifies the numerical solution. In this study θ is taken as 1 and Eq. 5.16 becomes

$$\left(\frac{[K_t]_{t+\Delta t}}{\Delta t} + [K]_{t+\Delta t}\right)\{H_n\}_{t+\Delta t} = \frac{[K_t]_{t+\Delta t}}{\Delta t}\{H_n\}_t + \{Q\}_{t+\Delta t} \qquad [5.19]$$

Eq. 5.19 is commonly called the backward method which is unconditionally stable as far as the time step is concerned. The Crank-Nicolson method ($\theta = \frac{1}{2}$) and the Galerkin method ($\theta = \frac{2}{3}$) may give more accurate solutions than the backward method. However, they often lead to oscillatory solutions which are troublesome. The forward method ($\theta = 0$) may result in either divergent or oscillatory solutions even though the explicit numerical procedure in this method is greatly simplified.

Iteration Techniques for Nonlinearity

In Eq. 5.19, $[K_t]_{t+\Delta t}$ and $[K]_{t+\Delta t}$ are functions of $\{H_n\}_{t+\Delta t}$. Thus Eq. 5.19 is nonlinear and requires an iteration technique to handle the nonlinearity numerically. The existing iteration techniques can be separated into two categories. One is called the *direct iteration* method, e.g., the Picard method, and the other is the *tangent method*, e.g., the Newton-Raphson's method. The direct iteration method is simple in numerical operation but inefficient in convergence when compared with the tangent method.

In a multiphase immiscible flow problem, nonlinearities arise due to variations in the fluid conductivities and the moisture capacities before the equilibrium state is reached. Because of these variations, numerical convergence faces difficulties in both iteration techniques

(Huyakorn 1983). Figure 19 shows an example of divergence while using the Picard method. In this figure, H_0 is the solution of the present time step t and H^{sol} is the correct solution of the next time step $t + \Delta t$. H^i represents the solution of iteration i. Figure 20 shows an example of divergence when the Newton-Raphson method is used. In this figure, ΔH is the *improvement* of the first iteration.

The direct iteration method with some modifications is used in this study. In Eq. 5.19, the known terms are $\{H_n\}_t$, $\{Q\}_{t+\Delta t}$, and Δt. The unknown terms $[K_t]_{t+\Delta t}$ and $[K]_{t+\Delta t}$ are required in order to solve for $\{H_n\}_{t+\Delta t}$. The iteration starts from the estimated values of $[K_t]^1_{t+\Delta t}$ and $[K]^1_{t+\Delta t}$ based on $\{H_n\}_t$. The superscript 1 indicates the first iteration. After $\{H_n\}^1_{t+\Delta t}$ is solved from Eq. 5.19, $[K_t]^2_{t+\Delta t}$ and $[K]^2_{t+\Delta t}$ are calculated based on

$$\lambda\{H_n\}^1_{t+\Delta t} + (1 - \lambda)\{H_n\}_t$$

where λ is a tuning factor. $[K_t]^2_{t+\Delta t}$ and $[K]^2_{t+\Delta t}$ are then substituted into Eq. 5.19 and solve for $\{H_n\}^2_{t+\Delta t}$. The iteration continues until

$$\left|H_i^n - H_i^{n-1}\right|_{t+\Delta t} \leq \varepsilon |H_i|_t$$

is achieved as the convergence criteria where ε is some specific fraction. Figure 21 shows an example of the modified direct iteration in which $\overline{H}_1$ is the *tuned* solution of the first iteration.

Summary

The finite element formulation is developed via the variational approach. The governing equations for the water and oil phases are coupled and result in a two-degree-of-freedom problem. A two-noded line element is used for the one-dimensional case and a four-noded quadrilateral element is used in the two-dimensional case. The backward time integration

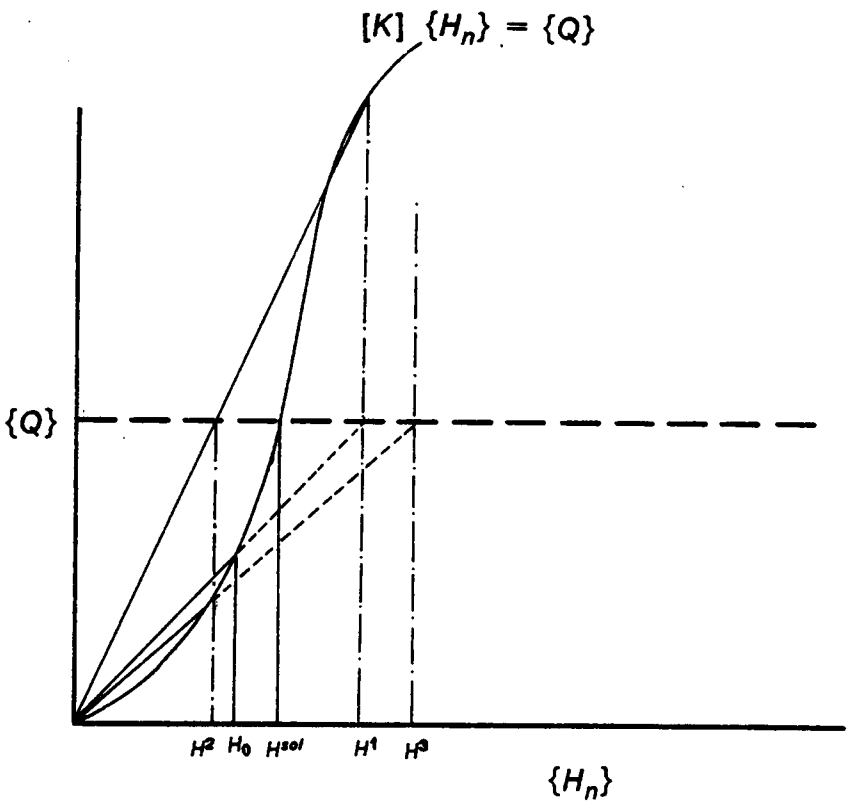

Figure 19. Example of divergence in using Picard method.

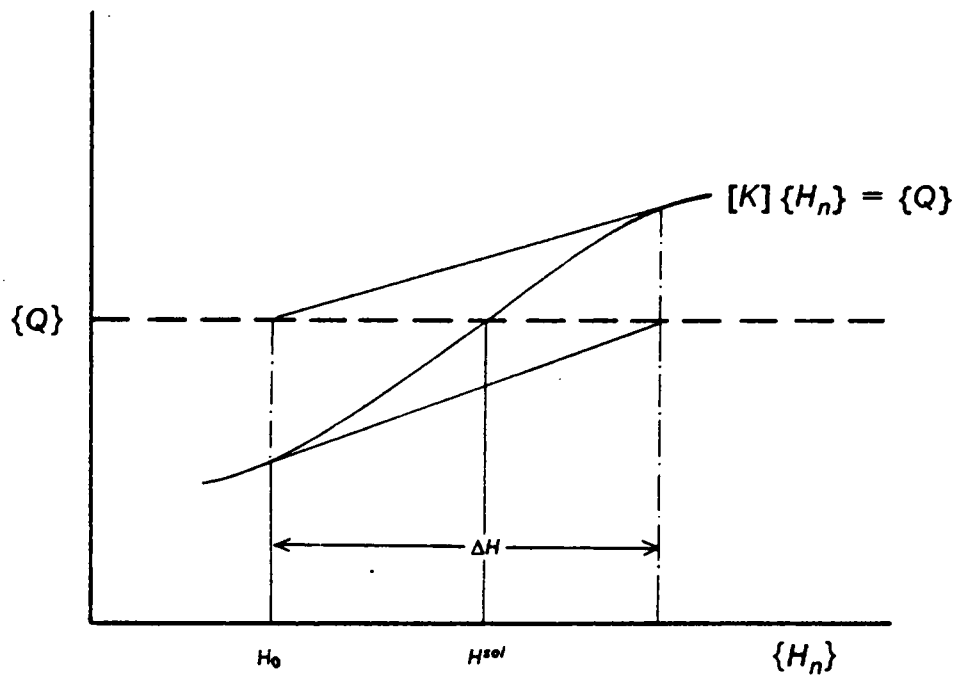

Figure 20. Example of divergence in using Newton-Raphson method.

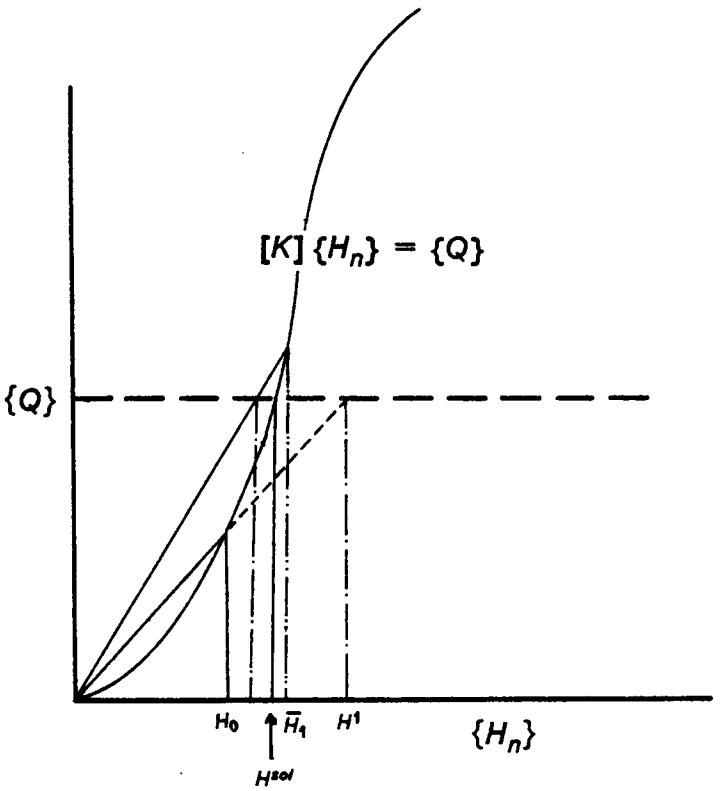

Figure 21. Example of convergence in using modified direct iteration method.

technique is incorporated in the numerical analysis along with a modified direct iteration procedure for the nonlinearities.

CHAPTER 6

Validation for Finite Element Model

Either field data or laboratory test results can be used to validate the developed finite element model for the multiphase immiscible flow problems. Unfortunately field data are seldom accessible from any project because of legal problems. This leaves laboratory test data results as the most readily accessible form of reliable verification.

Laboratory testing has the decided advantage of greater reliability as the tests are made under controlled conditions and the parameters are well determined; this provides a check on the finite element model which may be superior to a field test where unrecognized factors may have a significant influence.

Field data has its advantages. If tests are conducted in the field then the results are undoubtedly better for that particular site than a test conducted in the laboratory where some of the influences have been removed or altered. The field situation is more complex on account of the heterogeneous nature of the soil and the corresponding variability of associated properties. But for purpose of testing a mathematical model it can be successfully argued that

a numerical evaluation of the model based on controlled conditions is superior to the more complex situation.

This study uses parameters evaluated form laboratory tests for both of the reasons implied above. The tests are usually superior to field tests, and the laboratory tests are available.

The validation procedure used in this study is to estimate the parameters from the results of one kind of laboratory test. These parameters are then used in the numerical model to predict the results of the test. If the mathematical model successfully performs this operation, then it is used to predict the results of a different kind of laboratory test which utilizes the same parameters. If the finite element model successfully performs both of these tasks, then the formulation of the model is considered to be reliable.

Finite Element Programs

Two computer programs are developed to analyse three-phase immiscible problems. One is named IMF1D for the one-dimensional problem and the other is called IMF2D for the two-dimensional problem. The formulation for both of these programs is given in Chapter 5. A linear two-noded line element is used in IMF1D and a bilinear four-noded quadrilateral element is used in IMF2D. The backward time integration method and the modified direct iteration method are applied to both of these programs. Flow chart for IMF1D and IMF2D is given in Appendix B.

IMF1D vs. Laboratory Test Results

Static Test

There are three flow systems used for the static test to estimate the model parameters α, n, β_{aw}, β_{ao}, β_{ow}, S_{ro}, and S_{rw}. These flow systems are the air-water, air-benzene, and benzene-water system. The soil is the same as discussed in Chapter 4. In the air-water system, the soil sample is initially saturated with water. The air, under pressure, is then applied to the top of the soil sample. In the air-benzene system, the soil sample is initially saturated with benzene and air pressure is then applied to the top of the soil sample. In the benzene-water system, the soil sample is initially saturated with water. The benzene, under pressure, is then applied to the top of the soil sample. A detailed description of the static test is given in Chapter 4. All the test data are fitted by a single curve which is modelled by an empirical mathematical function with parameters α, n, β_{aw}, β_{ao}, β_{ow}, S_{ro}, and S_{rw}. Table 4 gives the parameters estimated from three static tests, the air-benzene, air-water, and benzene-water systems. These parameters are then used as the input data for the finite element program IMF1D.

The benzene-water flow system is then simulated by the finite element model for comparison. In Figure 22, the *S* shape curve represents the experimental results and the circles are the IMF1D predictions. The excellent match between the predicted and the measured results should not be a surprise because the comparison is made under static equilibrium conditions from which the parameters are derived. This indicates that the numerical model is performing satisfactorily, at least under static equilibrium conditions.

Table 4. Parameters from air-water, benzene-water, air-benzene systems.

Model Parameters		
$\alpha = .054$ /cm	$\beta_{ao} = 2.19$	$S_{raw} = 0.$
$n = 1.80$	$\beta_{ow} = 1.85$	$S_{rao} = 0.$
		$S_{row} = 0.$

Fundamental Material Properties		
Density of benzene	Porosity of soil	Saturated conductivity
$\rho_o = 0.88\ g/cm^3$	$\varphi = 0.42$	$K_{ws} = 23.33$ cm/hr
		$K_{os} = 44.1$ cm/hr

Subscript o stands for benzene.

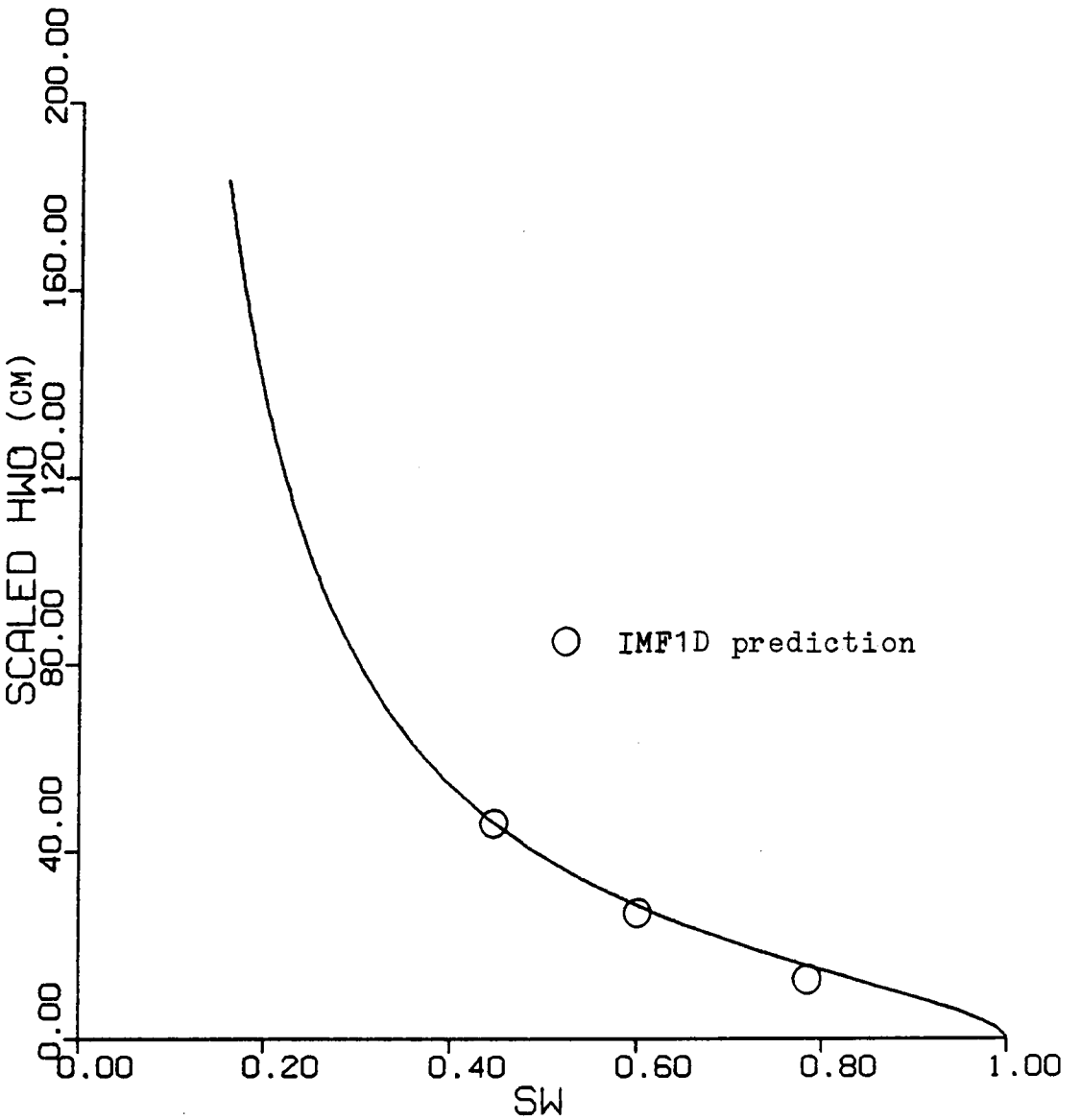

Figure 22. Static tests results and IMF1D predicted results.

Transient Test

Data on a transient test is available for the p-cymene and water system. In this transient test the p-cymene displaces the water. The transient test procedure is given in Chapter 4. Table 5 gives the parameters estimated from three static test data on the air-p-cymene, air-water, and water-p-cymene systems. These parameters are used in the finite element program IMF1D to predict the transient immiscible flow behavior.

In this transient test, the inflow of p-cymene should be equal to the outflow of water at any time instance. The calculated volumes of both the fluids at different time levels show that the mass balance is accurately met within the finite element program.

The result predicted by IMF1D and the result of the transient test are shown in Figure 23. In this figure, the horizontal axis is time in hours. The vertical axis is the outflow of water in cm^3. The transient test data are plotted in symbols and the finite element prediction is drawn as a solid line. Only a slight deviation between the tested and the predicted results is observed at the early time stages. This may be due to the induced instability when the p-cymene head is suddenly raised at the top of the soil sample and the water head is dropped simultaneously at the bottom of the soil sample. When these boundary heads are suddenly changed, the head gradient of p-cymene at the top of the soil sample and the head gradient of water at the bottom of the soil sample increase and these increases maintain at very high values for a period of time. The corresponding transient flow behavior may not be adequately modelled by using the parameters estimated under the static equilibrium conditions.

The reasonably good agreement between the predicted and the measured results shows that the parameters estimated from the static tests work quite well for the transient flow analysis. Both the mass balance calculated by the IMF1D program and the plotted results clearly validate the finite element formulation and show that the numerical model does follow the immiscible flow behavior.

Table 5. Parameters from air-water, p-cymene-water, and air-p-cymene systems.

Model Parameters		
α = .054 /cm	β_{ao} = 1.89	S_{raw} = 0.
n = 1.82	β_{ow} = 2.12	S_{rao} = 0.
		S_{row} = 0.

Fundamental Material Properties		
Denstiy of p-cymene	Porosity of soil	Saturated conductivity
ρ_o = 0.86 g/cm^3	φ = 0.42	K_{ws} = 23.33 cm/hr
		K_{os} = 41.4 cm/hr

Subscript o stands for p-cymene.

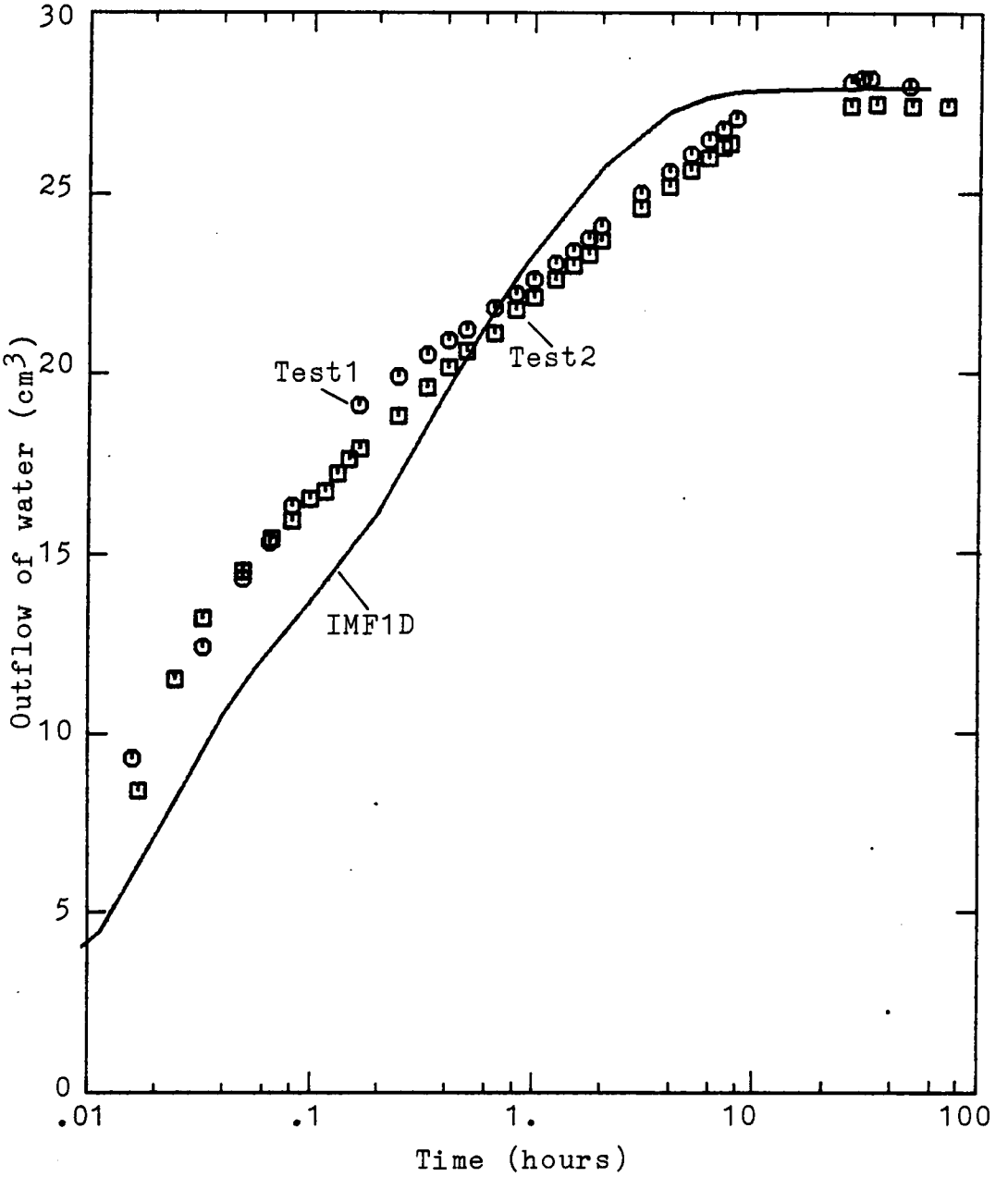

Figure 23. Transient test data and IMF1D prediction.

IMF2D Validation

The two-dimensional computer program IMF2D is used to simulate the one-dimensional transient test for validation purpose. This is done by using a column of two-dimensional rectangular elements with a uniform width of 5 cm. The thickness of the element is calculated such that the cross-sectional area of the element is the same as the soil sample. The material parameters and the initial condition used in IMF2D are the same as those used in IMF1D. The boundary conditions used in IMF2D are shown in Figure 24.

Figure 25 shows an excellent match between the IMF2D and IMF1D results for the same transient test simulation mentioned in the previous section. To further test the IMF2D program, the same finite element mesh is used with randomly assigned nodal numbers. Identical results are obtained. This validates the two-dimensional finite element program IMF2D.

Seepage

Two-dimensional transient test data and field data on three-phase immiscible flow are not available for comparison. In order to further validate the two-dimensional finite element program IMF2D, an example of seepage through an earth dam is analysed here. This is a case of unsaturated single-phase flow where water is the only flowing phase. The air phase is assumed to be atmospheric throughout the earth dam.

For this example, a homogeneous isotropic earth dam is taken as 40 m wide and 10 m high with a 2:3 upstream slope and a 1:2 downstream slope as shown in Figure 26. The base of the earth dam is assumed impervious. The material parameters of this example are given in Table 6.

The initial water table is assumed at the base of the dam. Suddenly the level of water on the upstream face is raised to 8 m above the base line while the downstream water table

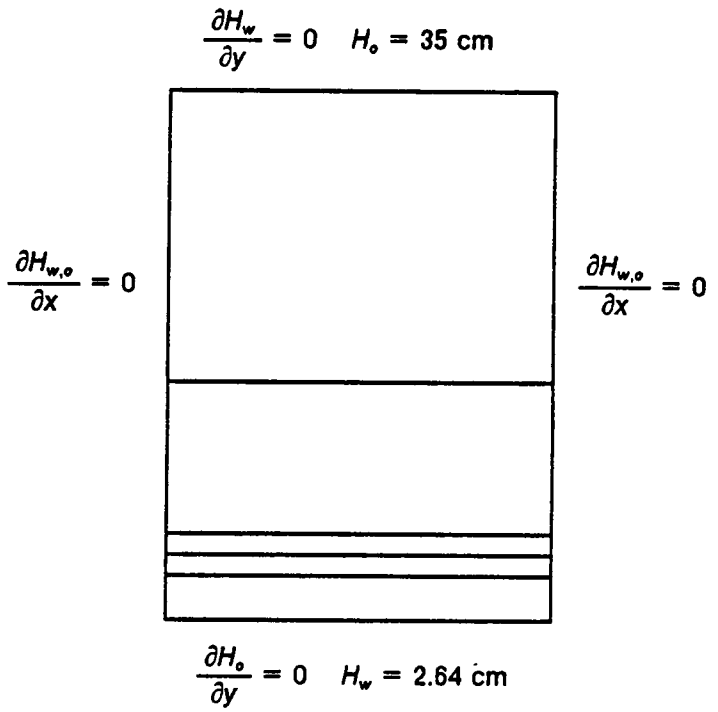

Figure 24. Boundary conditions of the soil column used in IMF2D.

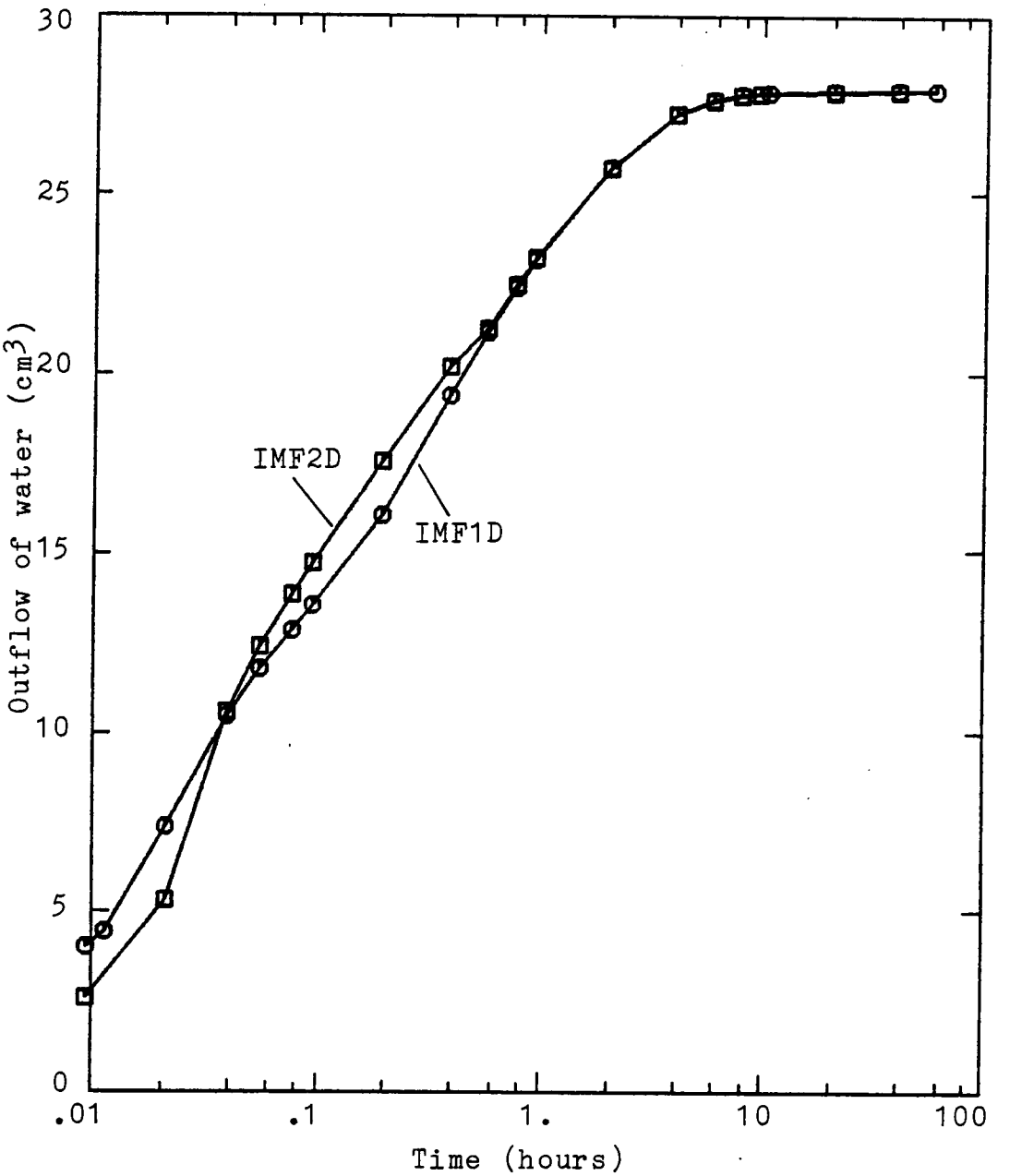

Figure 25. Predictions from IMF1D and IMF2D.

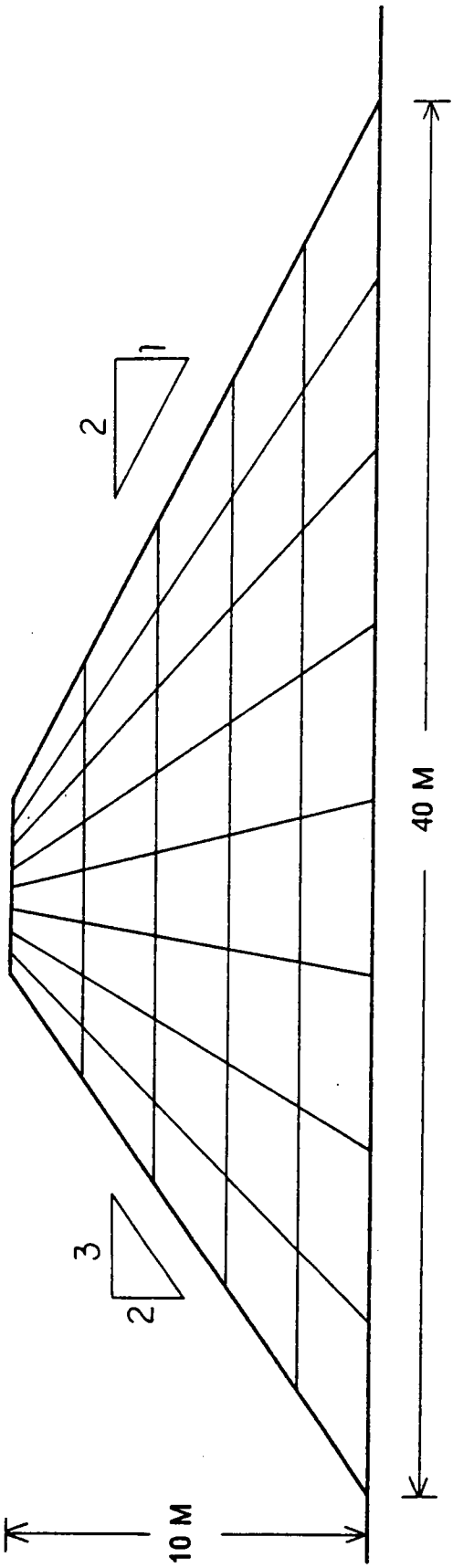

Figure 26. Finite element mesh of a homogeneous earth dam.

Table 6. Parameters used in the earth dam example.

Model Parameters		
$\alpha = 5$ /m	$\beta_{ao} = 2.0$	$S_{raw} = 0.$
$n = 1.84$	$\beta_{ow} = 2.2$	$S_{rao} = 0.$
		$S_{row} = 0.$

Fundamental Material Properties		
Density of oil	Porosity of soil	Saturated conductivity
$\rho_o = 0.8\ g/cm^3$	$\varphi = 0.3$	$K_{ws} = 0.05$ m/day
		$K_{os} = 0.005$ m/day

is kept at the baseline level. Figure 26 shows the finite element mesh consisting of 40 elements and 54 nodes. The initial time step Δt is taken as 20 days. The program IMF2D is used to analyse the problem. The oil head at each node is set equal to a constant negative value (-100 m) such that the oil content is zero and the oil phase is not significantly involved in the computation. Figure 27 shows the computed transient phreatic line at 24 days, 218 days, and at the final steady state condition (3124 days). The Casagrande's graphic solution (Harr 1962) is shown in dashed line for comparison. The computed steady state phreatic line deviates only slightly from the Casagrande's graphic construction. The computed length of the discharge surface is slightly longer than that of the Casagrande's solution. This example once again validates the finite element model.

Discussion

Factors such as the time step, the iteration technique, the initial condition, and moisture capacity terms, affect the performance of the numerical model. The effects of these factors are very difficult to evaluate in a general fashion on account of the complex nonlinearity involved.

Time Step

Since the backward method is used in the time integration, the time step Δt affects only the accuracy but not the stability of the numerical performance. However, the solution may become less accurate if the time step Δt is too large, especially in the early time stages. A rule-of-thumb on choosing a proper time step Δt is to set $\Delta t = L/K_s$ where L is the minimum length of the finite elements. Figure 28 shows the results of IMF1D using different time steps to simulate the transient test. It is observed that using large time steps yields a correct result after one cycle on a logarithmic time scale. Thus an initial time step $\Delta t = \frac{T}{10}$ is suggested

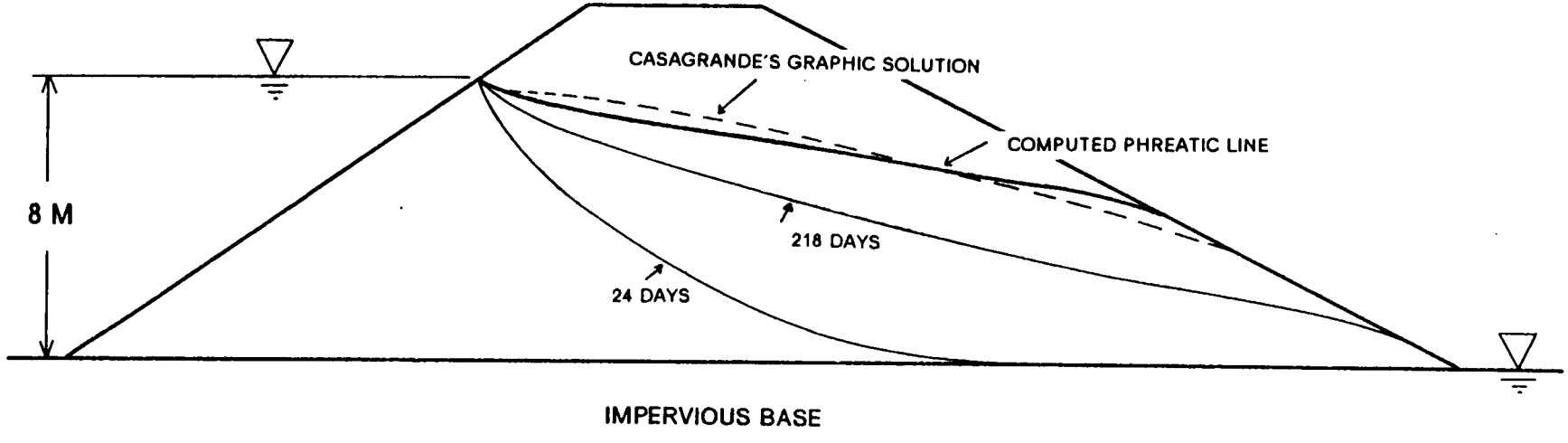

Figure 27. Computed phreatic line and Casagrande's graphic solution.

if only the results after time level T are of interest. This saves much computing time when long term behavior is desired. In IMF1D and IMF2D, the time step Δt is increased by an arbitrary factor DTT for each time step, i.e., $\Delta t_{i+1} = \Delta t_i \times DTT$. The value of DTT is usually set between 1 and 1.5 in this study.

Iteration Technique

As mentioned in Chapter 5, a modified direct iteration method is applied to handle the nonlinearities. A solution can be obtained by carefully choosing the tuning factor λ and the factor of convergence criterion ε. In general, using $0.3 \leq \lambda \leq 0.7$ and $\varepsilon \leq 0.05$, not more than 10 iterations are sufficient for obtaining a reasonable solution. Table 7 lists some results using different λ values and the resulting required number of iteration for convergence for the transient test simulation. It is noted that an acceptable result is obtained even though some nodal unknowns are not converged during the early time stages.

Initial Condition

It is noticed that the initial condition of each fluid phase affects the convergence especially during the early time stages. Table 8 lists some results of different initial conditions and the required number of iterations for convergence on a hypothetical transient flow problem. This hypothetical problem is similar to the laboratory transient test except that the initial condition is different. A reasonable assumption on the initial condition is that each fluid phase is under equilibrium conditions, i.e., initially there is either no flow or only steady-state flow. For a problem with initial conditions satisfying the above assumption, stability is well maintained in the early time stages.

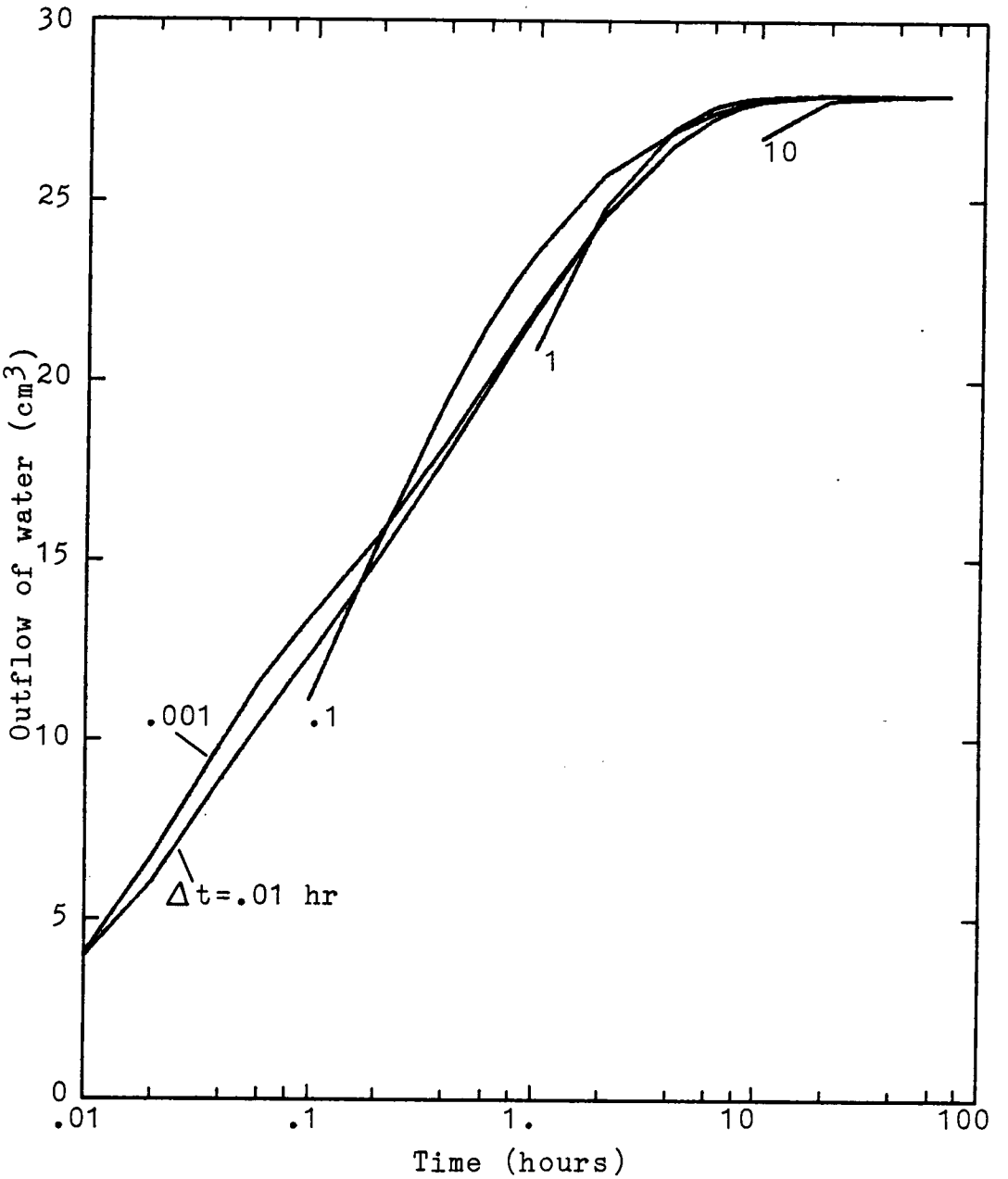

Figure 28. Effect of time step Δt .

Table 7. Tuning factor and required number of iterations.

Tuning factor λ	Number of iteration to converge	Time (hour) Δt = .01
.3	15	.01
	22	.02
	23	.03
	11	.05
	6	.09
	4	.11
.5	14	.01
	8	.02
	7	.03
	6	.05
	3	.09
	2	.11
.7	10	.01
	11	.02
	7	.03
	5	.05
	3	.09
	2	.11

Table 8. Initial condition and required number of iterations.

Initial condition	Number of iteration to converge	Time (hour) Δt = .01
Constant	14	.01
	8	.02
	7	.03
	6	.05
	3	.09
	2	.11
Linear	14	.01
	8	.02
	6	.03
	6	.05
	3	.09
	2	.11
Random	16	.01
	6	.02
	9	.03
	7	.05
	4	.09
	2	.11

Effect of Parameters α and n

There are mainly two basic parameters α and *n* involved in the constitutive model. To study the effect of these two parameters, the same transient test discussed before is analysed by changing α and *n*. Figures 29 and 30 show the effects of variations in α and *n* by ± 10% respectively. The parameter *n* shows a larger effect than does α. This can be justified by examining Eq. 4.6 or Eq. 4.8

$$\bar{S}_w = \left[1 + (\beta_{ow}\alpha h_{ow})^n\right]^{-1+\frac{1}{n}} \qquad [4.8]$$

in which the parameter *n* appears as a power. The scaling factor β and the parameter α appear along with the capillary head h_{ow} within the parentheses in the above equation. They should have the same effect.

Effect of Number of Elements

To evaluate the effect of spatial discretization on the accuracy of the numerical results, transient test simulations are carried out using 5-, 8-, 11-, and 17-element meshes. The initial time step Δt is 0.001 hr with the increasing factor DTT 1.1. Figure 31 shows a significant difference between simulations for 5-element and 11-element meshes but very little difference between 11- and 17-element solutions. It is concluded that the 11-element mesh is optimum for this specific transient test simulation.

Summary

The finite element program IMF1D is validated by comparing the computed results with both static and transient test data. The two-dimensional program IMF2D is verified by com-

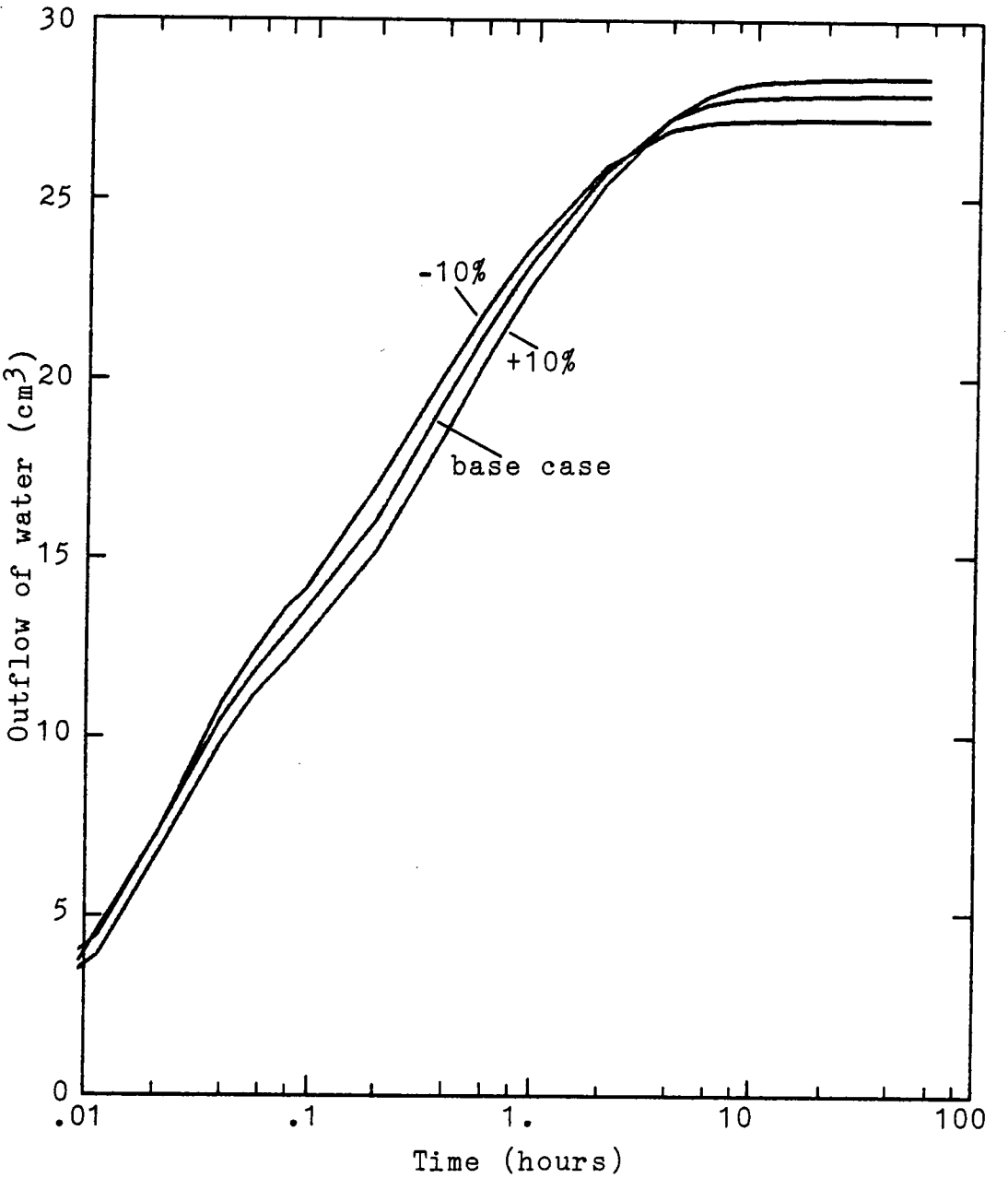

Figure 29. Effect of parameter α.

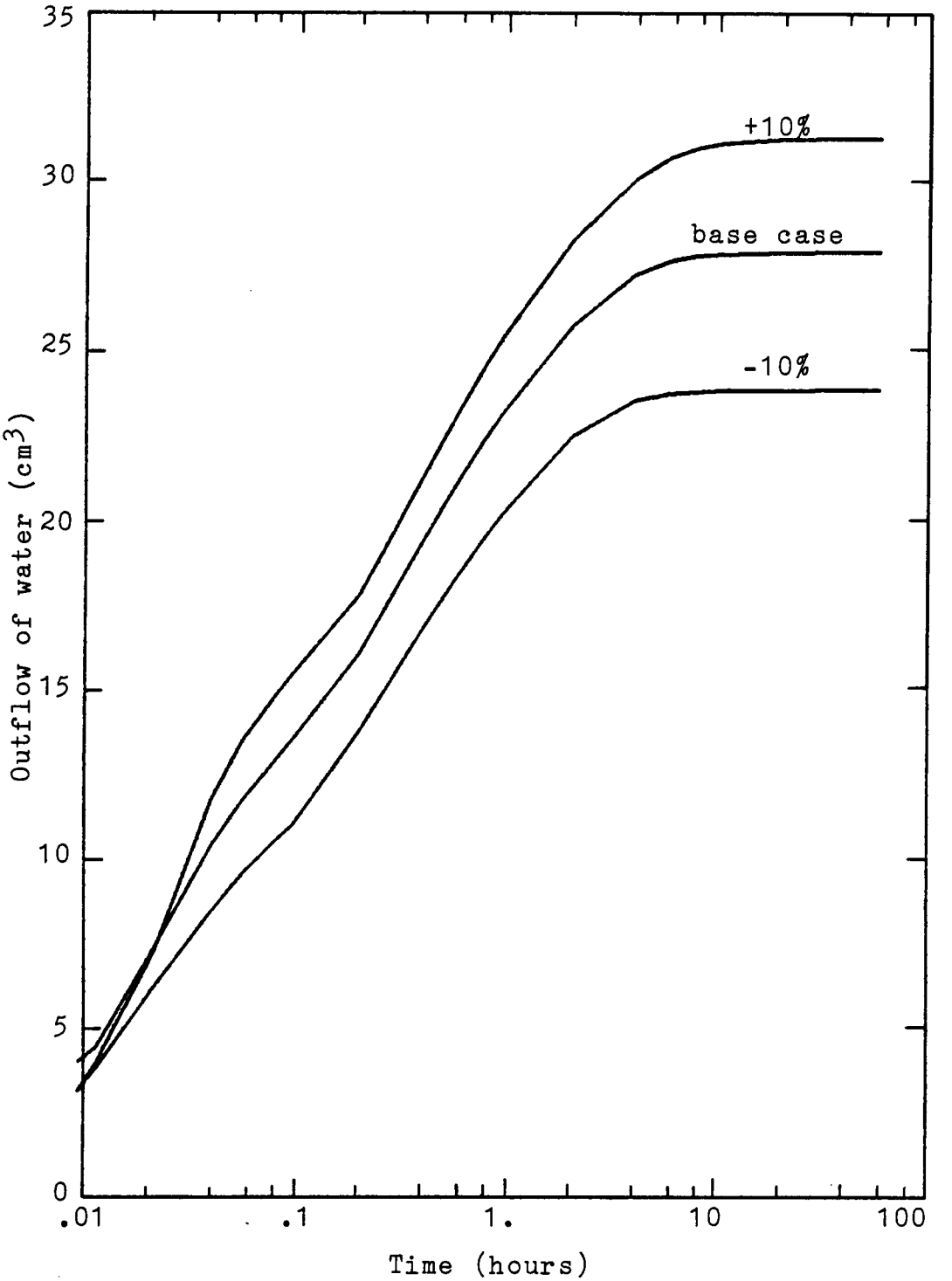

Figure 30. Effect of parameter *n* .

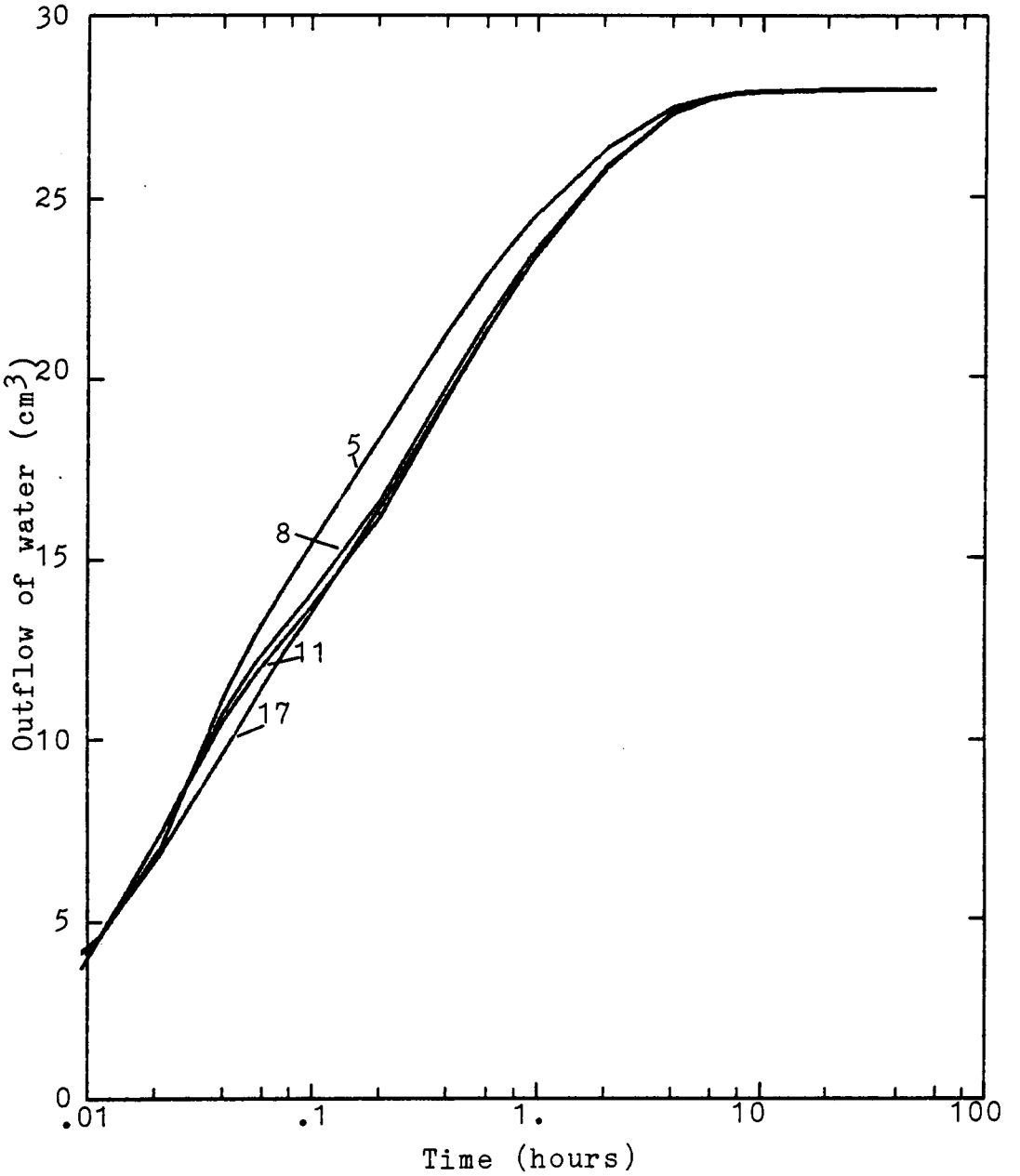

Figure 31. Effect of number of elements.

parison with the program IMF1D simulating the same problem. An example of seepage through an earth dam is presented which further validates program IMF2D. The effects of the time step, the iteration technique, the initial condition, and the model parameters are discussed. Suggestions for choosing the proper time step and tuning factor for iteration are presented.

CHAPTER 7

Application Problems

The finite element program IMF2D developed in this study is very general and can be applied to field problems of three-phase flow involving air, organic fluid and water. A commonly occurring problem and which is of the most interest to this study is the groundwater contamination due to leaking buried fluid storage tanks. In chemical and oil industries many different types of fluids are stored in steel tanks buried underground. Most of the organic fluids are immiscible with water. Due to aging and corrosion these tanks are worn out and leak. It is estimated (Edwards 1985) that as many as 350,000 of the nation's approximately 1.2 million service station tanks may be leaking by 1987. However, there is no case history with any scientific observation available now in the literature. For this purpose, it is proposed in the next phase of this research study that a large scale laboratory model test with controlled monitoring system are done. This laboratory model is expected to be built in the next two years. This will yield valuable information on the validity of the application of the finite element program IMF2D to a field problem. Here a typical field problem involving a leaking buried fluid storage tank is analysed to study the immiscible flow behavior. The effects of the

soil properties and the initial and boundary conditions imposed on both the oil and water phases are to be discussed.

Problem Description

The oil tank is 10 m wide and 2 m deep buried below the ground surface. The oil leaks from the bottom of the tank which is assumed to be fully filled up to the ground level all the time. The soil domain considered is 210 m wide and 16 m deep with an impervious base as shown in Figure 32 where the horizontal scale is 10 m/cm and the vertical scale is 5 m/cm. There are 11 cases studied in this chapter involving 7 different porous materials. The impervious base is taken as the datum for all the cases.

The material properties and the model parameters for the capillary function and fluid conductivities are assumed based on experimental data available (van Genuchten 1980, Parker et al. 1985). Also, at this stage, the laboratory data done for this study are the air-benzene-water and air-p-cymene-water systems with a sandy material as described in Chapter 6. Table 9 gives the material properties and model parameters used in all the cases. The major differences in Cases 1-3 are the fluid conductivities K and parameter α. These differences correspond to a clayey soil in Case 1, a silty soil in Case 2, and a sandy soil in Case 3. Among Cases 4-7 the fluid conductivities are different. Cutoff walls of various depths are used in Cases 8-11.

Cases 1 and 2

Case 1 is the study of a clay medium whereas in Case 2 the medium is silt. The finite element mesh consists 140 elements and 169 nodes as shown in Figure 33(a). This mesh is chosen after a comparison is made with the result from a finer mesh of 180 elements. The comparison of results shows no significant difference and indicates that a mesh of 140 ele-

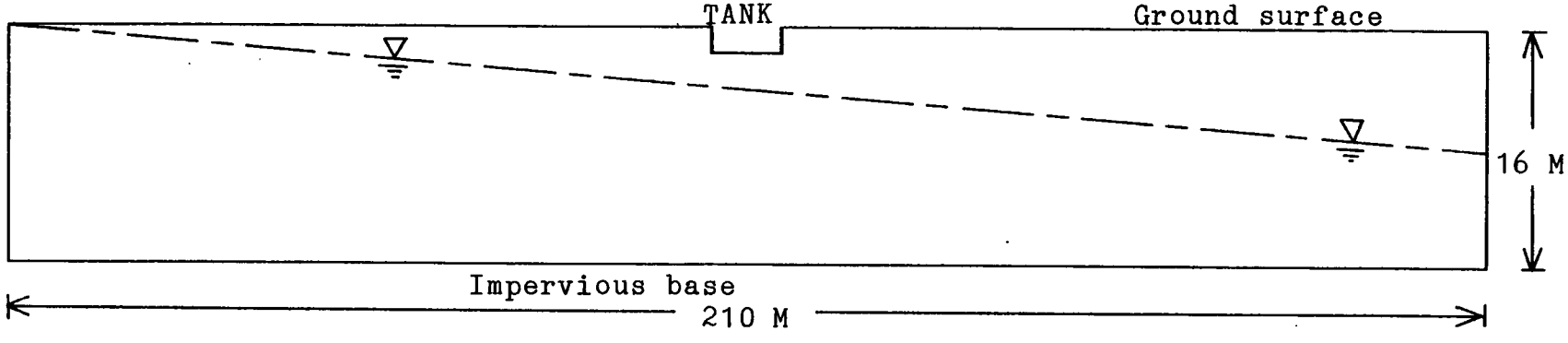

Figure 32. Oil tank and soil domain.

Table 9. Material properties and model parameters used in all the cases.

Case	Soil type	Porosity φ	Oil density ρ_o	K_{xws}	K_{yws}	K_{xos}	K_{yos}	α	n	β_{aw}	β_{ow}	β_{ao}	S_{rs}
1	clay	0.4	0.8	0.005	0.005	0.0038	0.0038	0.2	1.84	1.0	2.2	2.0	0.
2	silt	0.4	0.8	0.1	0.1	0.075	0.075	0.5	1.84	1.0	2.2	2.0	0.
3	sand1	0.4	0.8	2.0	2.0	1.5	1.5	5.0	1.84	1.0	2.2	2.0	0.
4	sand1	0.4	0.8	2.0	2.0	1.5	1.5	5.0	1.84	1.0	2.2	2.0	0.
5	sand2	0.4	0.8	1.5	1.5	2.0	2.0	5.0	1.84	1.0	2.2	2.0	0.
6	sand3	0.4	0.8	2.0	1.0	1.5	0.75	5.0	1.84	1.0	2.2	2.0	0.
7	sand4	0.4	0.8	2.0	0.5	1.5	0.375	5.0	1.84	1.0	2.2	2.0	0.
8	sand5	0.42	0.86	4.2	4.2	3.2	3.2	5.4	1.82	1.0	2.12	1.89	0.
9	sand5	0.42	0.86	4.2	4.2	3.2	3.2	5.4	1.82	1.0	2.12	1.89	0.
10	sand5	0.42	0.86	4.2	4.2	3.2	3.2	5.4	1.82	1.0	2.12	1.89	0.
11	sand5	0.42	0.86	4.2	4.2	3.2	3.2	5.4	1.82	1.0	2.12	1.89	0.
	wall	0.1		0.3	0.3	0.2	0.2	0.01	10.0	1.0	2.12	1.0×10^5	0.

Unit: Fluid conductivity K = *m/day* and parameter α = 1/m

ments is sufficient for this problem. In cases 1 and 2 the initial condition imposed for the oil phase is that the total head $H_o = -1$ m such that the oil saturation, S_o, is initially zero throughout the domain. The boundary conditions for the oil phase are all natural boundaries, i.e., no flow conditions, except at the bottom of the tank (see Figure 33(a)) where the total head of the oil phase is equal to 12.8 m which is equivalent head of water taking into account of the density of the oil. The total head of water is 16 m at the left boundary (CD) and 8 m at the right boundary (EF) for $t \geq 0$. The initial water table is 16 m at left (CD) and linearly decreases to 8 m at right (EF). Due to the low fluid conductivities in Case 1 (clay), the oil plume moves very slowly. The predicted oil plumes at 446, 1250, and 2910 days are plotted in Figure 34. The intensity of dots in this figure denotes the oil saturation ranging from 0.2 to 0. The predicted oil plumes at 446, 1250, and 2910 days in case 2 (silt) are shown in Figure 35. In this figure the density of dots represents the oil saturation ranging from 0.5 to 0. The variation of oil saturation at an element A (see Figure 33(a)) in case 2 is given in Figure 36. The oil saturation is 0.076 at 446 days and gradually increases to 0.312 at 2910 days.

Figures 37 and 38 show the variations in flow quantities of the whole soil domain for both oil and water phases in Cases 1 and 2 respectively. In these two figures, the oil content keeps on increasing with time. This is due to the assumption that the oil tank is fully filled all the time. In other words, there is a constant oil total head imposed at the bottom of the leaking tank. For water phase, the water content in Case 1 increases initially up to about 1600 days and then decreases. In Case 2 it increases up to 132 days and then decreases. At 1250 days, a net decrease of total water content is observed.

These observed behavior can be explained mathematically and physically. Initially the water pressure head is h_w, a negative number, at a particular element above the water table. Since the oil phase is absent initially ($S_o = 0$), the corresponding effective saturation of the water phase $\bar{S}_w$ of that element is calculated by Eq. 4.6

$$\bar{S}_w = \left[1 + (\alpha h_{aw})^n\right]^{-1+\frac{1}{n}} \qquad [4.6]$$

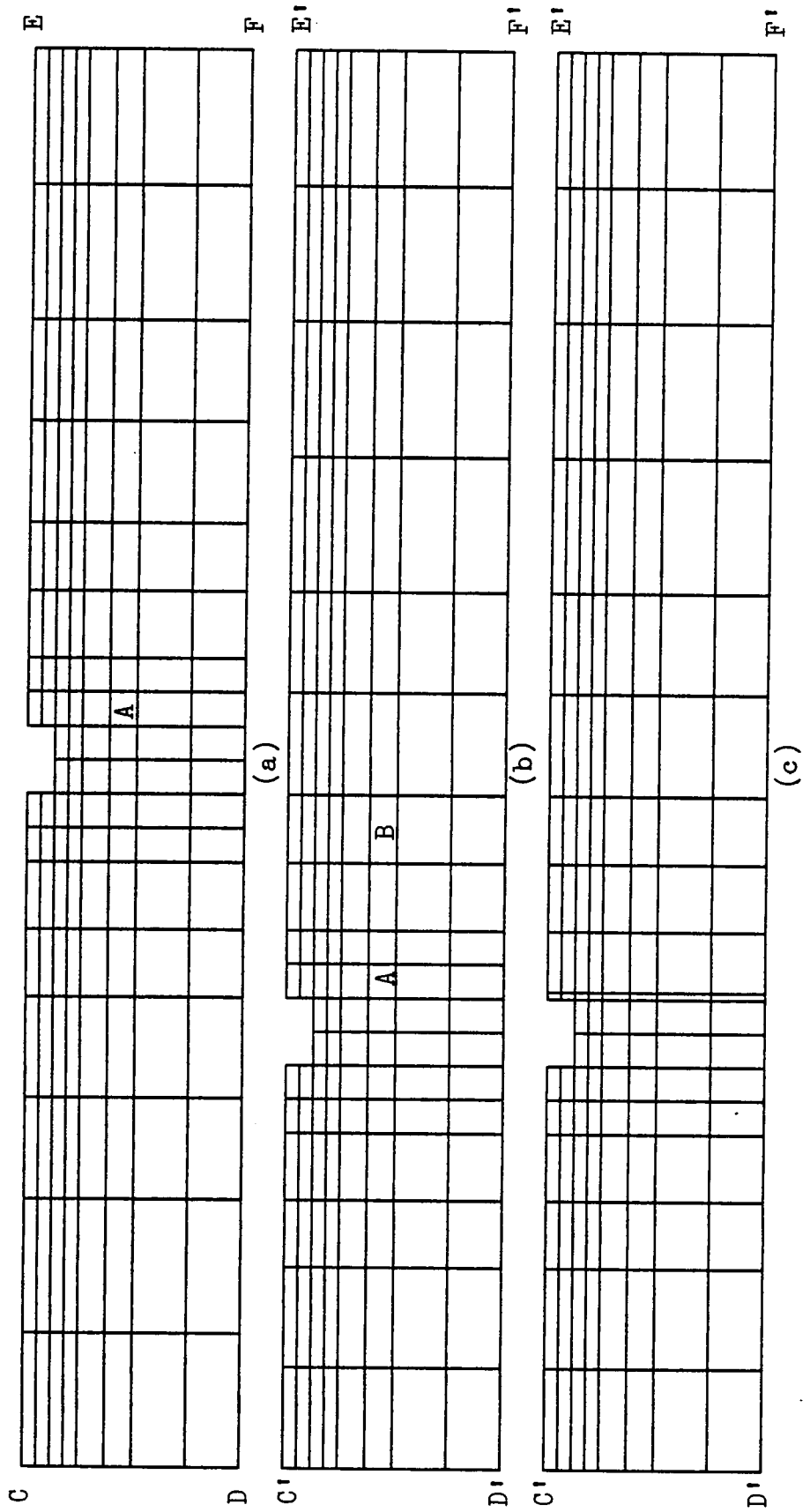

Figure 33. Finite element meshes used in Cases 1-2 (a), 3-8 (b), and 9-11 (c).

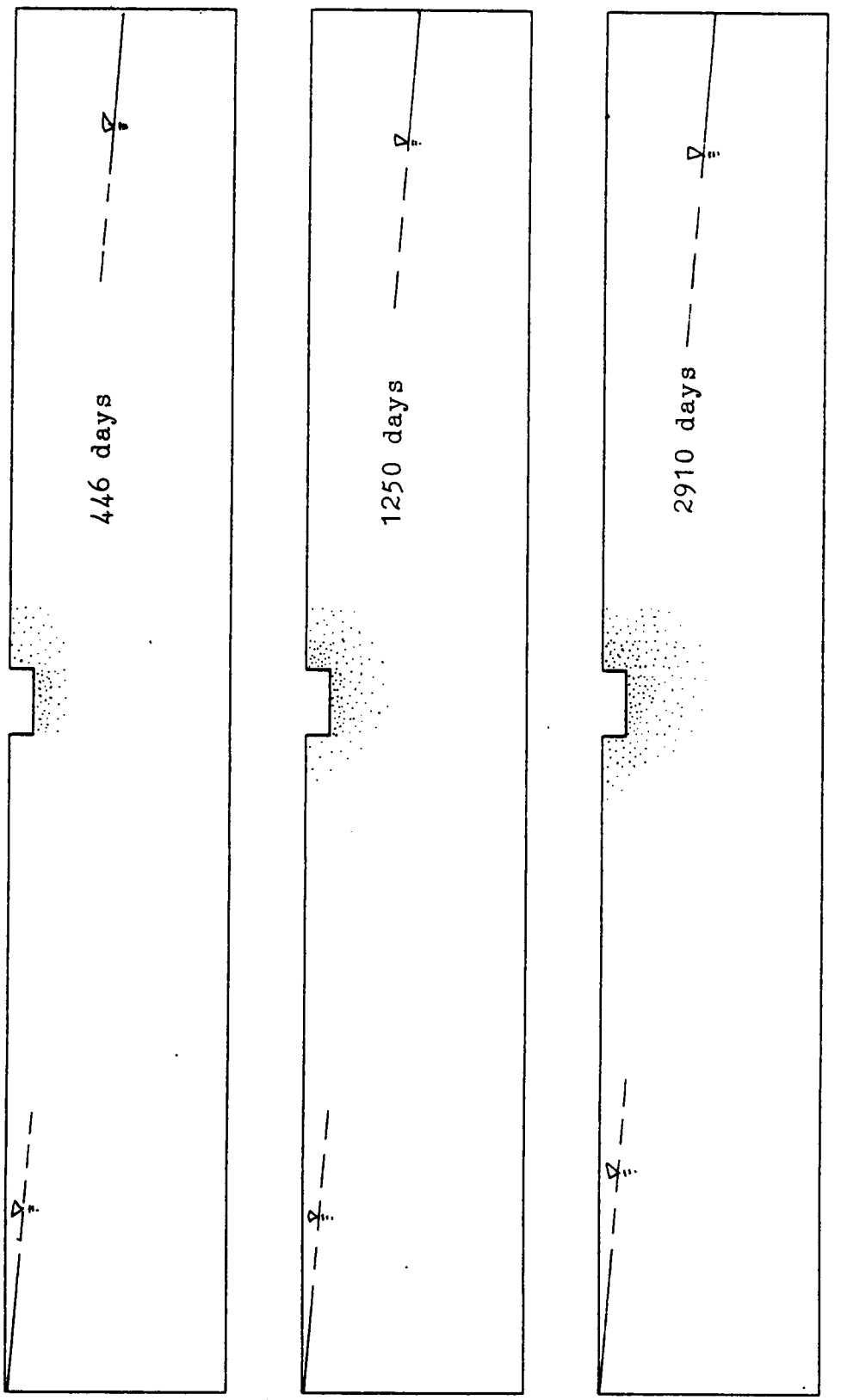

Figure 34. Oil phase plumes at 446, 1250, and 2910 days in Case 1.

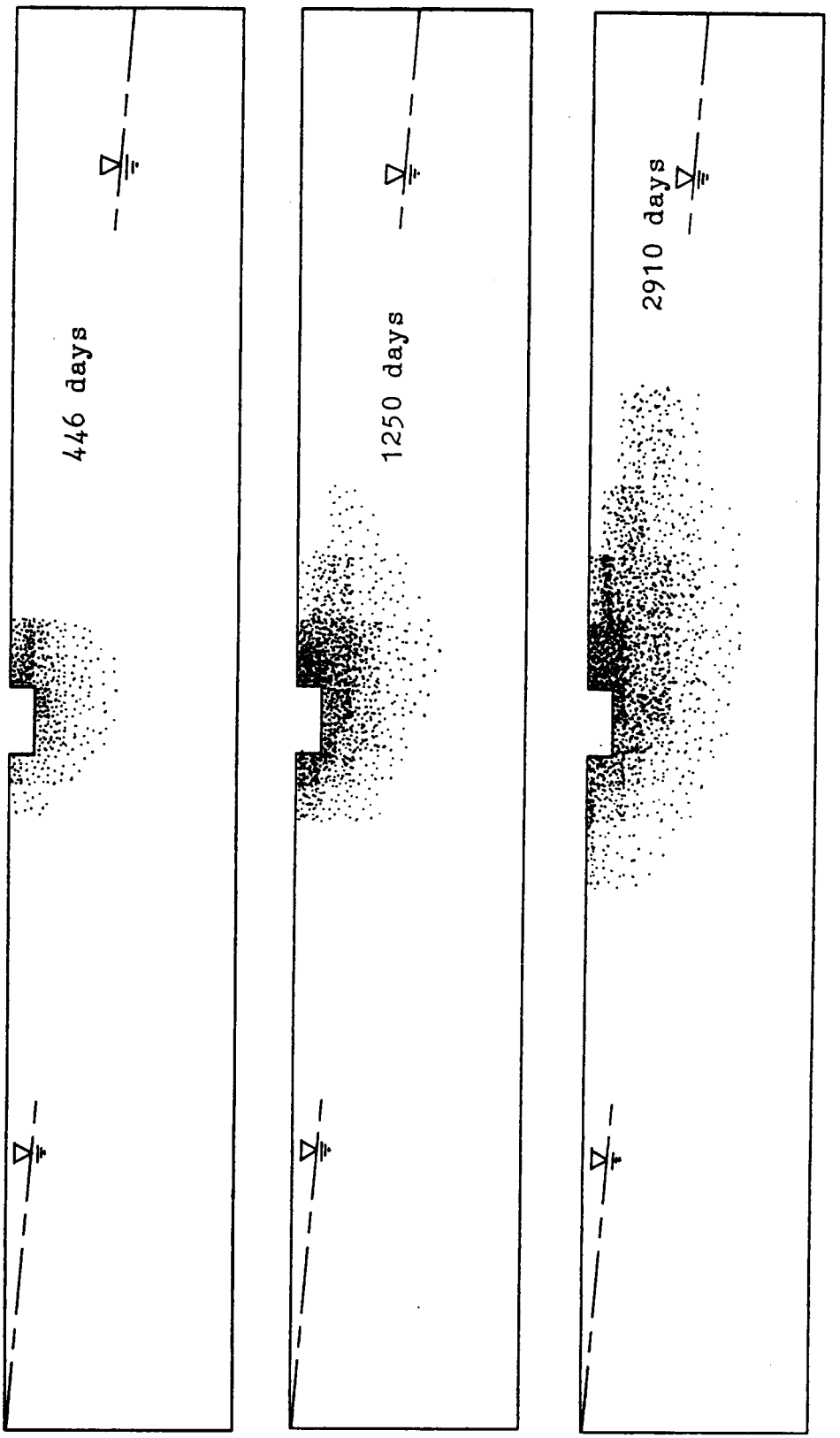

Figure 35. Oil phase plumes at 446, 1250, and 2910 days in Case 2.

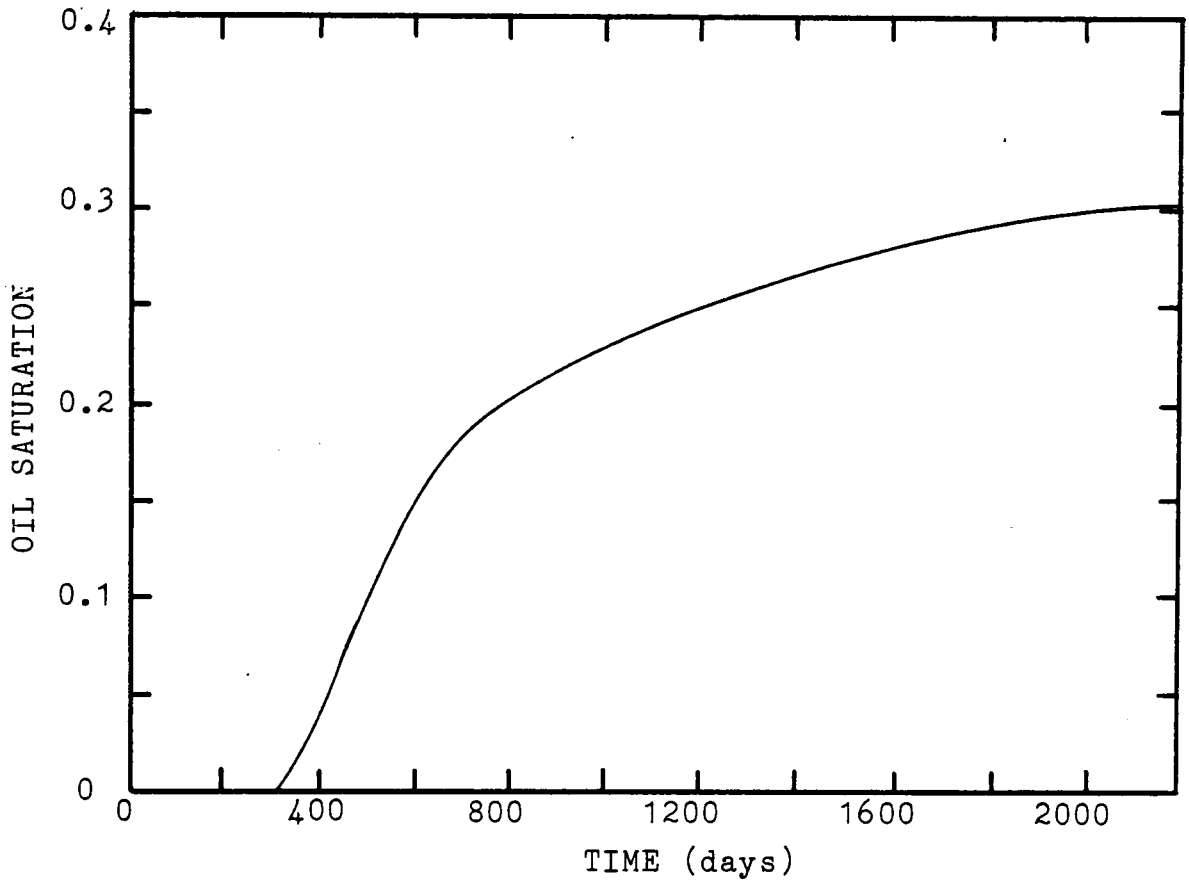

Figure 36. Variations of oil saturation at element A in Cases 2.

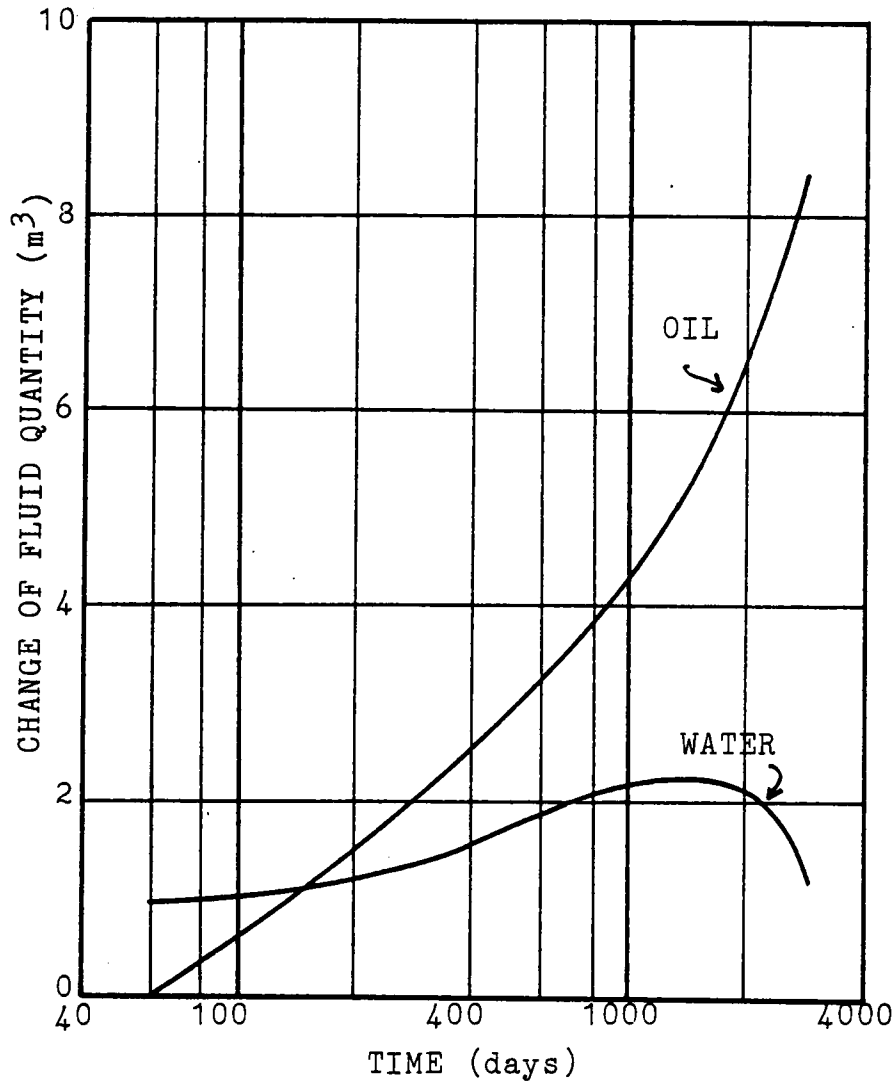

Figure 37. Variations in oil and water flows of the whole domain in Cases 1.

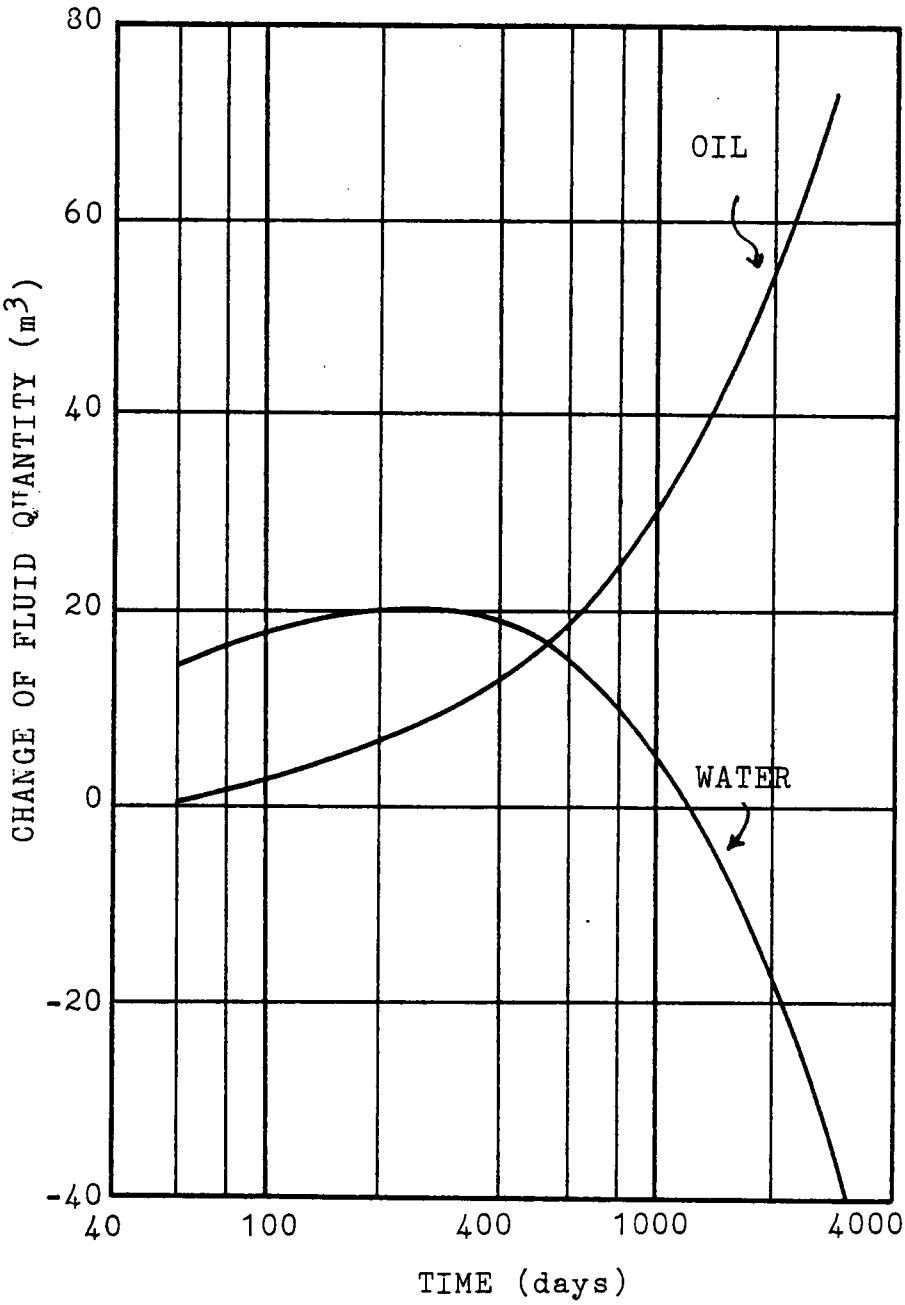

Figure 38. Variations in oil and water flows of the whole domain in Cases 2.

where $h_{aw} = -h_w$. As oil starts to flow, h_o increases. At a certain period of time (depending on the soil type and element location), $0 > h_o > h_w$ and $h_{ow} = h_o - h_w$. The corresponding $\bar{S}_w$ of this particular element is calculated by Eq. 4.8

$$\bar{S}_w = \left[1 + (\beta_w^{ow}\alpha h_{aw})^n\right]^{-1+\frac{1}{n}} \qquad [4.8]$$

Note that $\bar{S}_w$ calculated from Eq. 4.8 may greater than that from Eq. 4.6 if $\alpha h_{aw} > \beta_w^{ow}\alpha h_{ow}$ or $h_{aw} > \beta_w^{ow} h_{ow}$.

Physically speaking, the spreading of oil phase occupies the larger part of a pore. When the remaining part of the pore becomes small enough to hold water under a higher capillary head which is inversely proportional to the pore size, the wetting phase, water, can then be raised to a higher elevation than its initial elevation. Thus, for a certain period of time, some elements experience an increase not only on S_o but also S_w. This leads to an increase of water content of the whole soil domain as shown in Figures 37 and 38. The different flow behaviors between Case 1 and Case 2 are mainly due to the assumed larger pore size in silt than that in clay.

Case 3

This is the case of a sandy material with the properties and parameters given in Table 9. Because of the high fluid conductivities of oil and water in sand the oil plume moves toward right very fast. The right boundary (EF in Figure 33(a)) should be far away from the leaking tank such that the assumed natural boundary condition for the oil phase at right boundary does not significantly affect the flow behavior at the time level of analysis. Therefore, in this case the soil domain is modified and the finite element mesh is shown in Figure 33(b) with 140 elements and 169 nodes.

The initial water table is assumed 14.5 m at the left boundary (C'D') and linearly decreases to 6.48 m at the right boundary (E'F'). This corresponds to the same condition as in

the previous cases 1 and 2. The boundary condition for water phase is 14.5 m at left and 6.48 m at right which is a close approximation of the water phase boundary conditions in Cases 1 and 2. The initial and boundary conditions for oil phase are kept the same as in the previous cases.

The predicted oil plumes at 166, 305, and 572 days are shown in Figure 39 with the intensity of dots denoting the oil saturation ranging from 0.9 to 0. Because of the high fluid conductivities and larger pore size in this case, the oil plume moves much faster and the oil saturation is higher than those in Cases 1 and 2. In this case, the oil plume at 572 days (see Figure 39) spreads wider than the oil plume at 2910 days in Cases 1 and 2 (see Figures 34 and 35).

Case 4

This case is exactly the same as Case 3 except that the initial water table is raised to 16 m at left boundary and linearly decreased to 8 m at right boundary. This means that the water table is much close to the tank. The boundary conditions imposed for water phase are also changed to 16 m at left and 8 m at right. All the conditions for oil phase are the same as in case 3.

The predicted oil phase plumes at 166, 572, and 1070 days are shown in Figure 40 with the intensity of dots denoting the oil saturation ranging from 0.8 to 0. Due to the raised initial water table and the imposed water boundary conditions, the oil plumes spread considerably slower than those in Case 3. At 572 days, the oil plume penetrates 4 m below the ground surface in Case 4 while it is 11 m deep in Case 3.

An interesting phenomenon is observed in this case. Variations in saturation of the oil phase at two elements A and B are shown in Figure 41. The locations of elements A and B are given in Figure 33(b). The oil plume is seen to reach element A at 300 days. Oil saturation continuously increases to 0.56 at 750 days and then decreases. That is, initially the oil phase displaces the water phase at element A, and then the water phase starts to displace

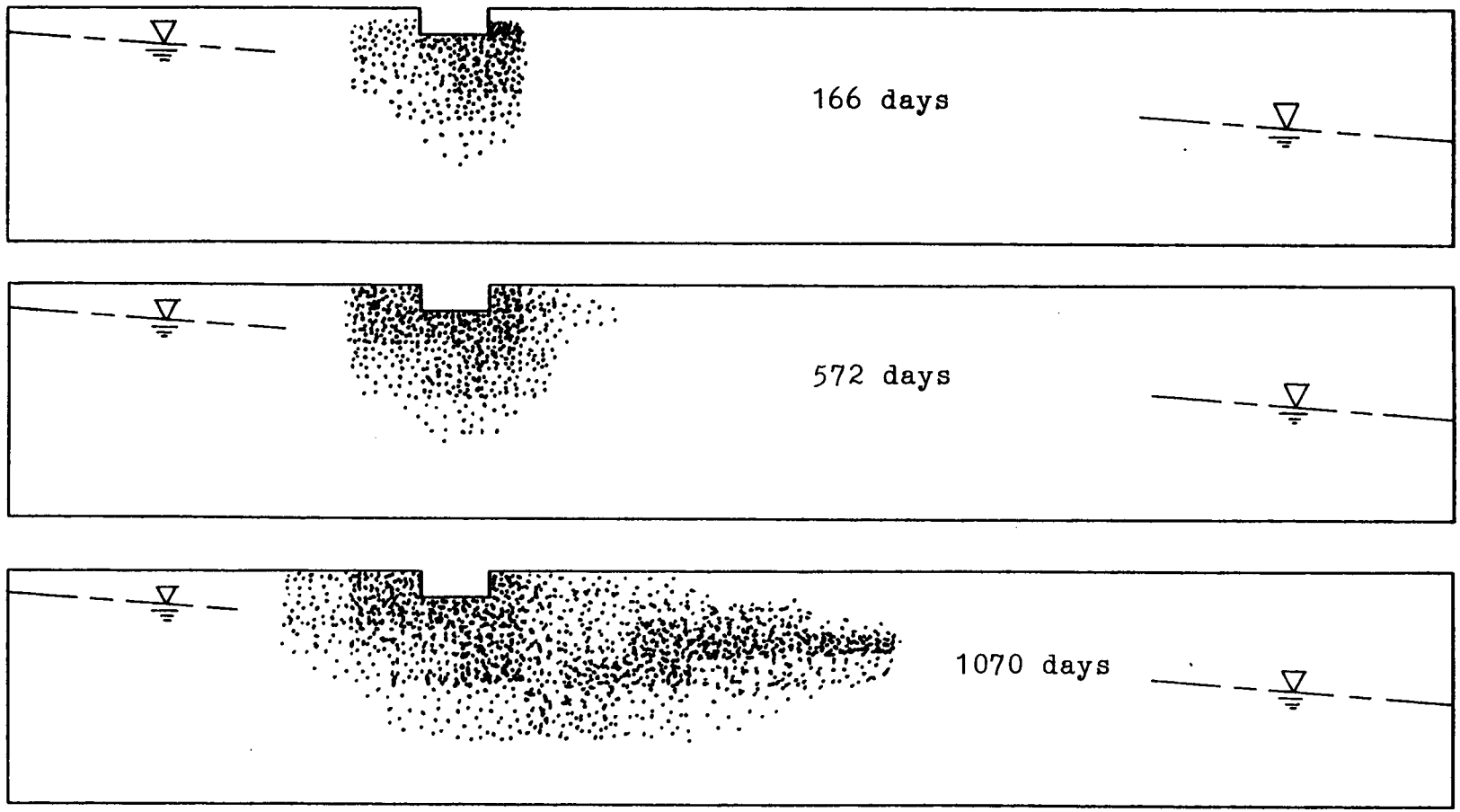

Figure 39. Oil phase plumes at 166, 305, and 572 days in Case 3.

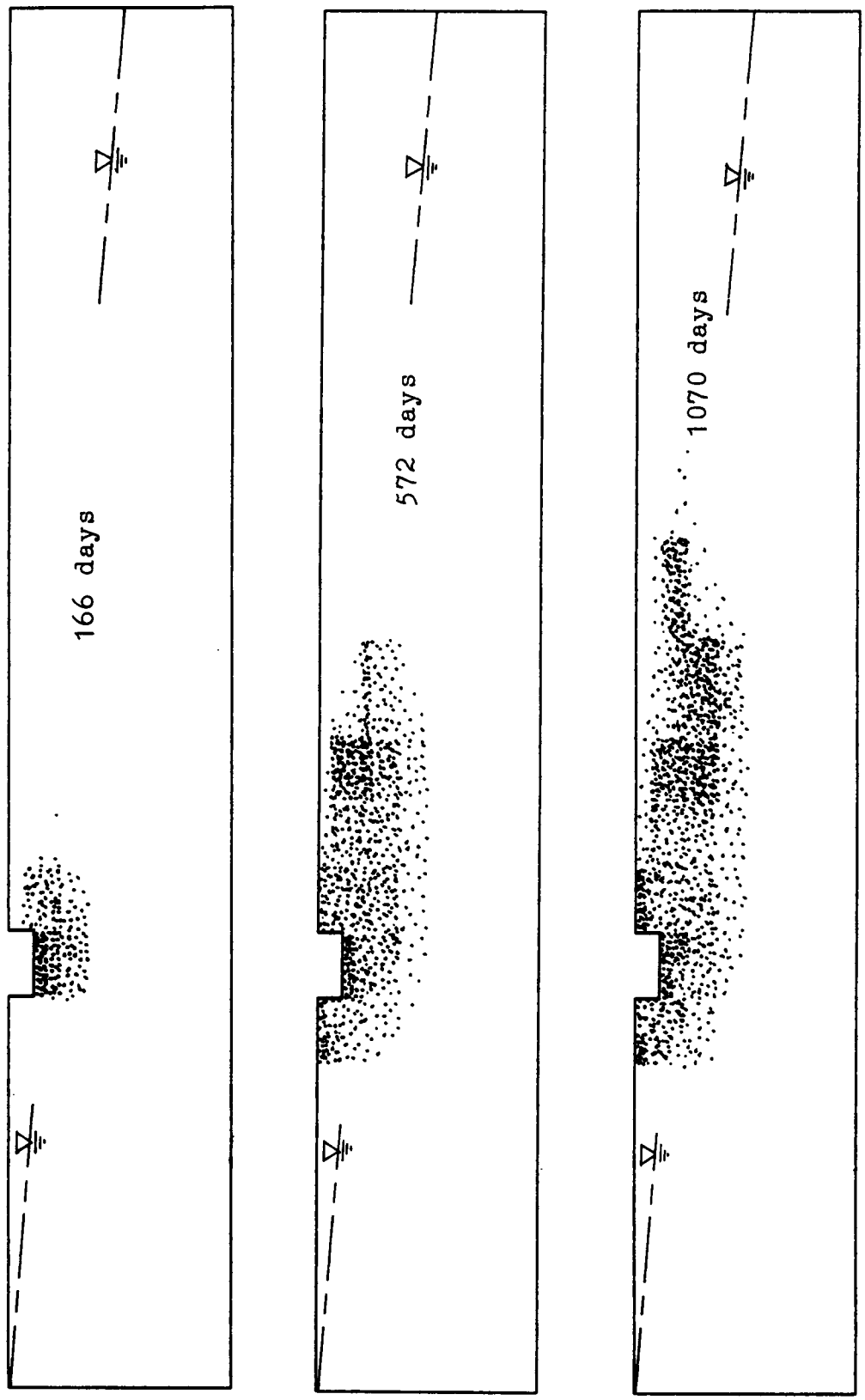

Figure 40. Oil phase plumes at 166, 572, and 1070 days in Case 4.

the oil phase. This is due to the differences in the fluid conductivities and densities between the water and oil. In this case the effect of fluid conductivities appears faster than that of densities while in Cases 1 and 2 the fluid conductivities are low and the effect of densities dominates the flow behavior. A similar situation is observed at element B which is located further away from the leaking tank than element A. The oil plume reaches element B at about 350 days and the peak of oil saturation, 0.67, occurs at 1000 days. The final oil saturation at element B is higher than that at A since the water table decreases toward the right boundary and elements A and B are at the same elevation.

Case 5

This case is similar to Case 4 except that the saturated fluid conductivity of oil phase K_{os} is 2 m/day which is higher than the saturated fluid conductivity of water phase K_{ws} , 1.5 m/day. The predicted oil phase plumes at 166, 572, and 1070 days are shown in Figure 42 with the intensity of dots denoting the oil saturation ranging from 0.8 to 0. Since the fluid conductivity of water is less than that in Case 4, water presents a higher resistance when displaced by oil. Furthermore, the oil conductivity is higher than that in Case 4, the density effect appears faster than it does in Case 4. These make the oil plumes spreading slower and penetrating less in depth compared with Case 4. Also noticed is that the oil phase does not spread toward up-stream while in Case 4 the oil phase reaches about 10 m upstream at 1070 days. The behavior shown in the previous case 4 for elements A and B is not observed in this case.

Cases 6 and 7

In these two cases, the effect of anisotropic fluid conductivities are studied. For the water phase, the saturated conductivities K_{xws} is 2 m/day in both cases and K_{yws} is 1 m/day in Case 6 and .5 m/day in Case 7. For the oil phase, K_{xos} is 1.5 m/day in both cases and K_{yos} is 0.75 m/day in Case 6 and .375 m/day in Case 7. The other properties, parameters, and conditions

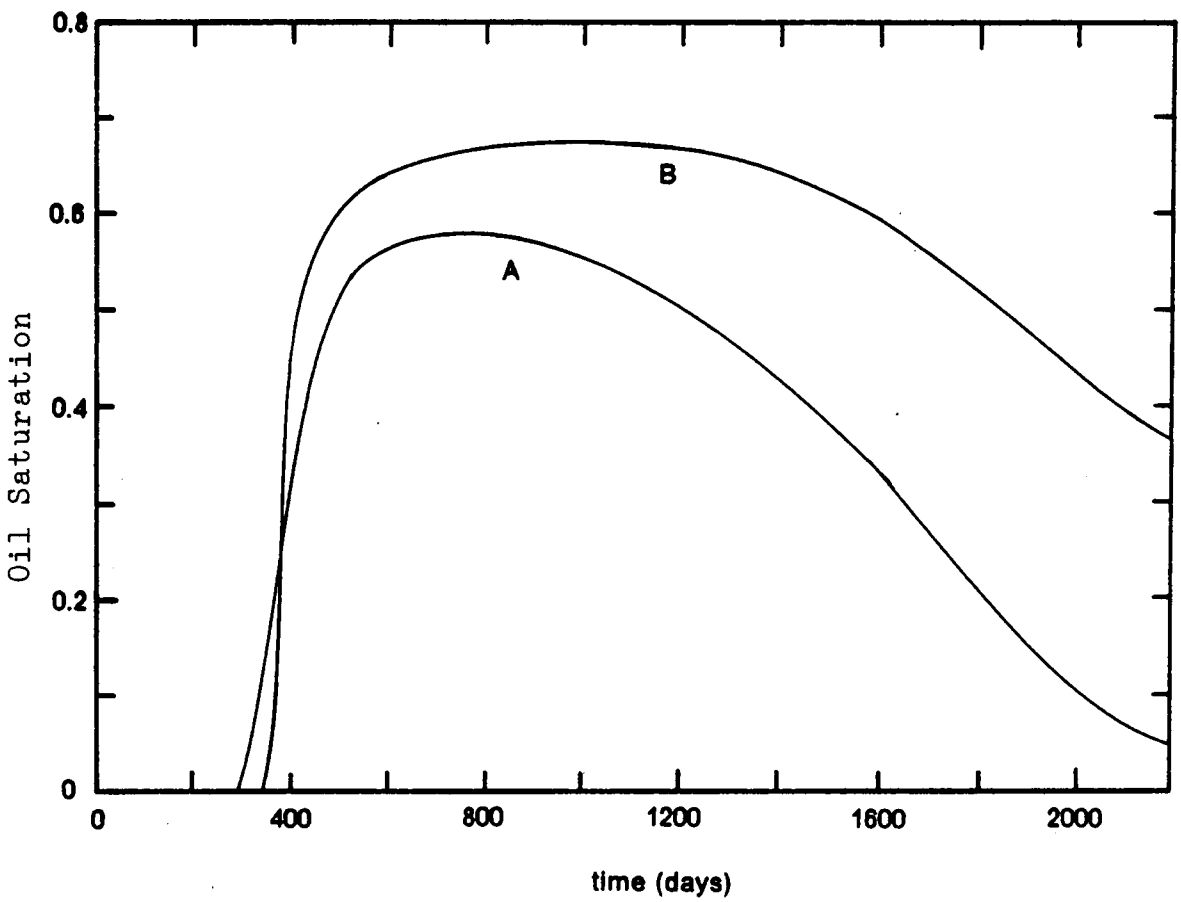

Figure 41. Variations in oil saturation at elements A and B in Case 4.

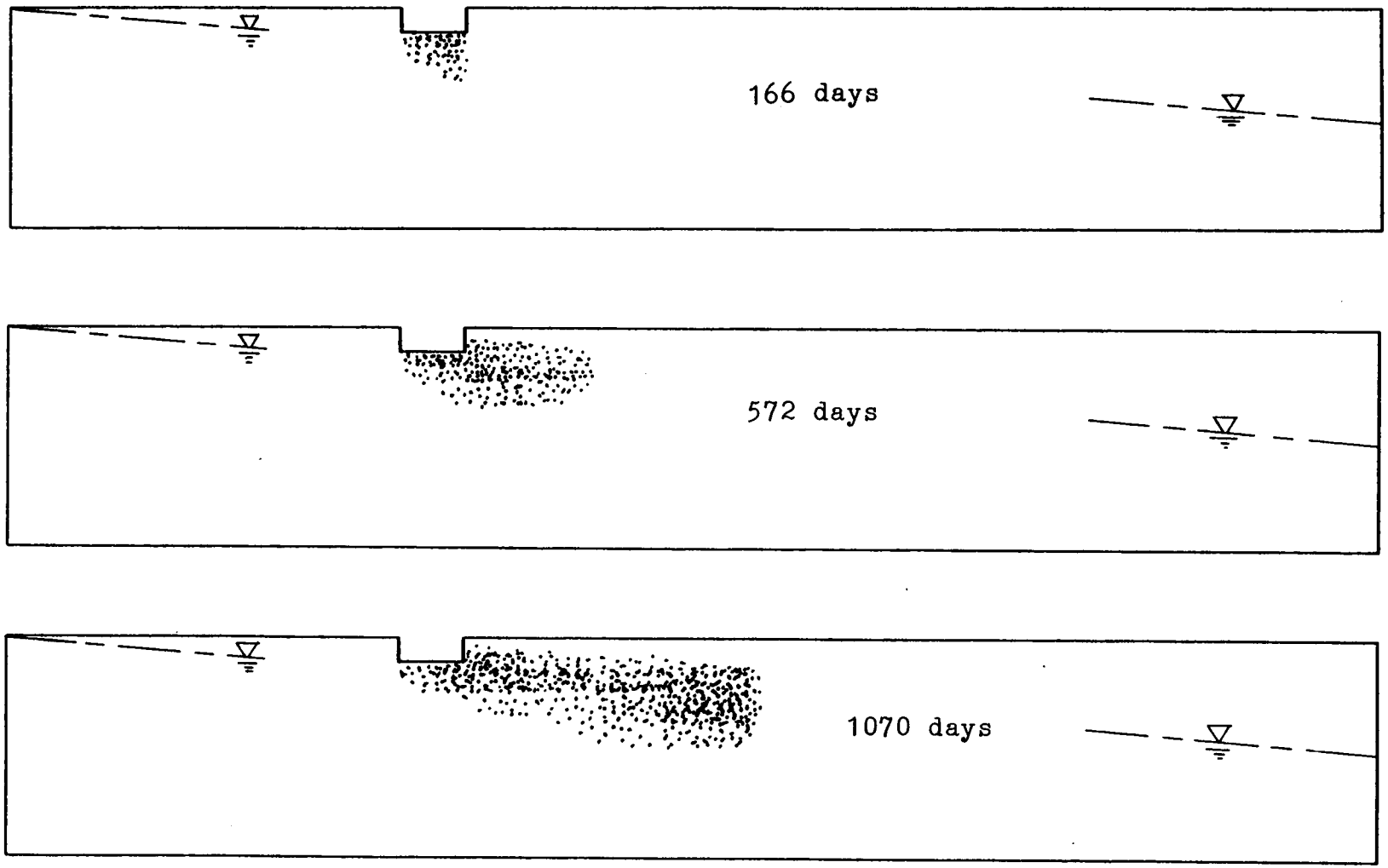

Figure 42. Oil phase plumes at 166, 572, and 1070 days in Case 5.

are the same as in Case 4. The predicted oil phase plumes at 166, 572, and 1070 days are shown in Figures 43 and 44 for Cases 6 and 7 respectively. The intensity of dots denotes the oil saturation ranging from 0.8 to 0 in both cases. Again, a slower and shallower spreading of the oil phase is observed in this case. This is due to the lower fluid conductivities in the vertical direction for both the oil and water phases. There is no oil spreading toward upstream as in Case 5. The slower oil phase spreading toward downstream is due to the coupled effect of the fluid conductivities in the vertical and horizontal directions even though the horizontal fluid conductivities are the same as those in Case 4.

Cases 8, 9, 10, and 11

In all these four cases a sandy medium is assumed. A cutoff wall is built adjacent to the leaking tank at the downstream side in Cases 9, 10, and 11. The function of the cutoff wall is to present a high resistance to the oil phase without blocking the water flow significantly. The material properties of the cutoff wall (see Table 9) is similar to those of the lower porous stone used in the laboratory transient test. The porous stone is made of fine copper particles. It presents a very high oil entry pressure such that the oil phase does penetrate through under the applied pressure. On the other hand, water can flow through the porous stone without facing significant resistance. Thus the function of the cutoff wall is to present a high resistance to the oil phase without blocking the water flow significantly. The cutoff wall is 1 m thick. The depth of the cutoff wall is 4 m, 6 m, and 8 m deep in Cases 9, 10, and 11, respectively, while there is no cutoff wall in Case 8. The material properties and model parameters for these four cases are given in Table 9. The initial and boundary conditions are the same as in Case 4. The finite element mesh used in these cases is shown in Figure 33(c).

For comparison, the predicted oil plumes at 166, 572, and 1070 days in each case are shown in Figures 45, 46, and 47, respectively, with the oil saturations ranging from 0.8 to 0. There is practically no difference in oil plumes among these four cases at 166 days. As time goes on, the oil phase spreads beyond the cutoff wall at 572 days in Case 9 (4 m deep wall)

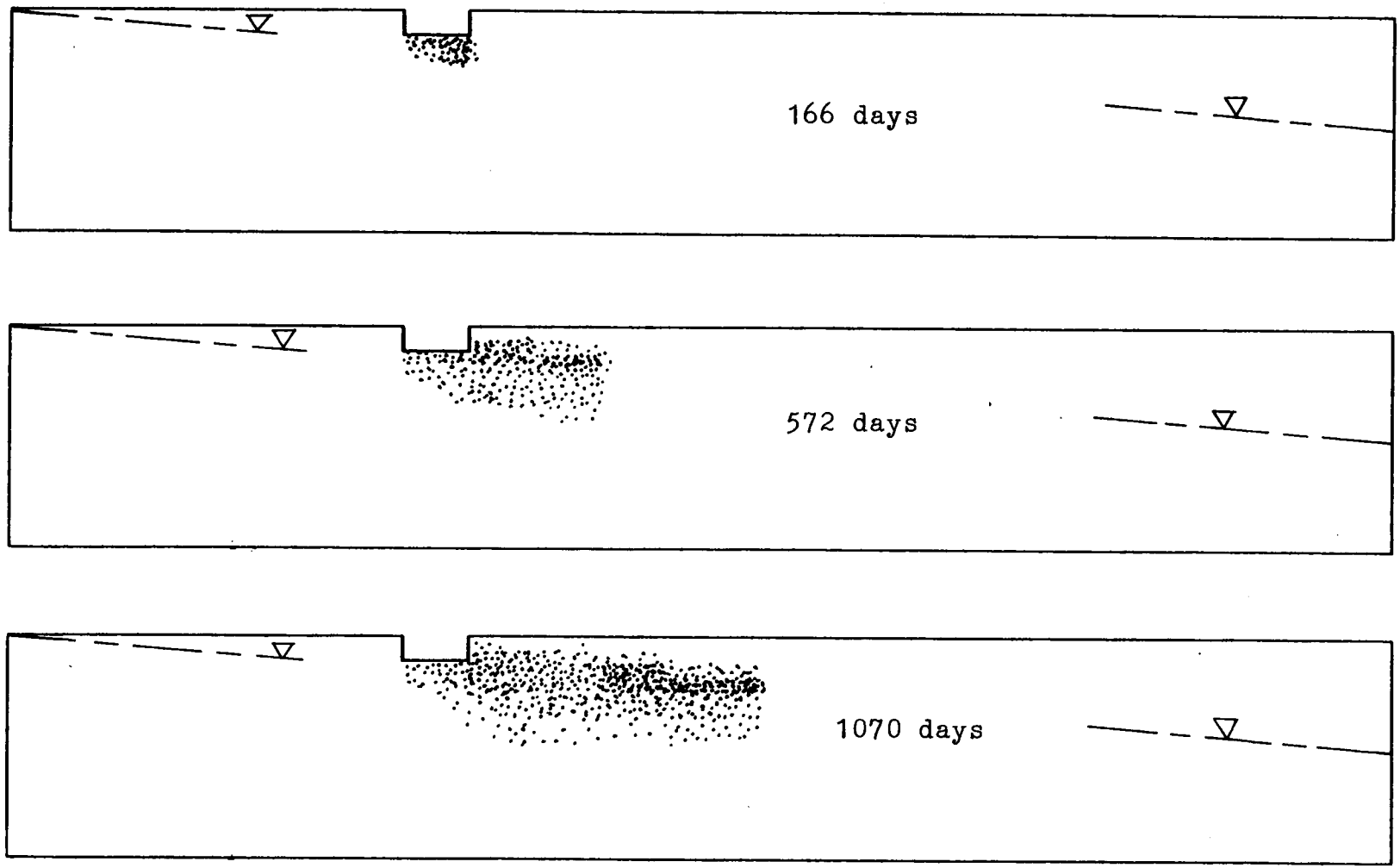

Figure 43. Oil phase plumes at 166, 572, and 1070 days in Case 6.

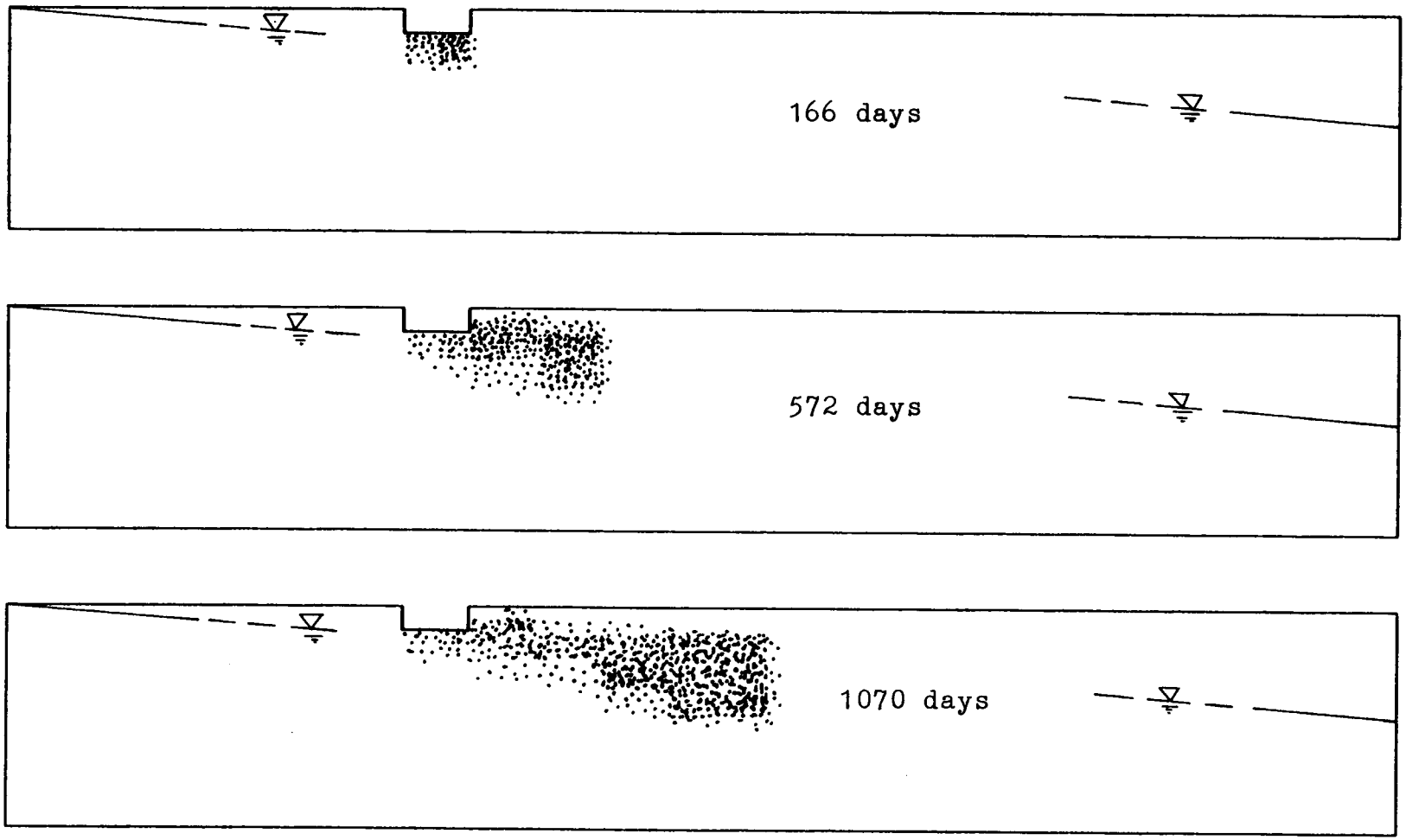

Figure 44. Oil phase plumes at 166, 572, and 1070 days in Case 7.

and at 1070 days in Case 10 (6 m deep wall). There is no oil spread beyond the cutoff wall in Case 11 (8 m deep wall) during the time period of analysis.

It is worth to note that the initial water table is only 2.67 m (H_w = 13.33 m) below ground level at the location of cutoff wall. Due to the characteristic of multiphase flow, the oil phase penetrates downward to a depth about 8 m below ground surface. A cutoff wall with a depth less than 8 m does slow down the spreading of the oil phase, as demonstrated in Cases 9 and 10. However, in order to fully prevent the leaking oil from spreading, a 8 m deep wall is required for this specific case.

Summary

A leaking buried storage tank subjects to different soil conditions as well as initial and boundary conditions is analysed. The predicted spreading of the oil plume is presented at different time levels. The effect of soil type (Cases 1, 2, and 3), water table elevation (Cases 3 and 4), and fluid conductivities (Cases 4, 5, 6, and 7) are described and discussed. Behaviors of the variations of oil saturation in Cases 1, 2, and 4 are described and explained. The effect of depth of a cutoff wall for preventing the oil phase from spreading is studied.

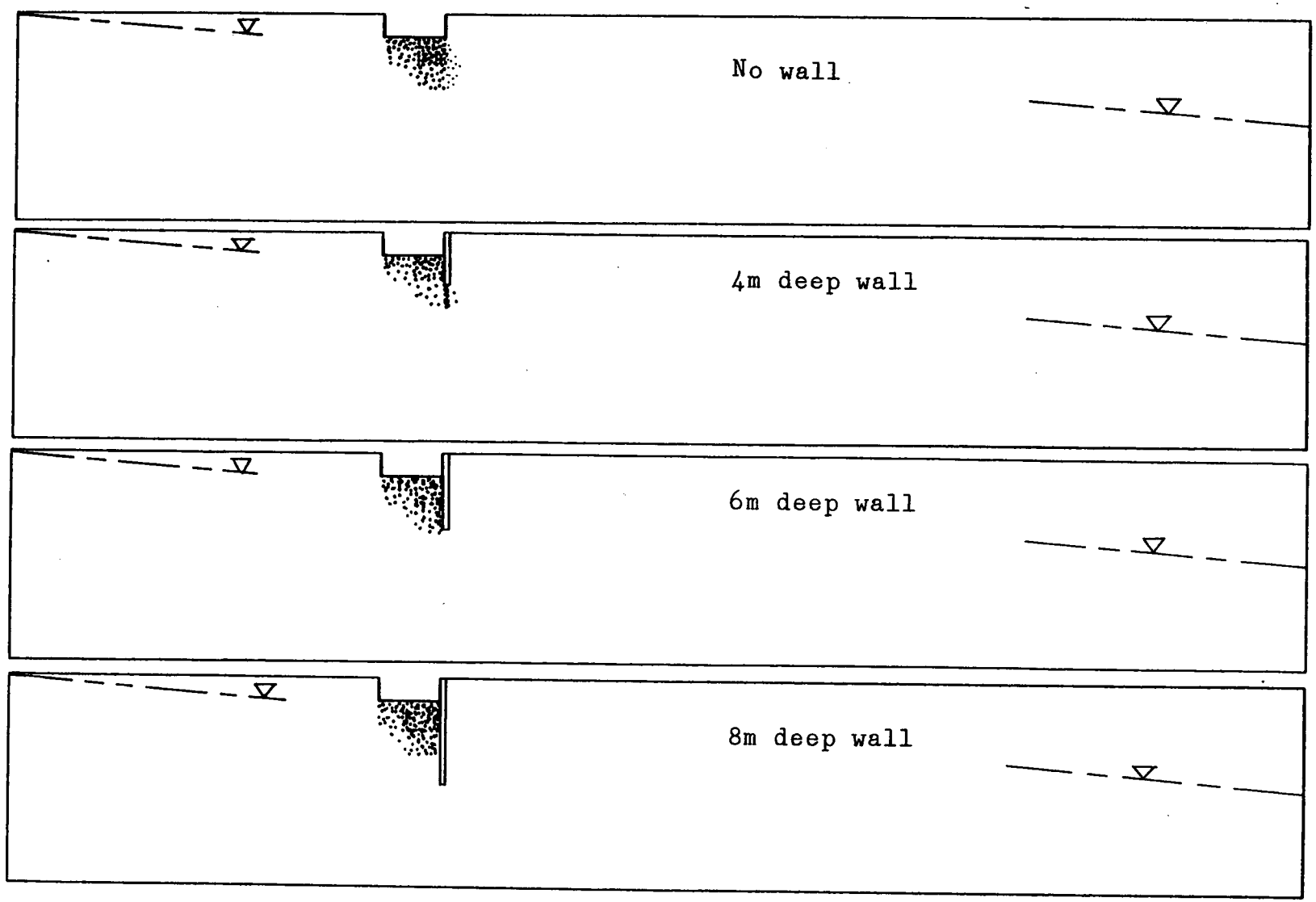

Figure 45. Oil phase plumes at 166 days in Cases 8, 9, 10, and 11.

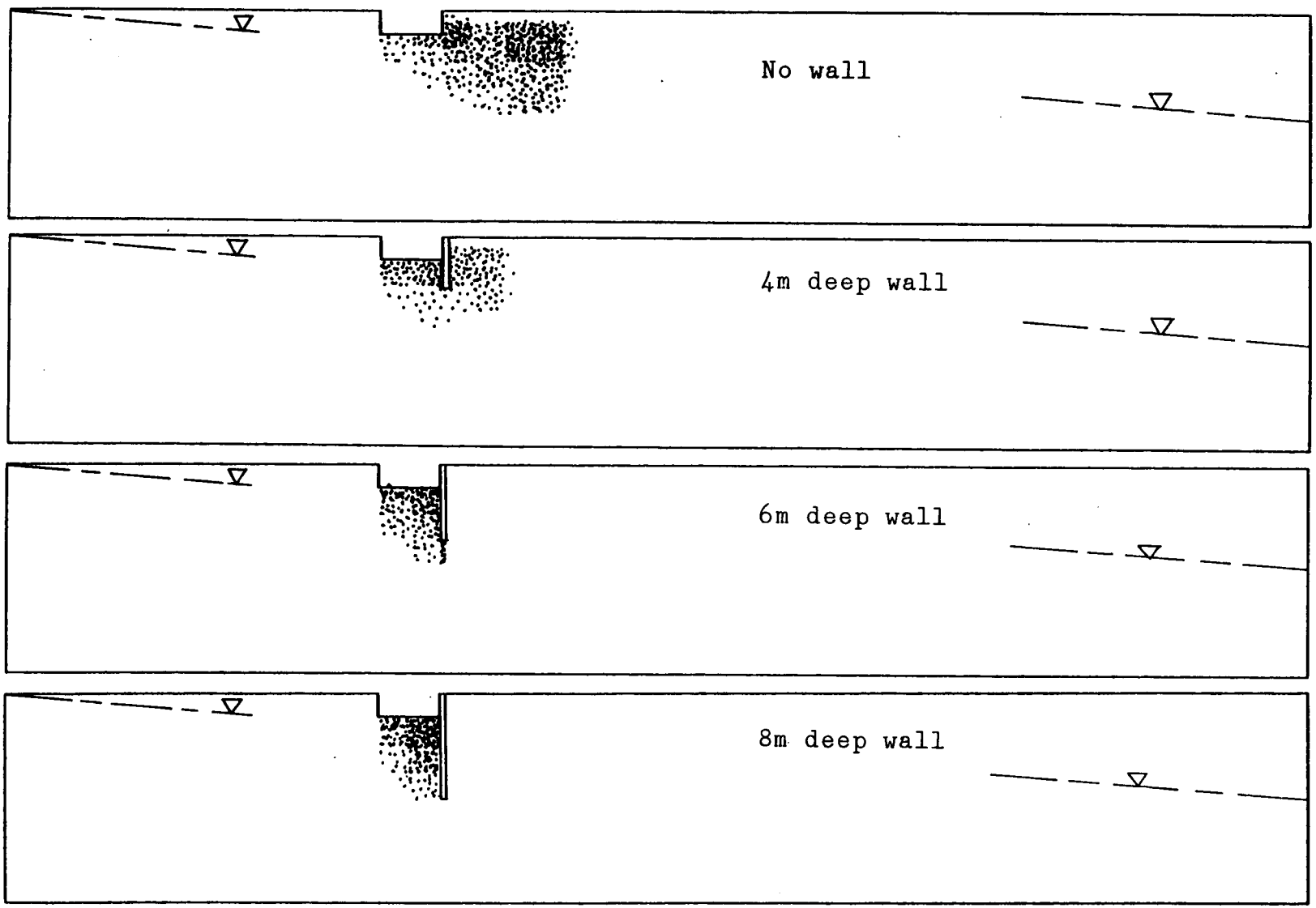

Figure 46. Oil phase plumes at 572 days in Cases 8, 9, 10, and 11.

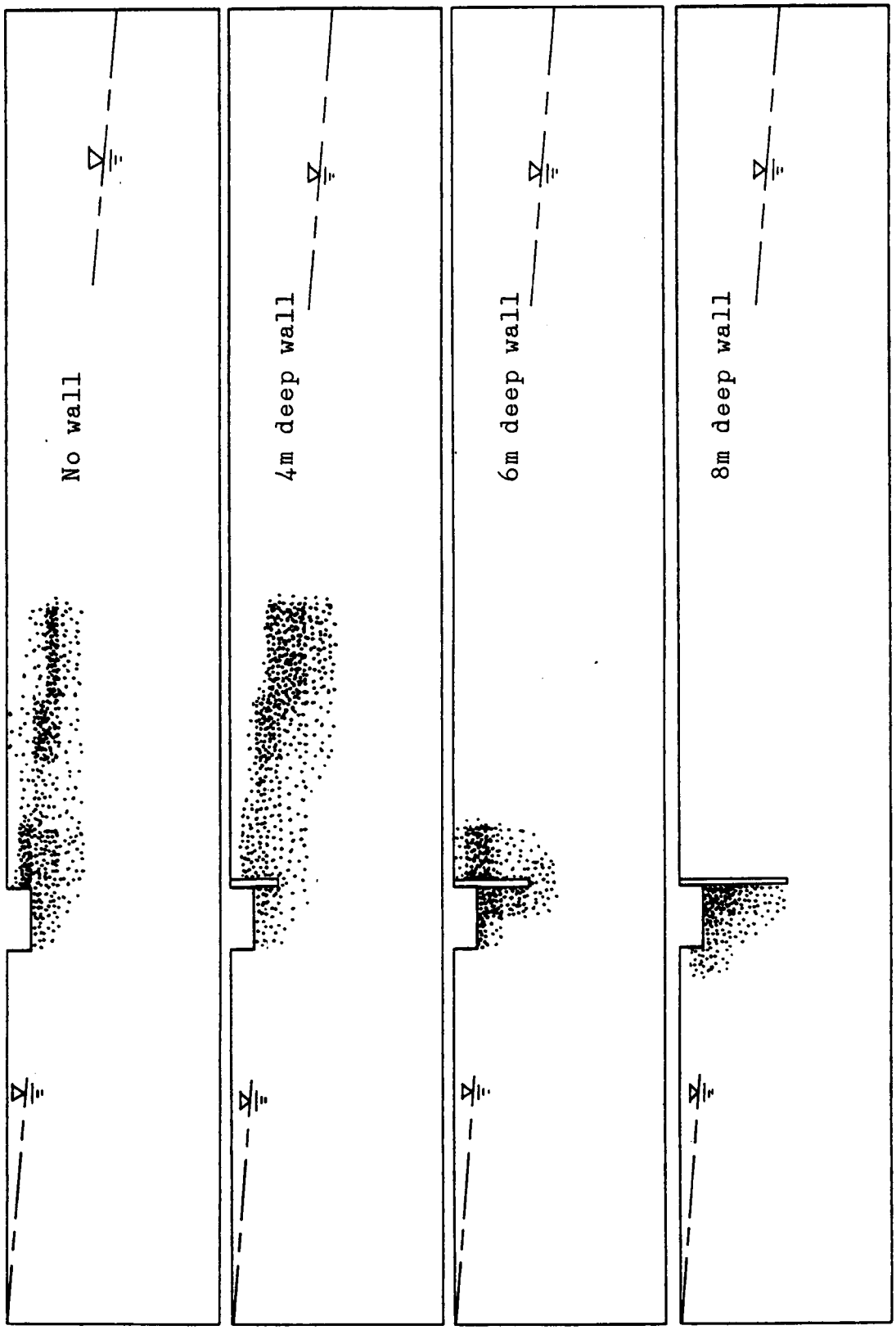

Figure 47. Oil phase plumes at 1070 days in Cases 8, 9, 10, and 11.

CHAPTER 8

Conclusions and Recommendations

This study has been concerned with simulation of the complex behavior of three-phase immiscible flow through soils. Special features of this study have been the use of van Genuchten's capillary function and Mualem's model for predicting relative fluid conductivities. A finite element model has been constructed and validated using laboratory tests.

Conclusions

Atmospheric air phase pressure, rigid porous materials and incompressible fluids are the assumptions made upon deriving the governing differential equations of immiscible flow. These are sound assumptions in dealing with groundwater contamination problems. The formulation leads to a coupled differential equations to be solved simultaneously. This is successfully accomplished using finite element method.

The capillary function proposed by van Genuchten (1980) can be applied to three-phase immiscible flow behavior. This has been done for the first time in this study.

The model for predicting the relative fluid conductivities in two-phase flow developed by Mualem (1976) can be adapted to three-phase immiscible flow. This modified model has been incorporated for the first time into the finite element formulation for three-phase immiscible flow.

For a successful culmination of this work it was necessary to evaluate the constitutive model parameters from laboratory tests. It was found that the parameters evaluated from three static tests of two-phase flow systems performed reasonably well in modelling the three-phase transient flow. The effects of model parameters and fundamental material properties were examined and showed that delicate laboratory tests are highly desirable.

In the numerical analysis, the effects of the time and spatial discretization were analysed and a simple rule was proposed for selecting a initial time step which can save much computing effort.

Convergence can be achieved using the modified direct iteration method which is simpler than the tangent method of iteration in computation.

From the study of simulating the buried leaking oil storage tank, it is concluded that the cutoff wall should be made of materials with high resistance only to the oil phase flow and should reach a certain depth below the water table. This depth depends on the soil condition, the water table, and the leaking oil and its head.

The finite element programs IMF1D (one-dimensional) and IMF2D (two-dimensional) are simple in structure but they have proven to be capable of handling severe nonlinearities involved in three-phase immiscible flow behavior. This study shows that the finite element technique has a great potential in analysing this type of flow problems. This study also shows the importance of the analytical derivation of the governing equations and the experimental analysis for the constitutive model.

Recommendations

Multiphase immiscible flow behavior is a complex and relatively new subject in geotechnical engineering. Since it is so new there are many areas requiring further study and research.

In a groundwater contamination problem, the spilled organic fluid may partially dissolve into the water phase. Also, due to the changes of pressure and temperature, it may vaporize and become gaseous phase. Water can also behave in the same manner. Thus the analytical study should be extended to model this interphase transfer.

It is noted that hysterisis in wetting and drying cycles of the capillary function may have an effect in some situations. This problem has not been attacked in this study and it is an area of some interest.

Model parameters α and n are affected by the pore size and pore size distribution in soils. Soil samples are commonly disturbed by sampling and transport. Thus some field test technique for a direct evaluation of these model parameters is highly desirable.

Severe nonlinearities are involved in the governing equations derived in this study. For this reason iteration techniques become very important as far as efficiency and accuracy are concerned. Any improvement made in the iteration technique for this specific problem is a contribution in this field as well as in numerical analysis.

Kerala

APPENDIX A

Explicit Form of Matrices

The explicit form of the matrices $[K]$ and $[K_t]$ in Eq.5.7 for the one-dimensional three-phase immiscible flow are

$$[K] = \frac{1}{l}\begin{bmatrix} K_w & -K_w & 0 & 0 \\ -K_w & K_w & 0 & 0 \\ 0 & 0 & K_o & -K_o \\ 0 & 0 & -K_o & K_o \end{bmatrix} \quad \text{and} \quad [K_t] = \frac{l}{6}\begin{bmatrix} 2C_{ww} & C_{ww} & 2C_{wo} & C_{wo} \\ C_{ww} & 2C_{ww} & C_{wo} & 2C_{wo} \\ 2C_{ow} & C_{ow} & 2C_{oo} & C_{oo} \\ C_{ow} & 2C_{ow} & C_{oo} & 2C_{oo} \end{bmatrix}$$

The bilinear shape functions [N] and its spatial derivatives [B] are

$$[N] = \frac{1}{4}\begin{bmatrix} (1-s)\ (1-t) \\ (1+s)\ (1-t) \\ (1+s)\ (1+t) \\ (1-s)\ (1+t) \end{bmatrix} \quad \text{and} \quad [B] = \begin{bmatrix} \frac{\partial N_1}{\partial x} & \frac{\partial N_2}{\partial x} & \frac{\partial N_3}{\partial x} & \frac{\partial N_4}{\partial x} \\ \frac{\partial N_1}{\partial y} & \frac{\partial N_2}{\partial y} & \frac{\partial N_3}{\partial y} & \frac{\partial N_4}{\partial y} \end{bmatrix}$$

APPENDIX B

Flow Chart of IMF1D and IMF2D

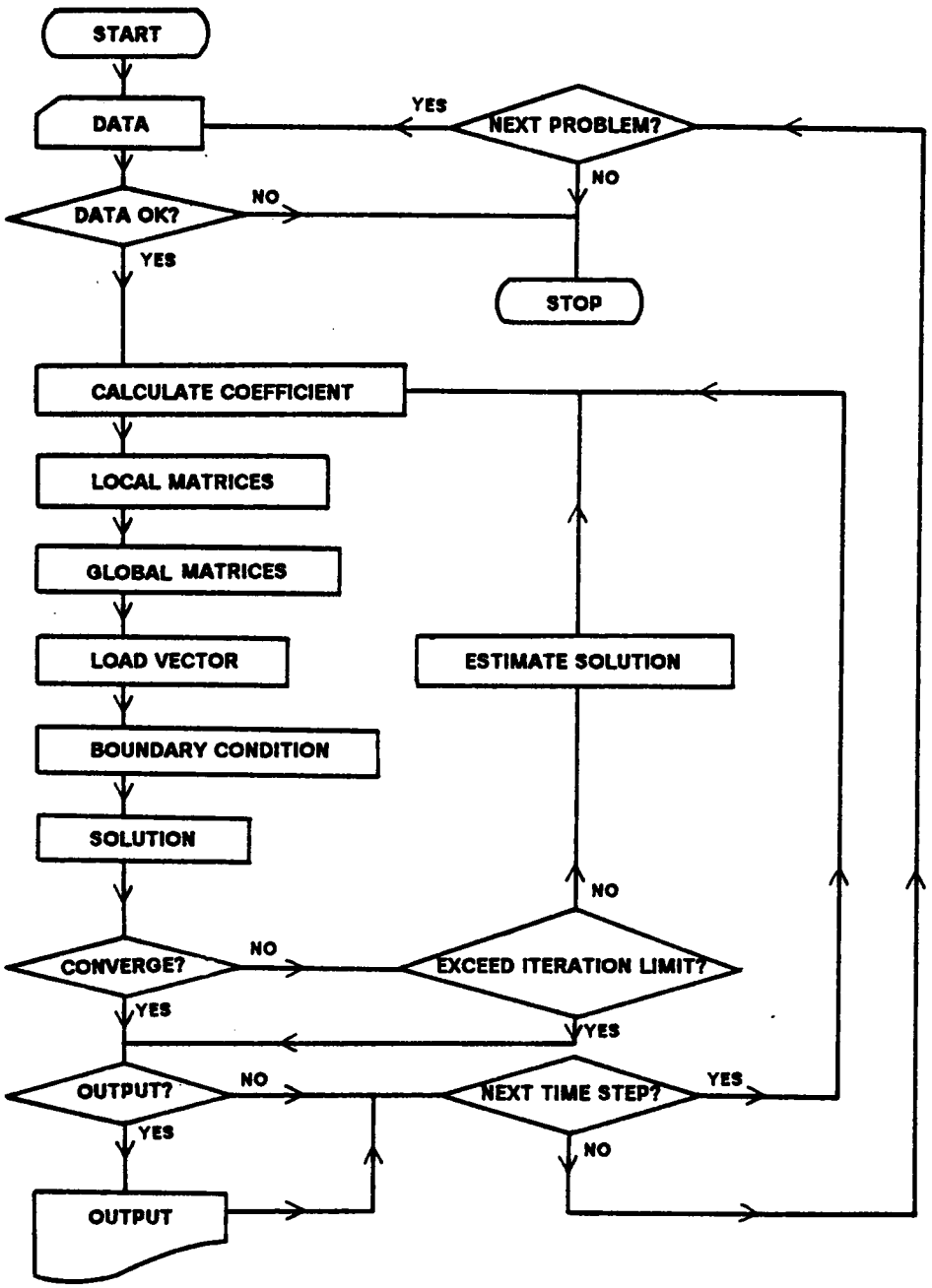

REFERENCES

Abriola, L. M. and Pinder, G. F. "A multiphase Approach to the Modeling of Porous Media Contamination by Organic Compounds, 1. Equation Development," Water Resources Research, Vol. 21, No. 1, January 1985a.

Abriola, L. M. and Pinder, G. F. "A multiphase Approach to the Modeling of Porous Media Contamination by Organic Compounds, 2. Numerical Simulation," Water Resources Research, Vol. 21, No. 1, January 1985b.

Adamson, A. W. Physical Chemistry of Surfaces, 2nd ed., Interscience, New York, 1967.

Amyx, J. W., Bass Jr., D. M., and Whiting, R. L. Petroleum Engineering, Physical Properties, McGraw-Hill, New York, 1960.

Bathe, K. J. and Wilson, E. L. Numerical Methods in Finite Element Analysis, Prentice Hall, New Jersy, 1976.

Bathe, K. J. Finite Element Procedures in Engineering Analysis, Prentice-Hall, NJ, 1982.

Bear, J. Dynamics of Fluids in Porous Media, American Elsevier Publishing, New York, 1972.

Belytschko, T. and Liu, W. K. "Computational Methods for Analysis of Transient Response," Recent Advances in Engineering Mechanics and Their Impaction on Civil Engineering Practice, Ed. by Chen, W. F. and Lewis, A. D. M., Vol. 1, Purdue University, May 1983.

Bettess, P. "Infinite Elements," International Journal for Numerical Methods in Engineering, Vol. 11, 1977.

Bikerman, J. J. Surface Chemistry Theory and Application, 2nd ed., Academic Press, New York, 1958.

Biot, M. A. "General Theory of Three-dimensional Consolidation," J. Appl. Phys. Vol.12, 1941.

Blake, F. C. "The Resistance of Packing to Fluid Flow," Trans. Amer. Inst. Chem. Eng. Vol. 14, 1922.

Bolt, G. H. and Groenevelt, P. H. "Coupling Phenomena As A Possible Cause for Non-Darcian Behavior of Water in Soil," Bull. IASH, No. 2, Vol. 14, 1969.

Botset, A. G. "Flow of Gas-Liquid Mixtures Through Consolidated Sand," Trans. AIME, Vol. 136, 1940.

Brebbia, C. A. (ed.) Finite Element Systems, A Handbook, 2nd ed., Springer-Verlag, New York, 1982.

Brooks, R. H. and Corey, A. T. "Hydraulic Properties of Porous Media," Hydrology Papers, Colorado State University, Fort Collins, CO, 1964.

Brown, H. W. "Capillary Pressure Investigations," Trans. AIME, Vol. 192, 1951.

Brownscombe, E. R., Slobad, R. L., and Caudle, B. H. "Laboratory Determination of Relative Permeability," Oil and Gas J. Vol. 51, 1950.

Buckley, S. E. and Leverett, M. C. "Mechanism of Fluid Displacement in Sands," Petroleum Development and Technology, Vol. 146, 1942.

Burdine, N. T. "Relative Permeability Calculations From Pore-Size distribution Data," Trans. AIME, Vol. 198, 1953.

Calhoun, J. C. Oil and Gas J. Vol. 50, 1951.

Carman, P. C. "Fluid Flow Through a Granular Bed," Trans. Inst. Chem. Eng. London, Vol. 15, 1937.

Carman, P. C. Flow of Gases Through Porous Media, Butterworths, London, 1956.

Carter, R. D. "Comparison of Alternating Direction Explicit and Implicit Procedures in Two-dimensional Flow Calculations," J. Soc. Petrol. Eng., No. 1, Vol. 7, 1967.

Casagrande, A. "Seepage Through Dams," Contribution to Soil Mechanics, Boston Society of Civil Engineers, Boston, 1940.

Casulli, V. and Greenspan, D. "Numerical Simulation of Miscible and Immiscible Fluid Flows in Porous Media," J. Soc. Petrol. Eng., No. 10, Vol. 22, 1982.

Collins, R. E. Flow of Fluids Through Porous Materials, Litton Educational Publishing, Texas, 1961.

Corey, A. T., Rathjens, C. H., Henderson, J. H., and Wyllie, M. R. J. "Three-phase Relative Permeability," Petroleum Transactions, Vol. 207, 1956. Cgaig, F. F. "The Reservoir Engineering Aspects of Water Flooding," Society of Petroleum Engineers of AIME, Monograph, Vol. 3, Dallas Texas, 1971.

Dean, J. A. (ed.) Lange's Handbook of Chemistry, 12th ed., McGraw-Hill, New York, 1979.

Diment, G. A. and Watson, K. K. "Stability Analysis of Water Movement in Unsaturated Porous Materials, 2. Numerical Studies," Water Resources Research, Vol. 21, No. 7, July 1983.

Douglas, J., Peaceman, D. W., and Rachford, H. H. "A Method for Calculating Multidimensional Immiscible Displacement," Trans. AIME, Vol. 216, 1959.

Dullien, F. A. L. Porous Media – Fluid Transport and Pore Structure, Academic Press, New York, 1979.

Eckberg, D. K. and Sunada, D. K. "Nonsteady Three-Phase Immiscible Fluid Distribution in Porous Media," Water Resources Research, Vol. 20, No. 12, December 1984.

Edwards, J. W. "Trouble in Oiled Waters," National Wildlife, October-November, 1985.

Fair, G. M. and Hatch, I. P. "Fundamental Factors Governing The Streamline Flow of Water Through Sand," J. Amer. Water Works Ass. Vol. 25, 1933.

Faust, C. R. "Transport of Immiscible Fluids Within and Below the Unsaturated Zone -- A Numerical Model," Geotrans Technical Report, No. 84-01, February 1984.

Fatt, I. and Dykstru, H. "Relative Permeability Studies," Trans. AIME, Vol. 192, 1951.

Freeze, R. A. "Three-Dimensional, Transient, Saturated-Unsaturated Flow in a Groundwater Basin," Water Resources Research, Vol. 7, No. 2, April 1971a.

Freeze, R. A. "Influence of the Unsaturated Flow Domain on Seepage Through Earth Dams," Water Resources Research, Vol. 7, No. 1, August 1971b.

Grandin, H. Fundamentals of The Finite Element Method, Macmillan Publishing Company, New York, 1986.

Harr, M. E. Groundwater and Seepage, McGraw Hill, New York, 1962.

Hinton, E. and Owen, D. R. J. An Introduction to Finite Element Computations, Pineridge Press, U.K., 1979.

Huppler, J. D. "Numerical Investigation of the Effects of Core Heterogeneities on Waterflood Relative Permeabilities," Trans. AIME, Vol. 249, 1970.

Huyakorn, P. S. and Pinder, G. F. Computational Methods in Subsurface Flow, Academic Press, New York, 1983.

Huyakorn, P. S. Thomas, S. D., and Thompson, B. M. "Techniques for Making Finite Elements Competitive in Modeling Flow in Variably Saturated Porous Media," Water Resources Research, Vol. 20, No. 8, August 1984.

Iberall, A. S. "Permeability of Glass Wool and Other Highly Porous Media," J. Res. Nat. Bur. Stand., Vol. 45, 1950.

Irmay, S. "Flow of Liquid Through Cracked Media," Bull. Res. Council of Israel No. 1, 5A, 1955.

Javandel, I. and Witherspoon, P. A. "Application of The Finite Element Method to Transient Flow in Porous Media," J. Soc. Petrol. Eng., Vol. 8, 1968.

Kutilek, M. "Non-Darcian Flow of Water in Soils (Laminar Region)," First IAHR Symp. Fundamentals of Transport Phenomena in Porous Media, Haifa, Israel, 1969.

Lambe, T. W. Soil Testing for Engineers, John Wiley and Sons, New York, 1951.

Lambe, T. W. and Whitman, R. V. Soil Mechanics, John Wiley and Sons, New York, 1969.

Lane, K. S. and Washburn, D. E. "Capillary Tests by Capillarimeter and by Soil Filled Tubes," Proc. Highway Research Board, 1946.

Lenhard, R. J. and Parker, J. C. "Use of Multiphase Retention Functions to Predict Fluid Behavior of Organic Liquid-Water-Air Fluid Systems in Porous Media," submitted to Water Resources Research, July, 1986.

Lewis, R. W., Morgan, K., and Johnson, K. H. "A Finite Element Study of Two-dimensional Multiphase Flow with Particular Reference to the Five-spot Problem," Computer Methods in Applied Mechanics and Engineering, Elseview Science Publishing, North-Holland, 1984.

Li, W. H. and Lam, S. H. Principles of Fluid Mechanics, Addison-Wesley Pub. Co., 1964.

Logan, D. L. A First Course in The Finite Element Method, Prindl, Weber, and Schmidt, MA., 1986.

Low, P. F. "Physical Chemistry of Clay-Water Interaction," Advances in Agronomy, Vol. 13, 1961.

Millington, R. J. and Quirk, J. P. "Permeability of Porous Solids," Trans. Faraday Soc. Vol. 57, 1961.

Mualem, Y. "A New Model for Predicting the Hydraulic Conductivity of Unsaturated Porous Media," Water Resources Research, Vol. 12, No. 3, June 1976.

Muskat, M. The Flow of Homogeneous Fluids Through Porous Media, McGraw-Hill, New York, 1937.

Narasimhan, T. N. and Witherspoon, P. A. "An Integrated Finite Difference Method for Analyzing Fluid Flow in Porous Media," Water Resources Research, Vol. 12, No. 1, February 1976.

Narasimhan, T. N. "Multidimensional Numerical Simulation of Fluid Flow in Fractured Porous Media," Water Resources Research, Vol. 18, No. 4, August 1982.

Neuman, S. P., Preller, C., and Narasimhan T. N. "Adaptive Explicit-Implicit Quasi Three-Dimensional Finite Element Model of Flow and Subsidence in Multiaquifer Systems," Water Resources Research, Vol. 18, No. 5, October 1982.

Nutting, P. G. "Physical Analysis of Oil Sands," Bull. Amer. Ass. Petr. Gelo., Vol. 14, 1930.

Osborne, M. and Sykes, J. "Numerical Modelling of Immiscible Organic Transport at The Hyde Park Landfill," Water Resources Research, Vol. 22, pp 25-33, 1986.

Parker, J. C., Kool, J. B., and van Genuchten, M. Th. "Determining Soil Hydraulic Properties from One-step Outflow Experiments by Parameter Estimation: II. Experimental Studies," Soil Science Society of America Journal, Vol. 49, No. 6, November-December 1985.

Parker, J. C., Lenhard, R. J., and Kuppusamy, T. "A Parametric Model for Constitutive Properties Governing Multiphase Fluid Conduction in Porous Media," submitted to Water Resources Research, June 1986.

Parsons, R. W. "Permeability of Idealized Fractured Rock," J. Soc. Petrol. Eng. 6, 1966.

Peery, J. H. and Herron, Jr. E. H. "Three-Phase Reservoir Simulation," Journal of Petroleum Technology, Vol. 21, February 1969.

Peaceman, D. W. Fundamentals of Numerical Reservoir Simulation, Elsevier North-Holland, Inc., New York, 1977.

Philip, J. R. "Flow Through Porous Media," Ann. Rev. Fluid Mechan., Vol. 2, 1970.

Pirson, S. J. Oil Reservoir Engineering, McGraw-Hill, New York, 1958.

Purcell, W. R. "Capillary Pressures – Their Measurement Using Mercury and The Calculation of Permeability Therefrom," Trans. AIME, Vol. 186, 1949.

Quon, D., Dranchuk, P. M., Allada, S. R., and Leung, P. K. " Application of The Alternating Direction Explicit Procedure to Two-dimensional Natural Gas Reservoirs," J. Soc. Petrol. Eng., No. 2, Vol. 6, 1966.

Rapoport, L. A. and Leas, W. J. "Relative Permeability to Liquid in Liquid-Gas Systems," Trans, AIME, Vol. 192, 1951.

Rapoport, L. A. and Leas, W. J. "Properties of Linear Waterfloods," Petroleum Transactions, Vol. 198, 1953.

Reddy, J. N. An Introduction to The Finite Element Method, McGraw-Hill, New York, 1984.

Remson, I. and Randolph, J. R. "Review of Some Elements of Soil Moisture Theory," U.S. Geol. Survey, Professional Paper 411-D, 1962.

Richtmeyer, R. D. Difference Methods for Initial-Value Problems, Interscience, New York, 1957.

Rose, H. E. "An Investigation into The Laws of Flow of Fluids Through Beds of Granular Material," Proc. Inst. Mech. Eng., Vol. 153, 1945.

Rose, W. "Some Problems of Relative Permeability Measurement," Proc. 3rd World Petrol. Congr. Sect. II, 1951.

Rose, W. and Bruce, W. A. "Evaluation of Capillary Characters in Petroleum Reservoir Rock," Trans. AIME, Vol. 186, 1949.

Rumer, R. R. and Drinker, P. A. "Resistance to Laminar Flow Through Porous Media," Proc. Amer. Soc. Civil Eng., No. HY5, Vol. 92, 1966.

Rusell, T. W. F. and Charles, E. "Effect of The Less Viscous Liquid in The Laminar Flow of Two Immiscible Liquids," Canad. J. Chem. Eng., Vol. 37, 1959.

Scheidegger, A. E. The Physics of Flow Through Porous Media, University of Toronto Press, 1960.

Scheidegger, A. E. "Statistical Hydrodynamics in Porous Media," J. Appl. Phys., No. 25, 1954.

Scheidegger, A. E. "On The Theory of Flow of Miscible Phase in Porous Media," Proc. IUGG General Assembly, Toronto, Vol. 2, 1957.

Segerlind, L. J. Applied Finite Element Analysis, John Wiley and Sons, New York, 1984.

Settari, A. and Aziz, K. "Use of Irregular Grid in Reservoir Simulation," Soc. Petrol. Eng. J., Vol. 103, 1972.

Shamir, U. "The Use of Computers in Ground Water Hydrology," Report No. 105, Hydrodynamics Lab., M.I.T., MA, 1967.

Shaw, F. S. Relaxation Methods, Dover, New York, 1953.

Silin-Bekchurin, A. I. Dynamics of Underground Water, Moscow University, Moscow, 1958.

Smith, G. O. Numerical Solution of Partial Differential Equations, Oxford University Press, New York, 1965.

Smith, W. O. "Capillary Flow Through An Ideal Uniform Soil," Physics, Vol. 3, 1933.

Snow, D. T. A Parallel Plate Model of Fractured Permeable Media, Dissertation, University of California, Berkeley, 1965.

Stone, H. L. "Probability Model for Estimating Three-Phase Relative Permeability," Journal of Petroleum Technology, Vol. 249, February 1970.

Swartzendruber, D. "Non-Darcy Flow Behavior in Liquid-Saturated Porous Media," J. Geophys. Res. No. 3, Vol. 4, 1962.

Swartzendruber, D. "The Flow of Water in Unsaturated Soils," Flow Through Porous Media (de Wiest, R. J. M. Ed.) Chap. 6, Academic Press, New York, 1969.

van Genuchten, M. Th. "A Closed-form Equation for Predicting the Hydraulic Conductivity of Unsaturated Soils," Soil Science Society of America Journal, Vol. 44, No. 5, September 1980.

van Genuchten, M. Th. "A Comparison of Numerical Solutions of the One-dimensional Unsaturated-Saturated Flow and Mass Transport Equations," Advanced Water Resources, Vol. 5, March 1982.

van Genuchten, M. Th. "An Hermitian Finite Element Solution for the Two-dimensional Saturated-unsaturated Flow Equation," Advances in Water Resources, Vol. 6, June 1983.

van Meurs, P. "The Use of Transparent Three-dimensional Models for Studying The Mechanisms of Flow Processes in Oil Reservoirs," Trans. AIME, Petrol., Vol 210, 1957.

von Engelhardt, W. and Tunn, W. L. M. The Flow of Fluids Through Sandstones, translated by Witherspoon, P. A. from Heidelberger Beitr. Mineral Petrog. Vol. 2, Ill. State Geol. Survey, Circular 194, 1955.

Ward, J. C. "Turbulent Flow in Porous Media," Proc. Amer. Soc. Civil Eng. No. HY5, Vol. 90, 1964.

Watson, K. K. "Experimental and Numerical Study of Column Drainage," Proc. Amer. Soc. Civil Eng. Hydraul. Div. No. HY2, Vol. 93, 1967.

Weige, H. J. and Bruce, W. A. "The Restored State Method for Determination of Oil In Place and Connate Water," Drilling and Production Practices, Amer. Petrol. Inst., Vol. 166, 1947.

Wesseling, J. "Principles of Unsaturated Flow and Their Application to The Penetration of Moisture into The Soil," Tech. Bull. Inst. Land and Water Res. No. 23, Wageningen, The Netherlands, 1961.

Wyllie, M. R. J. and Spangler, M. B. "Application of Electrical Resistivity Measurements to Problems of Fluid Flow in Porous Media," Bull. Amer. Ass. Petrol. Geol., Vol. 36, 1952.

Zienkiewicz, O. C. The Finite Element Method, 3rd Ed., Mcgraw-Hill, New York, 1977.

Zienkiewicz, O. C., Kelly D. W., and Bettess, P. "The Coupling of the Finite Element Method and Boundary Solution Procedures," International Journal for Numerical Methods in Engineering, Vol. 11, 1977.

The vita has been removed from the scanned document